Ink-Gel Simultaneous Embedded 3D Printing

Author:

Adrian van Driel

Supervisor:

Dr Reuben Govender

Department of Mechanical Engineering

University of Cape Town

2024

Plagiarism Declaration

I, Adrian van Driel, hereby:

1. I know that plagiarism is wrong. Plagiarism is to use another's work and pretend that it is one's own.
2. I have used the IEEE convention for citation and referencing. Each contribution to, and quotation in, this report from the work(s) of other people has been attributed and has been cited and referenced.
3. This report is my own work.
4. I have not allowed, and will not allow anyone to copy my work with the intention of passing it off as their own work or part thereof.

I know the meaning of plagiarism and declare that all the work in the document, save for that which is properly acknowledged, is my own. This thesis/dissertation has been submitted to the Turnitin module (or equivalent similarity and originality checking software) and I confirm that my supervisor has seen my report and any concerns revealed by such have been resolved with my supervisor.

Signed by candidate

Adrian van Driel

Department of Mechanical Engineering

University of Cape Town

19 July 2024

Abstract

3D printing has improved by leaps and bounds. The gains include both the hardware and software. With 3D printers increasingly becoming staples of many a laboratory and engineering workshop, naturally comes the application of 3D printing to ever more significant issues. Some of these new applications encouraged the use of 3D printing to solve problems involving printing materials that do not solidify in the near-instantaneous manner that most existing methodologies used in 3D printing require. The material requirements of liquid or gel materials that may take minutes or even hours to solidify prompted the invention of embedded 3D printing. Embedded 3D printing is a methodology whereby a liquid is 3D printed into a support gel that supports the printed material's form until it can cure.

This project aims to design and test a prototype that may increase the useful print volume of an embedded 3D printer modified from an existing low-cost fused deposition modelling type 3D printer. To create parts using embedded 3D printing in the past, a support bath needed to be prepared before printing and the printed material nozzle needed to be longer than the shortest axis of the part. With that design, the requirement for a long nozzle to print larger parts introduces some problems. More extended nozzles require more pressure to extrude material, are more likely to clog than shorter nozzles, create more of a disturbance in the support gel and are more susceptible to deflection over the nozzle's length. A need was identified to print support gel on demand and, in that way, make an embedded printer that could expand the useful print volume without increasing the length of the nozzle.

Various sub-assemblies were designed, tested, and iteratively improved until the entire assembly could be tested together to achieve simultaneous printing of the printed material and the support gel. This assembly would be called the Dual Ink-Gel Extruder (DIGEX). The printed material and the support gel were mixed in the same lab as the 3D printer, and the rheological properties of several concentrations of the support gel were tested and analysed to best enable simultaneous printing. Printed material and gel deposition methodologies were developed for this purpose, and their performance was analysed for best results. Several iterations of the electrical hardware, the software, and the slicer configurations were tested and iterated for use with DIGEX. These improvements culminated in a result that could successfully demonstrate the concept of simultaneous dual extrusion. However, some new complications were introduced in the printing process that need further iterations and research to enable large-format embedded 3D printers.

Acknowledgements

I have many people that I am eternally grateful for helping me bring this project across the finish line in a state that I am genuinely proud of. In no particular order:

I need to thank Dr Reuben Govender; his advice and understanding of the issues inside and outside of this project I encountered ensured that I could keep treading water, even when I felt I had jumped into the deep end at times.

My thanks to everyone at BISRU; you were there to commiserate and aid when I hit a snag and equally there to celebrate the victories, big and small, along the way.

Thank you to the team at CME. Your patience and enthusiasm during my testing in your laboratory smoothed out any bumps when I would have otherwise tripped over unforeseen obstacles.

Thank you to those in the Chemical Engineering Department who helped me over the weeks of testing I did in your laboratory. I absolutely could not have done what I did without your help.

Thank you to the good people in the Electrical Engineering Department who helped me when I was utterly stumped over the confounding electrical interference issues I ran into while trying to build the 3D printer. Your advice and aid turned a disaster into a footnote.

My thanks are also extended to Carst & Walker for giving samples of Carbopol 980 and 990 powder. The amount freely given was far more than I could have hoped for, and I am grateful for their generosity.

Another business I must thank is Gripper, who met in person to discuss my needs for the pumps I was building and supplied the necessary fittings as requested, even when I didn't know what I wanted.

Last but certainly not least, I must thank my family and close friends. Sharing my enthusiasm for what I was doing at UCT and allowing me to think aloud when chewing on a difficult problem helped more than you could ever know—a special thanks to those who even read parts of or even entire draft versions of this document. Your feedback is invaluable and helped make a document that I treasure today.

Table of Contents

Table of Figures

Table of Tables

Nomenclature

3D printing	-	Method of additive construction whereby a three-dimensional part is made from a digital 3D model
Ink	-	Material in embedded 3D printing to be used in smaller amounts to be supported by the support gel
Support gel	-	Material within which the ink material is embedded during embedded 3D printing for support
CAD	-	Software used to create 2D or 3D designs (Computer Aided Design)
SLA	-	A type of 3D printing using ultraviolet light to cure resin in a layer-by-layer fashion (Stereolithography)
SLS	-	A type of 3D printing using lasers to sinter powders (Selective Laser Sintering)
FDM	-	A type of 3D printing using thermoplastic selectively deposited to create 3D models (Fused Deposition Modelling)
Hot end	-	Heater and nozzle assembly of an FDM 3D printer, used to melt and deposit molten thermoplastic
Print head	-	Assembly mounted onto a carriage to be moved about to deposit molten thermoplastic material selectively, usually includes the heater and nozzle assembly and can also be called the hot end in FDM 3D printing
Build volume	-	The volume within which a 3D printer can create a part
Extruder	-	The assembly pushing thermoplastic filament to the hot end in FDM 3D printing
Ink deposition needle	-	The nozzle used to deposit the ink in embedded 3D printing
Tool changing	-	The automatic process of changing the tools to increase the capabilities of the machine using a tool changer

1. Introduction

3D printing is an additive process whereby a part is created by adding material instead of removing material from a larger part, unlike many other more traditional manufacturing methods. 3D printing has rapidly grown in capability in the last decade while reducing the overall cost of the machines involved.

3D printers' strengths lie in creating geometries like complex organic cavities and internal lattices that would be difficult or impossible using other methods. Additionally, low-volume, customized parts can be made to fit the desired purpose. However, traditional 3D printing technologies are often limited to materials that rapidly solidify after being printed or are already solid before printing.

Embedded 3D printing was developed to enable the use of input materials with longer solidification times. Embedded 3D printing is a method whereby a liquid material is extruded from a nozzle or needle tip into a support bath that traps the material where it may remain liquid or can solidify and be extracted after solidifying. Using embedded 3D printing, materials that are too soft for other extrusion-based 3D printers or are liquid at room temperature may be 3D printed. This method may also eliminate the need for support and enable materials like silicones and bio-inks to be 3D printed [1].

Embedded printing does have some limitations. A major limitation has been the size of the prints possible using embedded 3D printers. This limitation stems from the need for the needle injecting material into the support bath to be longer than the shortest axis of the produced part [1].

1.1. Aims of the study

This work aimed to tackle the size constraint inherent in many embedded 3D printer designs and develop a method to massively increase the possibilities regarding printing large parts and enable large format embedded 3D printing.

Additionally, this study aimed to achieve printing quality, as seen in previous iterations of embedded 3D printers, but it should be able to print much larger parts than has been generally done before.

1.2. Scope, limitations and constraints

Some generic limitations were placed on the study to keep it in line with a mechanical engineering masters dissertation:

- Custom parts were limited to what could be easily produced at low cost.
- The prototypes would not need to be useable outside a laboratory.

Some limitations were also applied that are more appropriate for the development of embedded 3D printing:

- The ink and support gel combinations are limited to similar combinations found in previous projects [2].
- Only ink and gel combinations that could be printed at room temperature were used. Ink or gels that require heating were left for future project development.
- The printer would be constructed using an existing low-cost, consumer-level 3D printer.
- No custom electronics should be constructed.
- Existing firmware and 3D printing software should be used.

1.3. Key outcomes

As a first step, an existing 3D printing platform was converted to an embedded 3D printer using an existing successful design for an embedded 3D printer [3]. Building and testing an embedded 3D printer based on a proven embedded 3D printer design gave valuable insight into how best to design a new working prototype that would fulfil the aim of this study.

Once a prototype had been developed, a gel deposition system was added to the embedded 3D printer to allow automated switching between ink and support material deposition. Testing commenced on the sub-systems, and iterative improvements were made until the embedded printer could reliably produce parts on a scale that had been difficult to achieve before.

2. Literature review

Significant research needed to be undertaken to develop a solution to the problem of the limited size of embedded 3D printing build volumes. This research started by looking into 3D printing more generally. Once a good foundation of knowledge was built up, embedded printing was focused on. Further research was done on the factors influencing embedded printing. This research on embedded printing and the factors influencing ultimate print success was used to best proceed with the project's development.

2.1. General overview of 3D printing development and technologies

3D printing or additive manufacturing is the process of creating a 3-dimensional object from a digital file by laying down material layer-by-layer until the 3D print is complete.

Generally, the digital object is cut into 2D "slices", thin cross-sections of the object, to make these layers in software. The "Slicer" software takes a computer-aided design (CAD) model generated from software such as Autodesk Inventor or Solidworks and makes these slices. Once the Slicer is done, the output is a set of movement and tool action instructions for the printer, usually in the form of G-code. The G-code file is transferred to the 3D printer as a complete file or line-by-line. The 3D printer microcontroller interprets the G-code to enact motion, temperature or tool parameter changes.

This approach allows an individual with CAD skills and a 3D printer to quickly design and produce unique parts. Additionally, additive manufacturing allows a user to create geometries that are impossible when using other techniques.

2.1.1. History of 3D printing

The technology of 3D printing is older than one might realize. The first instance of a machine called a 3D printer can be attributed to Hideo Kodama in 1981 [4]. Kodama's machine was an early form of stereolithography apparatus (SLA) 3D printing. A photosensitive resin was deposited, layer-by-layer, and cured by ultra-violet light into a functional shape for the user. An image from Kodama’s patent on 3D printing is shown in Figure 1.

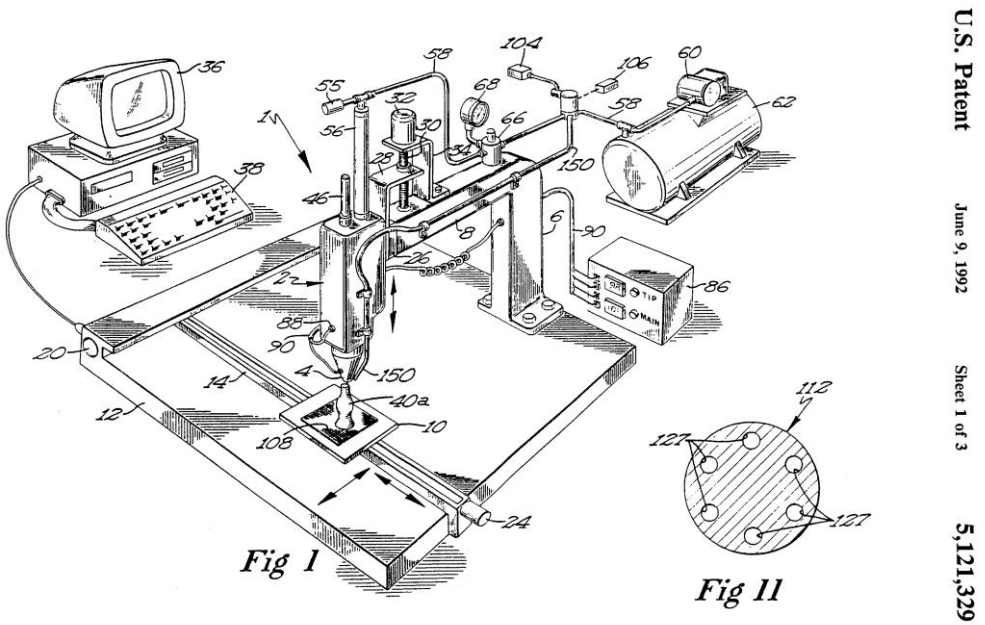

Figure 1: *The first granted patent for a fused deposition modelling 3D printer* [5]

In 1986, French researchers developed a similar technology whereby a laser was used to cure liquid monomers instead of layers of resin [4]. In the same year, the first patent for SLA printing was submitted by an American, Charles Hull. In 1988, he founded the 3D Systems Corporation, selling the SLA-1, the first commercial 3D printer [4].

1988 also marked the year Carl Deckard of the University of Texas submitted the first patent for Selective Laser Sintering (SLS) [4]. Like the previously mentioned French researchers, SLS printing uses lasers, but unlike the French researchers, powders are sintered instead of resins.

Around the same time, Scott Crump developed fused deposition modelling (FDM) 3D printing [4]. This 3D printing technology extruded softened thermoplastics through a heated nozzle to form the user-specified geometry. FDM is used in most low-cost 3D printers available today.

In the following years, many companies experimented with different implementations of 3D printing. These early printers were typically expensive, difficult to use and unreliable. In 2005, the RepRap project was started by Adrian Bowyer [4]. RepRap was an open-source project to make 3D printers that may be used to manufacture print parts for further 3D printers (self-replicating rapid prototyping).

Once the FDM patents submitted in the late 80s became public domain in 2009, the door was opened to hobbyists and smaller companies to innovate on the FDM technology. From that point onwards, FDM 3D printers became more accessible and cheaper. These machines becoming more commonplace while more individuals have access to learning CAD modelling skills and software ensured that FDM 3D printers have an essential place in many workshops and laboratories.

2.1.2. Existing 3D printing technologies

Several additive manufacturing technologies are used today, including: Vat Photopolymerization, Material Jetting, Binder Jetting, Material Extrusion, Powder Bed Fusion, Sheet Lamination, and Directed Energy Deposition [6]. This review will focus on the more commonly available 3D printer technologies, namely Vat Photopolymerization, Material Extrusion and Powder Bed Fusion. More comprehensive reviews of other additive manufacturing technologies can be found at [7] and [8].

2.1.2.1. Stereolithography Apparatus (SLA)

SLA is a Vat Photopolymerization type additive manufacturing technology. It uses an ultraviolet laser to selectively cure an ultraviolet-curable resin, layer by layer, to reproduce the user-defined geometry. Typically, in modern SLA printers, a platform is lowered into a resin vat until it is very close to the bottom of the vat, where a laser shines onto the platform or the existing, already cured model attached to the platform. This process is known to produce very high detail and accurate models since the size of the reproducible detail is only limited by the diameter of the laser beam used [9]. An example of an SLA 3D printer is shown in Figure 2.

Figure 2: *An example of an SLA 3D printer* [10]

Digital Light Processing (DLP) and Masked Stereolithography Apparatus (MSLA) are both evolutions of SLA printing[10]. Instead of a single laser being used, an image is projected onto the platform or the existing print. Prints can be completed far more quickly using these methods. Additionally, since an entire layer is printed simultaneously, adding parts to a print job does not necessarily increase the print time[10]. A drawback of these approaches is that the printed quality is limited by the resolution of the displayed image and some pixelation may result that would not be seen in SLA 3D printed parts, which are the result of a smoothly drawn path using a laser. Anti-aliasing and higher pixel-density displays have reduced the pixelation effects and increased the surface finish of DLP and MSLA 3D printed parts[9].

It should be noted that when working with resin 3D printers, some irritation or toxic side effects may be experience in more sensitive users. It is thus advised that the user post process the print to make sure all the uncured resin has been washed off or cured while needing some personal protective equipment to keep resin of the skin and to keep the user from breathing in the fumes[9].

2.1.2.2. Selective Laser Sintering (SLS)

SLS 3D printers use Powder Bed Fusion additive manufacturing. SLS printers typically use a laser that sinters powders in a bed to recreate a user-specified geometry [11]. Once the laser has finished with a layer, a roller will spread a new layer of powder over the existing layer so that the laser may sinter the next layer. This method applies to both thermoplastic polymers and metal powders, though different laser wavelengths are typically needed for these.

An advantage SLS has over most SLA or FDM-derived techniques is that no separate support material is required, as the unbonded powder supports the next layer. This factor and that the unused powder is reusable for the next SLS print job gives SLS a claim as the lowest waste 3D printing method [11]. The properties of the powder can be changed as needed to suit the user's use case. Despite all this, the complexities of safely handling the fine powder have meant that SLS printers have primarily been restricted to laboratories or specialised engineering workshops. Figures from the patent detailing the SLS process are shown in Figure 3.

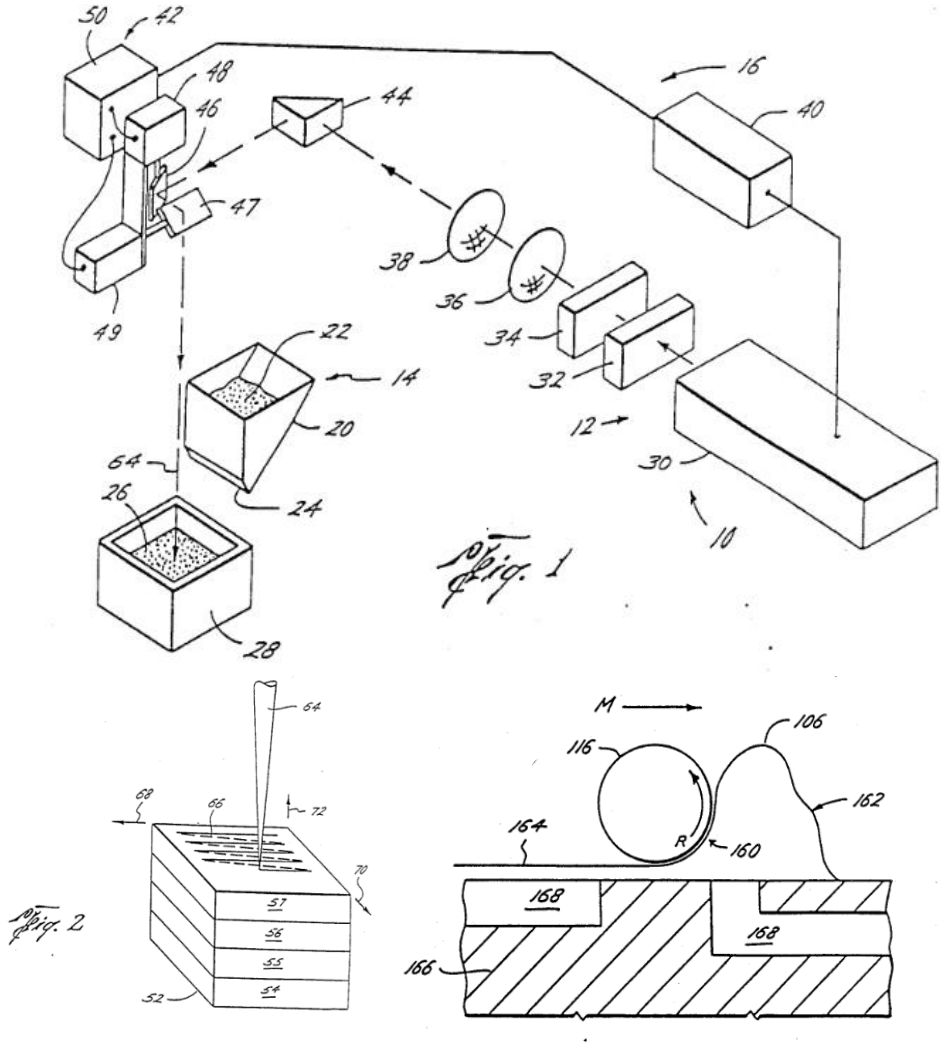

Figure 3: *Figures from the Selective Laser Sintering with Assisted Powder Handling patent where a roller lays out an even layer of powder before a laser is directed to sinter the powder along a pre-defined path* [12].

2.1.2.3. Fused Deposition Modeling (FDM)

FDM is a method of 3D printing where heated thermoplastic is extruded out of a nozzle. Material is laid down layer by layer until the user-specified geometry is finished. Usually, an FDM machine will accept a plastic filament of a specific diameter to push through a motor assembly called the extruder. The extruder drives the filament to the hot end assembly, where the plastic filament is softened and extruded from the nozzle.

This technology is also known as fused filament fabrication (FFF) after Stratasys made "fused deposition modelling" and "FDM" their trademark in 1991 [5]. The technology has since become public domain. Generally thought of as one of the simplest methods of 3D printing, while being typically low-cost and versatile, FDM machines dominate the hobbyist 3D printing market. An example of one of these hobbyist machines is shown in Figure 4.

Figure 4: *An example of an FDM 3D printer* [13]

2.1.2.3.1. FDM movement

There are several methods of moving the print head of an FDM 3D printer. These include Rectilinear Cartesian, Delta, SCARA, and Polar, among others. The method focused on in this work will be cartesian since it is by far the most ubiquitous. Most 3D printer cartesian movement can be further broken down into pure cartesian and CoreXY movement. Some motion systems are shown in Figure 5.

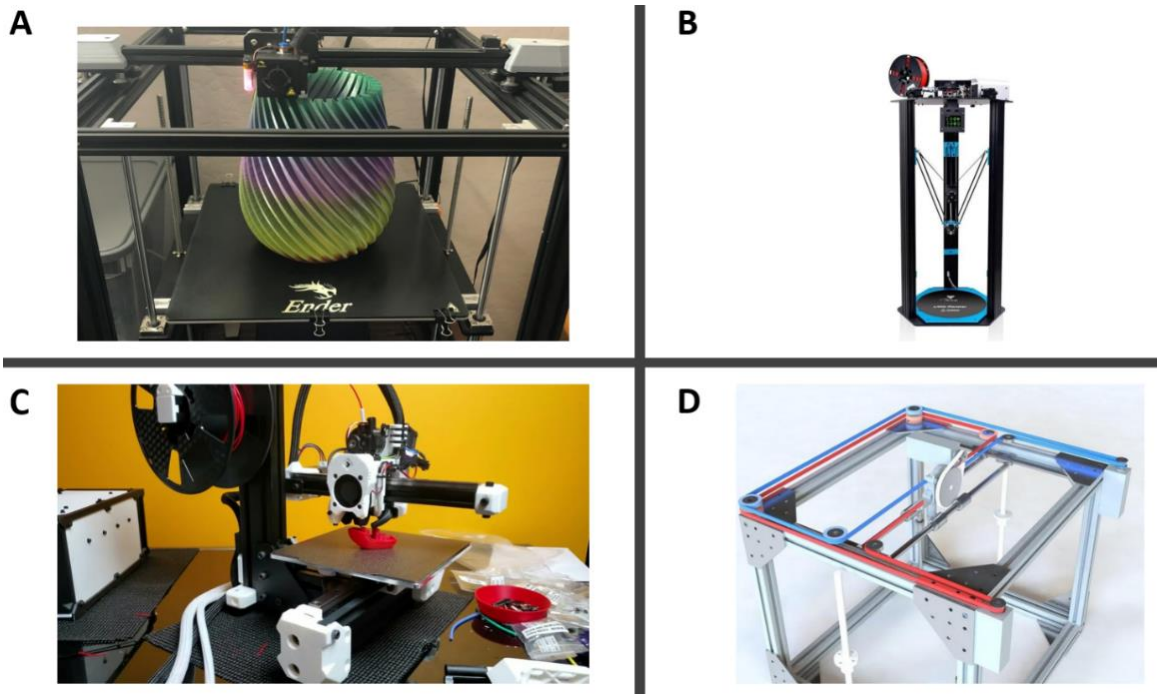

Figure 5: *Some motion systems typically used in FDM 3D printers. A is an example of cartesian movement* [14]*, B is an example of delta movement* [15]*, C is a bed slinger* [16] *and D uses CoreXY movement* [15]

In cartesian movement, the hot end is moved in the x, y, and z directions, with one or more motors assigned to each direction. No motors are assigned to more than one direction. This simplicity in the movement makes controlling the print head easier but generally results in prints taking longer as the print head cannot reach the same print speeds as other methods that use combinations of two or more motors to control the movement of the print head. Since one or more motors are responsible for the movement of each axis, it often means that the most straightforward approach is to mount one of the motors to a gantry that needs to move, resulting in other motors always being at a disadvantage since the disadvantaged motors need to move the print head, the gantry the print head is mounted to, as well as the motor mounted to that gantry.

In CoreXY movement, a complicated arrangement of belts allows two motors to simultaneously drive the print head, usually in the x-y plane and a separate motor for the perpendicular axis to that plane. Using two motors to drive a print head can increase the speed at which one can print but does come with additional complexity due to the arrangement of the belts. Additionally, CoreXY FDM 3D printers require more maintenance as their much longer belts can stretch more noticeably over time.

In bed-slinger-type cartesian 3D printers, the bed is moved along the y-axis and the hot end is moved in the x-z plane, as used in the extremely popular Creality Ender 3 and Prusa MK3. Bed-slinger machines are often the cheapest of all the FDM printers but suffer from issues related to the bed's swinging or 'slinging' back and forth. These issues are related to the print bed's weight and the print's weight, which increases over the duration of the print. The relatively large inertia of the bed can cause noticeable vibrations in the print job and can cause shifted layers and failed print jobs as the motor driving the bed fails to accelerate and decelerate a too-heavy bed. Additionally, the maximum print speed of a bed slinger is generally slower than an equivalent cartesian 3D printer that does not use a bed slinger design.

2.1.2.3.2. FDM extrusion

Two extrusion methods are typically used, depending on where the extruder is mounted. If the extruder assembly is mounted on the hot end, it is called a direct drive extruder. Direct drive extrusion is beneficial for controlling filament flow out of the hot end, but the added weight and inertia of the extruder on the hot end may cause artefacts in the printed parts. When the extruder assembly is mounted away from the hot end, typically on the frame of the printer, it is called a Bowden extruder. Mounting the extruder on the frame is done to limit the weight of the hot end, allowing faster printing and a reduction of artefacts related to the weight and inertia of the hot end. Still, some precision in controlling the filament flow out of the hot end is lost. In this setup, the extruder pushes the filament down a tube called a Bowden tube to the hot end. A comparison of these two extrusion methods is shown in Figure 6.

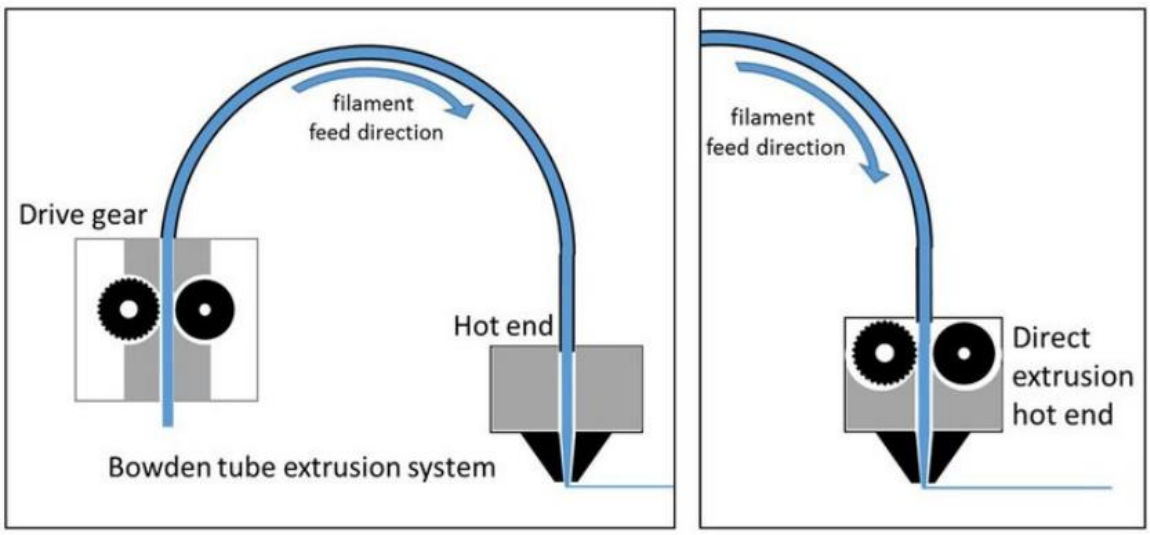

Figure 6: *Comparison of different methods of extrusion in FDM printers* [17]

Hybrid extrusion systems are also available where a master extruder is mounted to the frame while a smaller slave extruder is mounted to the hot end to try and capitalize on the benefits of both methods while minimizing the issues associated with both techniques. This method has not been broadly implemented due to the increased complexity of such a setup.

2.1.2.3.3. Pellet Extruders

This variant of FDM does not use thermoplastic filament but rather thermoplastic pellets, which are poured into a hopper above the hot end, where the molten plastic is extruded from the hot end. In every other way, a pellet extruder functions nearly identically to a regular FDM printer [18]. The hopper adds weight to the hot end assembly, reducing the speed at which a user can print, however the pellets are cheaper than filament rolls (which often made from pellets).

2.1.2.3.4. Paste Extruders

Paste extruders are similar to FDM, except the extruder is not pushing a thermoplastic filament into the hot end but instead pumping a paste through the nozzle that might or might not need to be heated, unlike an FDM hot end which requires heating to melt thermoplastics.

This technique is used when printing foods, ceramics or concretes [19][20][21]. Paste extruder applications can range from printing sculptures in sugar, chocolate or ceramics, among other materials, to even printing the walls of entire houses using concrete. Paste extruders are more scalable than other printing methods, allowing for printing larger objects in this context.

2.2. Embedded 3D printing development and use

2.2.1. Functionality of Embedded 3D printing

In embedded 3D printing, a print head equipped with a nozzle is moved to print an object, layer by layer, until the object is completed. This is similar to FDM 3D printing, but a liquid ink is extruded instead of a thermoplastic. The liquid ink is extruded into a gel support bath that holds the ink in place (see Figure 7), while the ink cures by several different means, depending on the ink used. Once the print job has been completed, the part can be removed from the gel or the excess gel can be dissolved, washed away, or cured to make the support gel part of the finished part.

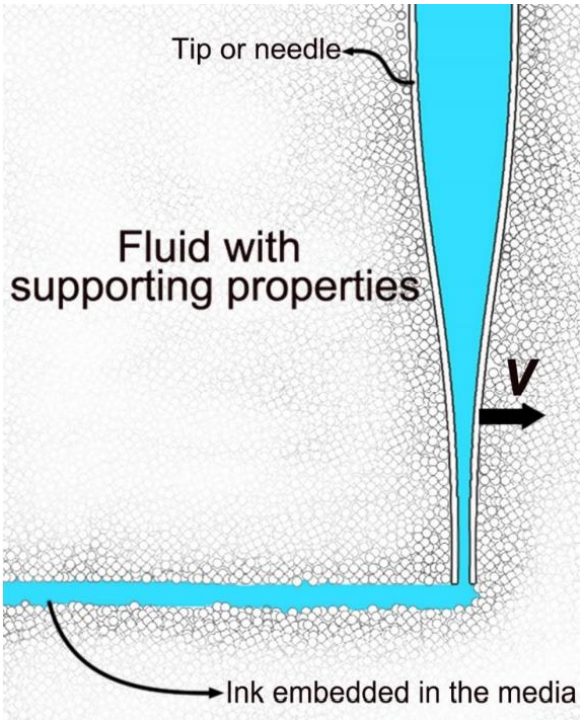

Figure 7: *In embedded 3D printing, a nozzle extrudes liquid ink into a support gel* [1]

The benefit of this method is that parts may be made using quite soft materials once solidified or materials that are liquids at room temperature. Additionally, this method does not need support for the printed parts since the part is printed entirely in a gel that supports it from every side (such as the powder in SLS 3D printing). These benefits allow the creation of parts that are impossible to make using any other manufacturing method. Embedded 3D printing can even print soft silicone parts, biomedical implants, or transplants [22].

2.2.2. Development of embedded 3D printing

In 2004, Gratson *et al.* wrote "Direct writing of three-dimensional webs" in the scientific journal, Nature [23]. This article was an important, early step in showing how one could use, in their words, a "three-axis micropositioning device" to sequentially build layered, patterned structures in a coagulation reservoir. Nine years later, in 2013, Mannoor *et al.* demonstrated a method of creating cybernetic implants in "A 3D Printed Bionic Ear", where they showed how one could use embedded 3D printing to create custom, cybernetically enhanced implants [24], shown in Figure 8.

Figure 8: *Cybernetic implant in a printed bionic ear* [24]

In 2015, Hinton *et al.* published a research article titled 'Three-dimensional printing of complex biological structures by freeform reversible embedding of suspended hydrogels' [25] wherein an additive manufacturing method called Freeform Reversible Embedding of Suspended Hydrogels (FRESH) was described and demonstrated.

Hinton *et al.*'s method used low-cost materials and components to emphasize the accessibility of this technology. The materials used were a gelatin mixture for the support gel and a sodium alginate mixture for the part material. The printer itself was a modified Printrbot Jr, which cost $400 at the time.

With the introduction of this variant of FDM printing with its benefit to the medical industry recently becoming more apparent with Hinton *et al.*'s paper and its low cost of entry, a flurry of research has been done to investigate different methods of extrusion and the viability of other materials as ink-support gel combinations.

2.2.3. Use cases for embedded 3D printing

Embedded 3D printing shows strong potential in soft robots, sensors, organ models and tissue engineering [1]. Each of these use cases gain unique advantages through embedded 3D printing that may not be attained using other methods of manufacture.

2.2.3.1. Embedded sensors and soft robots

The first instances using the words "embedded 3D printing" are related to sensors and soft robot 3D printing. Before this, the technique was referred to as "direct writing". Embedded 3D printing can be advantageous in strain sensor manufacturing, where conductive ink is printed in a model before curing, which can then be used to measure the strain the model experiences after printing [26]. Embedded sensors created in this manner may flex with the model and can measure internal strains to the part that a surface-mounted strain gauge may not measure. In this use case, the ink may remain liquid and the support gel cures and makes up the model with the ink trapped within it.

Similarly to embedding sensors in a model, a circuit may be embedded in a soft robot before curing using embedded 3D printing. These circuits can be biologically inspired. When creating soft robots, embedded 3D printing, lithography, moulding, and embedded 3D printing may be combined to make the robot, as shown in Wehner et al. [27]. Wehner printed an entirely soft robot, mimicking the form of an octopus, with the ability to move its tentacles without needing a hard circuit built into it.

2.2.3.2. Organ modelling and tissue engineering

An organ model is a part that accurately recreates the geometry of an organ, often for use in education, see Figure 9. Having a soft model that accurately recreates the external and internal geometry of an organ can be helpful to those studying medicine. It may be particularly useful to those preparing for a particular surgery as one could operate on the model, with the model including as much or as little detail as required [28].

When using embedded 3D printing for organ models, removing the support that the print is embedded within becomes essential. This is due to the part being made up by the ink material and the support gel not being necessary in the part after printing. As embedded printing progressed, development has driven the use of inks that can cure and support gels that can be removed after the print has been completed [28].

Extending the idea of creating organ models using embedded 3D printing makes those organs biocompatible to potentially act as transplants or implants. To this end, much research has been done in tissue engineering to create biocompatible bio-inks to be used as the inks to create embedded 3D prints that may be customised to a patient's individual needs [29][30]. Living cells may be kept alive through the printing process in these bio-inks and, once inserted in the patient, may multiply and assimilate with the patient's tissue. These living cells may be derived from the patient's material and, one may hope, avoid rejection from the patient's immune system.

Figure 9: *A model heart made using embedded 3D printing* [29]

The development of biomedical-embedded 3D printing is vital for those waiting for organ transplants. In the USA, in 2020 alone, nearly 6500 people were removed from the organ transplant list because they had died before receiving a transplant [31]. Biomedical-embedded 3D printing has the potential to save the lives of tens of thousands of people worldwide and improve the lives of many more.

A more niche use is to create cybernetically enhanced organs that may be implanted into an organism to augment their abilities [24]. Once tissue engineering coupled with embedded 3D printing gains more traction in research, cybernetic enhancement using embedded 3D printing may become a more popular field of study.

2.2.4. Support gel and ink requirements

Various materials are used in embedded 3D printing, with many more being investigated for suitability as support gels or inks for different applications. For this reason, this section will not be extensive. Still, it will give the reader an idea of the breadth of the materials used in embedded 3D printing and the correct pairing of support and inks for the different use cases for which an embedded 3D printer may be used.

In the early work on embedded 3D printing, Pluronic F127 was often used as a thermoreversible (a material whose properties can be reversed by heating) support gel [32] and is still widely used today in other areas of embedded 3D printing. Later, when the printing of sensors and flexible robots using embedded 3D printing was investigated, silicone thickener-based support gels became more popular [33]. An example of embedded 3D printing being used to create a soft robot is shown in Figure 10.

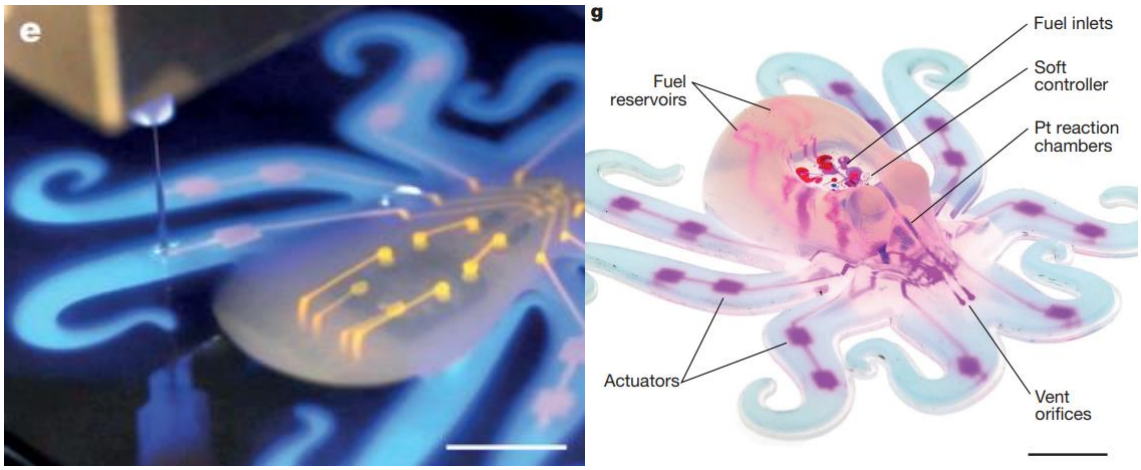

Figure 10: *A soft robot made using embedded 3D printing* [27]

In soft robots and sensors, the circuitry would be printed with conductive ink. Both the support gel and conductive ink would then be cured together. The support gel could have been made with polyacrylamide (PAAm) as a rheological modifier and polydimethylsiloxane (PDMS) due to its optical and electrical properties[27].

In tissue engineering and creating organ models, the ink must be biocompatible while having a non-trivial combination of flow, thermal and mechanical properties. The appropriate pairing of support gel and ink is also needed to achieve the correct characteristics in the finished part with sufficient detail. If the pairing of the materials is not done well, then necessary features may be lost, the part may not cure in the support gel sufficiently, or living cells in a bio-ink may die due to the environment provided by the support gel not being appropriate. For tissue engineering applications, the combination of bio-ink and support gel is often a bespoke arrangement to meet complex requirements[34].

2.2.5. Influencing factors in embedded 3D printing

2.2.5.1. Gel selection

When printing using the embedded 3D printing technique, the support gel is pushed aside when the ink deposition needle moves through the gel and ink is deposited. After this, the support gel must almost immediately return to the evacuated space and trap the recently deposited ink. The supported gel should generally not move except for the volume immediately around the ink deposition needle.

With this in mind, a gel with a well-defined yield stress works well. This yield stress is the point below which the gel acts more like a solid, and above the yield strength, the gel flows like a fluid. The yield strength of the support gel limits the stirring in the gel and helps maintain the quality of the already printed part [25].

It is then vital to make the ink-gel pairing such that they resist diffusing and dissolving. Over time, this would negatively affect the quality of the printed part as the ink dissolves into the surrounding gel instead of the part being distinct from the support gel [35].

Depending on the materials used and the desired characteristics of the printed part, some consideration needs to be made regarding how the part needs to be solidified. For example, if UV light needs to be used to cure just the ink, it would be advisable to use transparent support gel. If the ink requires a chemical reaction to solidify, a support gel can be created that enables that reaction to occur when the ink is deposited in the support bath. If the support gel is all that is needed to cure, and the ink may stay liquid or solidify over time without any intervention, then consideration should be given to a gel that the user can cure without affecting the ink embedded within [36].

2.2.5.2. Ink deposition needle geometry

A significant issue is the limits in the size of embedded 3D prints. Most 3D printers have a well-defined build volume within which an object may be 3D printed. This build volume is the maximum dimensions a 3D printer can produce within. On top of this, support gels often need a container to hold them because they are not viscous enough to hold their shape when unconstrained. This container will likely be much smaller than the total build volume of the 3D printer [37]. The container (which already limits the x, y and z dimensions of the 3D printed object) is usually filled before the time with support gel. The selected ink deposition needle must be as long or longer than the part's total z-height to print in this volume [38]. A long needle, however, has other problems like deflection issues, disturbing the gel more, more significant pressure drops across the needle and a greater likelihood of the needle clogging during regular printing [37].

When the needle travels through the support gel, it will experience viscous drag forces, as shown in Figure 11. The needle can be considered a cantilever beam with a distributed load over the submerged length of the needle. The viscous drag forces increase proportionally with the depth of the needle being submerged, and the deflection increases by the fourth power of that length [39]. Large deflections due to excessively long or delicate needles can result in inaccuracies in the final printed object [38].

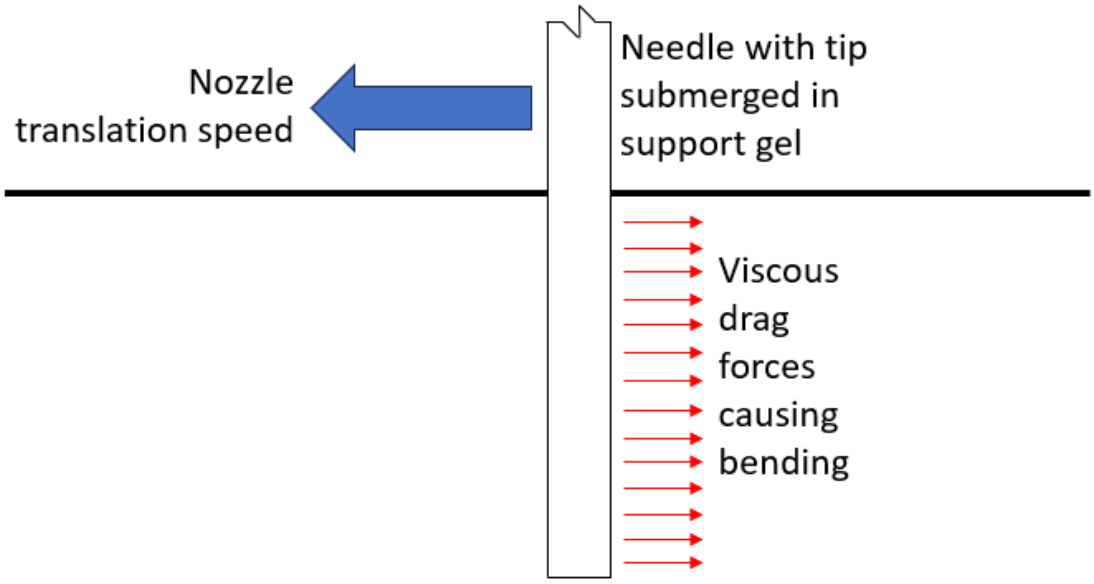

Figure 11: *Viscous drag forces experienced while the needle translates through the support gel*

Combatting deflection by making the needle thicker also comes with its issues. As the needle's outer diameter increases, more drag is experienced by the needle, causing more disturbances in the support gel, which can lead to reduced part quality as the support gel becomes stirred by the needle travelling through it [40].

With this all in mind, one should balance the needle length such that the needle is not so long as to risk issues with deflection but not so short that the support gel may not properly support the print. Additionally, one should balance the needle diameter so that the needle is strong enough to resist deflections adequately but not so thick that it disturbs the part in the support gel.

2.2.5.3. Print speed, extrusion rate and pressure

Focussing now on disturbances, an FDM bed-slinger-based embedded 3D printer could cause issues by disturbing the printed part while it is being printed as the entire support bath is moved backwards and forwards along the x or y axis, possibly causing the support gel to slosh along with the bed. The increased weight of a support volume of gel also has a practical limit on how large the support volume can be since a single stepper motor will likely be responsible for accurately moving and stopping that weight.

When printing in a support gel, it is essential not to disturb the gel that is not immediately needed to trap recently deposited ink. Excessively high print speeds can cause the needle to disturb large parts of the support bath, ruining the quality of the printed part [40].

Inconsistent line width, the diameter of printed material, can also be seen often in embedded 3D printing. The variations in line width can be caused by a mismatch in the ink-gel pairing where the ink is not trapped well by the gel and allowed to run or form droplets [2]. It can also be caused by an extrusion pump that does not evenly apply pressure to the fluid being pumped, as shown in something like a peristaltic pump [41]. This can be seen as inconsistent ink lines in the gel instead of cleanly printed ink lines.

Even if the ink-gel pairing is good, part quality depends on the balance between print speed, extrusion rate, and pressure. When printing too fast, significant disturbances can be caused by the forces applied to the support gel [28], sloshing the volume around and likely causing inconsistent extrusion as the ink pumping mechanisms produce insufficient extrusion pressure or flow rate.

Noting the factors relating to print speed, extrusion rate and pressure, it is important to select a printer motion system and an ink deposition pump appropriate for the use in embedded 3D printing, such that the material may be deposited at a reasonable rate using a system that does not cause disturbances in the printed part.

2.2.5.3.1. Needle extrusion pressure

Pressure must be applied to extrude ink through the needle. The required amount of pressure can be determined using the Hagen-Poiseuille equation [42]:

$$\Delta p = \frac{8\mu L Q}{\pi R^4} \tag{2-1}$$

Where Δp is the pressure difference across the needle, μ is the dynamic viscosity of the ink, L is the length of the needle, and R is the internal diameter of the needle.

If the pressure is too high, at best, the motor driving the pumping assembly will skip, and some minor defects will appear in the printed part. At worst, permanent damage to the pumping assembly will be done.

2.2.5.4. Temperature of extrusion

The gel or ink temperature will affect the viscosity of the printed fluid, and its importance in embedded printing depends on the ink-gel pairing [43]. A supported gel that is too cool may not properly trap the ink embedded within it, as the higher viscosity of the gel slows the closure of the needle path. If it is too warm, the gel may not hold the ink well enough and allow it to flow within it. It may also be susceptible to turbulence as it becomes more liquid-like than gel-like.

If the ink is too cool, it could cause inconsistencies or blockage during printing. If the ink is too warm, it could cause the ink to leak out of the nozzle when the ink should not be printing, affecting the quality of the printed object. Temperature becomes even more crucial when printing with inks containing living cells or needing to cure in the support gel. Living cells require specific conditions to be provided by the support gel [44][29]. The same goes for inks that need particular conditions to cure or need that curing to be delayed until after being printed [28].

2.2.5.5. Instabilities of embedded 3D printing

Four main instabilities have been identified that occur in embedded 3D printing. These are illustrated in Figure 12.

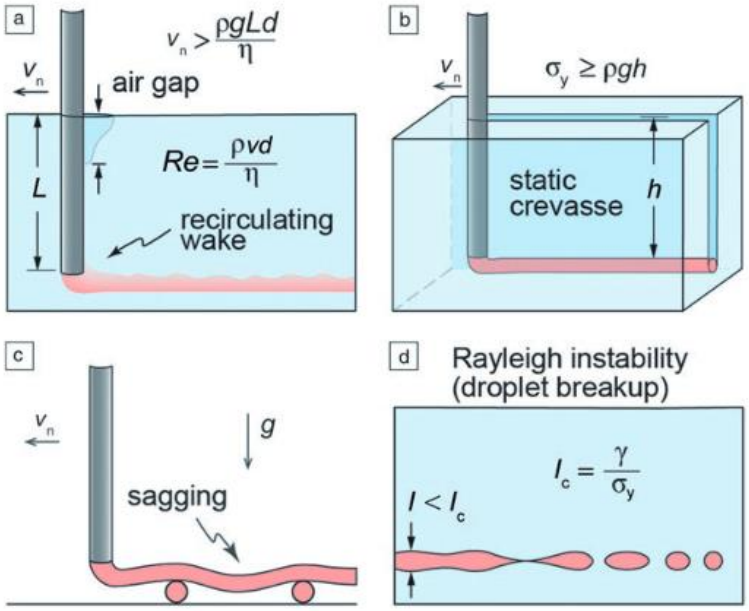

Figure 12: *Four different ways instabilities may occur in embedded 3D printing. The first instability, 'a', is called recirculation wake, 'b' is static crevasse, 'c' is sagging and 'd' is droplet breakup* [40]

2.2.5.5.1. Recirculating wake

When the ink needle is translating through the support gel, a region of instability can form behind the needle, which is described by Equation 2-2 [40]:

$$v_n > \frac{\rho g L d}{\eta} \tag{2-2}$$

Where v_n is the nozzle translation speed, ρ is the density of the support material, g is gravitational acceleration, L is the submerged needle length in the support material, d is the diameter of the needle, η is the dynamic viscosity of the support material.

When trying to print at higher needle translation velocities, it becomes crucial to manage these instabilities since they will affect the quality of the printed part. One may print with lower-diameter needles or higher-viscosity support materials to avoid instabilities at higher speeds.

For this work, the following formula can be used to determine the minimum allowable printing depth of support gel required to avoid instabilities:

$$L < \frac{v_n \eta}{\rho g d} \tag{2-3}$$

2.2.5.5.2. Support gel crevasse formation

A crevasse will appear behind the translating needle, with its depth being determined by hydrostatic pressure and the support material's yield stress [40] as defined by Equation 2-4.

$$\sigma_y \geq \rho g h \tag{2-4}$$

Where σ_y is the support material's yield stress, ρ is the support material's density, g is the gravitational acceleration, and h is the height of the crevasse.

To avoid the static crevasse affecting the printed part, one must print at a depth greater than the height determined by the following relation derived from Equation 2-4:

$$h = \frac{\sigma_y}{\rho g} \tag{2-5}$$

2.2.5.5.3. Sag due to gravity

Sag can be caused by gravity, even in embedded printing, which is specifically designed to manage sag. To prevent sag, match the density of the support gel and the printed ink as closely as possible[40]. Another method to prevent sag is to print on a sacrificial structure, similar to what is seen in FDM printing[1].

2.2.5.5.4. Interfacial tension driven droplet breakup

When interfacial tension between the support material and printed ink is too great, it may break up continuous printed features into droplets. This breakup happens when the feature diameter is smaller than the critical diameter described in Equation 2-6 [40]:

$$I_c = \frac{\gamma}{\sigma_y} \tag{2-6}$$

Where I_c is the critical feature diameter, γ is the interfacial tension between the support material and the printed ink, and σ_y is the yield stress of the support material.

When droplet breakup of printed features occurs, the rate of ink extrusion should be increased to increase the feature size, the interfacial tension between the support material and the printed ink should be reduced, or the yield stress of the support material should be increased.

3. Prototype requirements and constraints

As has been previously discussed, there are several requirements that the prototype must meet. This chapter will outline these and the approach to evaluate the efficacy of the solutions and the system as a whole.

3.1. Firmware

Per the constraints outlined in the Introduction, the author is not expected to create firmware specific to this project. Instead, an existing 3D printer firmware should be adapted for this project.

This project requires that the firmware have the following functionality:

- Easy, fully functional user configuration
- Cold extrusion
- Tool changing

Iterative user configuration is essential for this project. Editing the configuration of the 3D printer in firmware without reflashing will expedite the testing of those edits.

Cold extrusion refers to extruding at or below room temperature in 3D printing. Since the extruded materials may already be liquid at room temperature, allowing cold extrusion is essential, but many 3D printers have safeguards against printing below temperatures that would liquefy plastic.

Tool changing support in firmware will be necessary since the printer must extrude ink and gel. The materials used as inks typically have different properties from gels, and other "tools" will be needed to print them.

3.2. Motion system

Per the constraints, the author will not need to create their own motion system. An existing 3D printer may be used as a base on which to build the functionality of an embedded printer, an example of a previous attempt in work done elsewhere is shown in Figure 13. The motion system further needs to be able to move the mass of the toolhead or multiple toolheads at a reasonable printing speed. The motion system should have an x, y and z axis, with all the axes allowed to have minimum and maximum limits.

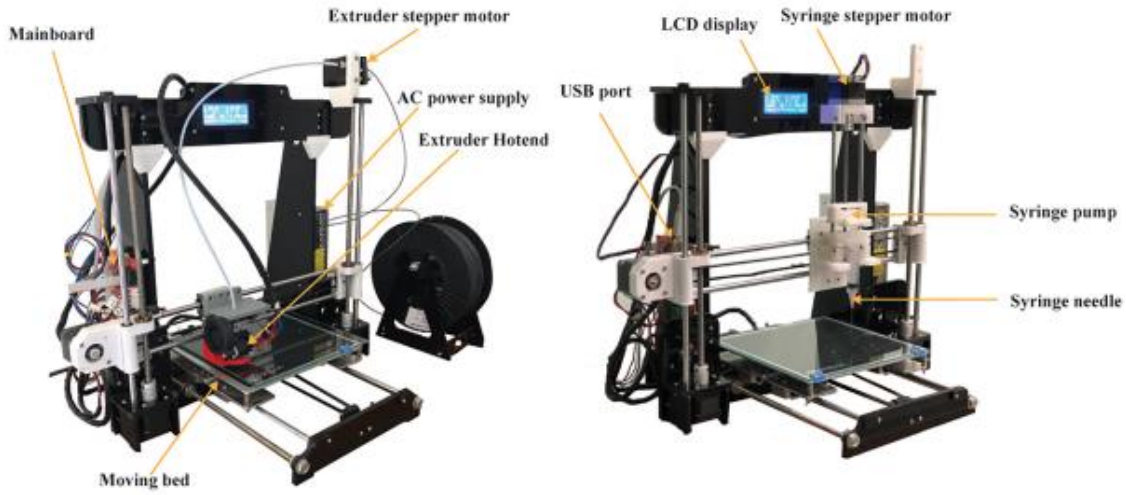

Figure 13: *The conversion of an FDM printer to an embedded 3D printer* [45]

The motion system should be able to move a toolhead at an accuracy equivalent to other consumer-level 3D printers. The Creality Ender 3 was identified as a suitable example of a consumer-level 3D printer. Its motion system typically uses NEMA 17 stepper motors and 20-toothed GT2 pulleys [46]. A motion system that reasonably matches or exceeds this requirement should work well for this project.

3.3. Ink-gel dual extrusion

To achieve an increase in the size of the printed parts achievable by embedded 3D printing without increasing the length of the ink needle, consideration was given to printing a support bath as needed to ensure the ink is always printing in ample support gel. The different ways this could be achieved are described in Section 3.3.1.

3.3.1. Tool changing methods

One may consider manually adding gel as needed throughout a print. Considering that longer FDM 3D prints can take well over 8 hours to complete larger jobs, this is not feasible. Continual application of gel needs to be via an automated process.

In FDM 3D printing, this is called "tool changing". It is called "tool changing" because the software and firmware that 3D printers use see different extruders (motor-driven mechanisms for extruding material) as "tools". This "tool changing" is then used to control the process of switching from one tool to another, conceptually similar to automatic tool changers seen in CNC mills. There are numerous ways this is done in 3D printers, as shown in Figure 14:

1. Tool Changer – The toolheads sit ready to the side of the print volume, and as needed, the print head automatically swaps out the entire toolhead.
2. Switching head – The toolheads are attached to the same mounting plate, and the printer swaps between them as needed.
3. Mixing head – Most of the hardware is shared between the toolheads, except the motors driving the extruded material.
4. Dual Extruder – Two toolheads are attached to the same mounting plate. In this case, both heads can work at the same time.
5. Independent Dual Extrusion – Two toolheads are attached to the same gantry. The two heads can move independently of one another on a single axis.
6. Recoating Blade – A blade or arm that spreads new material over the top of the existing build volume. Recoating blades are used in SLS 3D printing.
7. Reservoir Feed – A valve or gate is opened or closed as needed, or gravity pulls the material from a reservoir as material is depleted in the bath. This technique is sometimes used in SLA and DLP 3D printing.

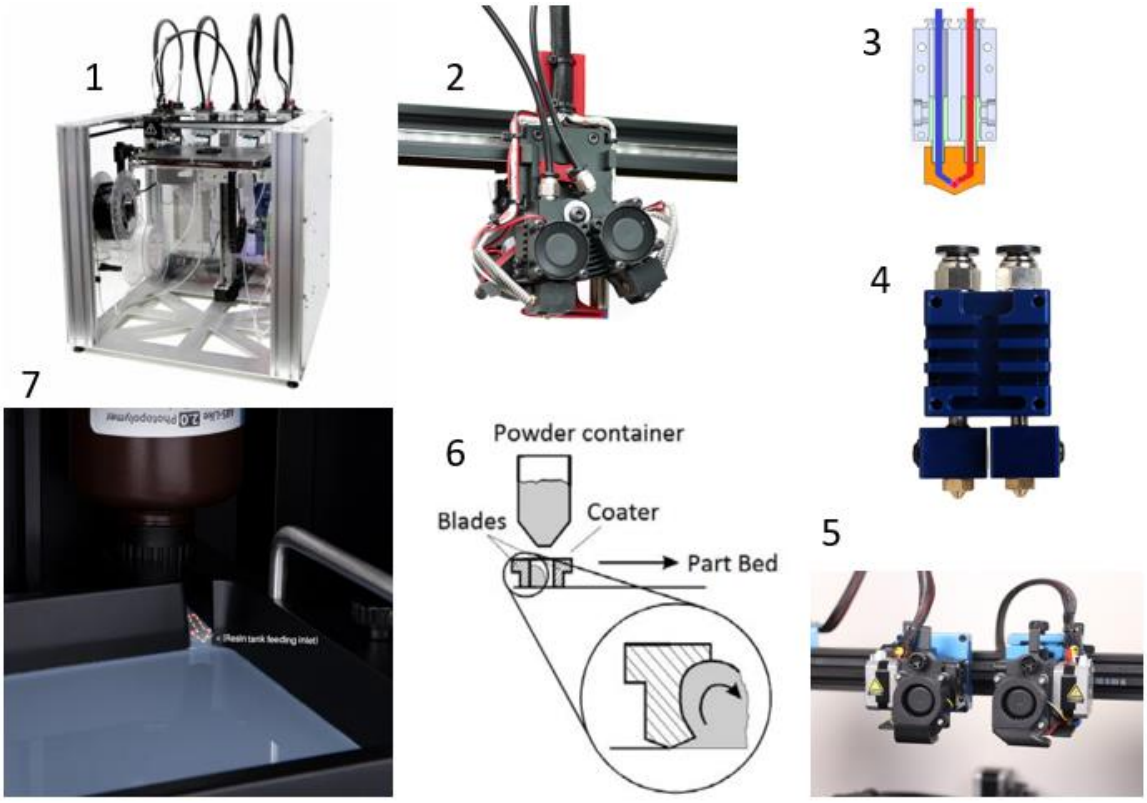

Figure 14: *A collection of dual extrusion methods. 1 is a tool changer* [47]*, 2 is a switching head* [48]*, 3 is a mixing head* [49]*, 4 is a dual extruder* [50]*, 5 is an independent dual extruder* [51]*, 6 is a recoating blade* [52] *and 7 is a reservoir feed* [53]

Knowing these are all possible options, one should then start to consider what other requirements will be required of the solution:

- Toolhead weight – Increased toolhead weight slows printing speeds and decreases part quality.
- Compactness – The solution should be compact within the print volume to make more volume available for printing.
- Mechanical simplicity – The simpler the solution, the lower the likelihood of mechanical issues or more expensive or specialised workshop work required.
- Cost – If possible, the tool changing mechanism should be low-cost to stay within this project's scope.
- Ease of configuration – Configuration of the firmware should not require significant edits to the basic functionality of the firmware to keep within the scope of this project.
- Ink extrusion quality – This project aims to reproduce parts similar to previous works with embedded printers.
- Gel extrusion quality – Quality gel extrusions are required to avoid malformed ink parts being constructed within that gel.
- Likelihood of voids – If the ink or gel has voids, the quality of printed parts will suffer.
- Tool change speed – Inks and gels used in embedded 3D printing may remain liquid for a limited time, ensuring quick tool change speeds can guarantee more productivity.

- Flexibility – A variety of materials may be printed using an embedded printer. Some flexibility in the tools' ability to extrude multiple different materials is desirable.

Typically, in these tool change systems, an additional requirement is needed for the firmware and the control boards to accommodate the extra sensors and motors required by these systems. A control board should be selected to enable interaction with these additional electronics. To this end, 3D printer microcontroller boards with the ability to control two or more print heads should be considered or the use of software and firmware that may use additional microcontrollers in parallel with one another.

3.3.2. Pumping methods

The pumping mechanisms directly control the material flow rate during the extrusion process in embedded 3D printing. Listed below and shown in Figure 15 is a summary of a few options with some positives and negatives:

1. Centrifugal pump – High flow rate but less precise control of flow rate.
2. Diaphragm pump – Good overall accuracy but complex and flow pulsates.
3. Gear pump – Compact and simple design, low pulsation, but requires precise manufacturing.
4. Peristaltic pump – Similar to the diaphragm pump, it has good accuracy but flow pulsates.
5. Lobe pump – Similar to gear pump, but more complex than gear pump, with lower pulsations.
6. Piston pump – Precise and consistent but generally low flow rate.

Figure 15: *Some varieties of pumps that may be used in an embedded 3D printer. 1 is a centrifugal pump, 2 is a diaphragm pump, 3 is a gear pump, 4 is a peristaltic pump, 5 is a lobe pump and 6 is a piston pump* [54]

Any pump used in this project should be relatively:

- Low cost to manufacture or acquire
- Low complexity
- Able to pump small amounts of material accurately and consistently

Gel extrusion may have different requirements, like a higher flow rate and lower consistency than ink extrusion. With this in mind, the ink-pumping extrusion method may differ from the gel-pumping extrusion method.

A piston pump has been shown to perform well in terms of depositing ink on demand [55][37][45]. These generally work by using a NEMA17 motor to turn a threaded rod where rotational movement may be used to cause linear movement of a syringe plunger, forming a syringe pump. This form of a piston pump appears to be well understood in this application and will continue to be used in this project for the ink deposition system.

3.3.3. Ink deposition system

The volumetric flow rate of the material and the translation speed of the components responsible for the deposition of the extruded material are related to one another; as the translation speed increases, generally, the required flow rate of printed material increases, and vice versa. One can then return to consumer FDM printers to inform them of a target translation speed. Consumer-level 3D printers typically have a nozzle translation speed of 10-100 mm/s. Hinton *et al.* aimed for a typical speed of 20 mm/s [35]. 20 mm/s is well within the normal capabilities of consumer-level FDM 3D printers, requiring no new developments outside the print speed suggestions made in Section 4.11. This range of translation speeds can inform the volumetric flow rate once the extrusion apparatus was selected.

The detail required can be determined from previous works based on consumer 3D printers. In the 2016 paper by Hinton *et al.*, they used 0.14, 0.28 and 0.4 mm needles on their syringe pump to print PDMS inks [35]. This range of nozzle diameters is comparable to those used in consumer-level FDM 3D printers.

3.3.4. Gel deposition system

When extruding gels, the resolution requires far less refinement since the gel is only needed to support the printed part and will most likely be discarded afterwards. It is for this reason that the mechanism that delivers the gel must chiefly deposit in such a way as to minimise air bubble entrapment in the gel and consistency in the layers. Air bubbles should be avoided since they can be voids that recently printed ink may flow into, degrading the final part quality. The consistency of gel extrusion should be maintained to prevent the recirculation wake and crevasse formation instabilities mentioned previously.

The use of a syringe pump, like what has been used before [30][37][45], requires the gel deposition system to be able to work in tandem with and around the ink deposition system as well as the ink syringe pump.

4. Design decisions

Decisions can be taken on how best to design the prototype using the knowledge from Chapter 2 and the requirements and constraints in Chapter 3. This was an iterative process whereby the initial decisions were often augmented by the results generated in Chapter 6. This chapter begins by selecting an ink, gel and printer. A printer firmware and an appropriate microcontroller were then chosen for this use case.

Testing was then done with the Replistruder [3] extruder, developed by Hinton et al., to inform further design decisions. Having put together an embedded printer using the Replistruder, decisions were made to build an ink-gel dual extruder prototype. Finally, the instabilities detailed in Section 2.2.5.5 were considered and integrated into the decisions made.

4.1. Ink selection

There are a variety of inks available for use in embedded 3D printing. It becomes essential then to list some requirements to reduce the number of available options. The following requirements were identified:

- Good pairing with the selected gel
- Readily available at low cost
- No need to support living cells

With this all in mind, the bio-inks like alginate, collagen and GelMA could be ruled out since there is no need to support living cells as a part of this project. That leaves the synthetic gels, of which the choices are epoxies, photoresists, silicones and urethanes as shown in Figure 16. From previous work done at the University of Cape Town done by Brinkley [2], Ecoflex 00-30 is available for use in this project. Matching this with an appropriate support gel will satisfy the requirements listed above. One should note that some safety precautions should be taken when handling uncured Ecoflex 00-30.

Noting the safety concerns surrounding handling potentially hazardous substances, it was prudent to also use another liquid ink material during the testing stages of this project. This ink would not be required to be able to cure like Ecoflex 00-30 but should resist dissolving or diffusing into the support gel.

Some success has been seen using custard as a makeshift ink in other work done at the University of Cape Town during the testing stages of other embedded 3D printing projects. A similar approach was followed for this project.

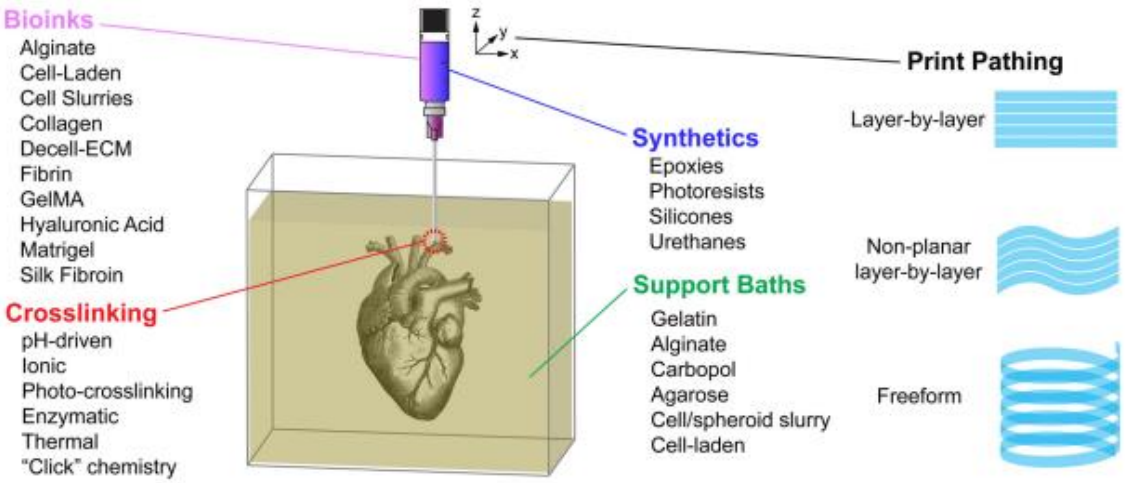

Figure 16: *Several combinations of inks and gels can be paired with varying results for use in embedded 3D printing* [56]

4.2. Gel selection

With an appropriate ink selected, gel selection can be somewhat easier. The gel's requirements are similar to the list of requirements provided for the ink selection, taking care now to ensure that a good pairing is made with the selected ink.

Referring to Section 2.2.5.1, a gel that resists defusing with Ecoflex 00-30 should be selected. Additionally, the gel is not required to support living material, allow UV curing or participate in a chemical reaction. Carbopol 1342 has been paired with Ecoflex 00-30 in previous work done by Brinkley [2], although with limited success. More success has been seen with Carbopol 940 [35], and thus, the project aim was to acquire that Carbopol or a similar hydrogel instead.

4.3. Printer selection

Several consumer-level 3D printers have been used as a base on which to build embedded 3D printers in other embedded 3D printing projects. All of the 3D printers adapted to become embedded 3D printers that the author knows of are FDM 3D printers, owing to the similarities of the hardware used between FDM and embedded 3D printers. Various printer brands have been used in other embedded 3D printing projects including Prusa, Creality and Makerbot. A selection of Creality 3D printers was already available for this project at the University of Cape Town.

A Creality Ender 5 was selected for its application in this project because of its motion system. It uses a modified cartesian motion system, with a single motor responsible for motion per axis. NEMA 17 motors drive the x, y and z axes with 200 steps per revolution. The x and y axes are belt driven around 20-tooth GT2 pulleys, and the z-axis uses an 8 mm lead screw. These specifications are similar, if not the same, as the Creality Ender 3 on which the resolution requirements were based, see Section 3.2. An example of an Ender 3 and an Ender 5 are shown in Figure 17.

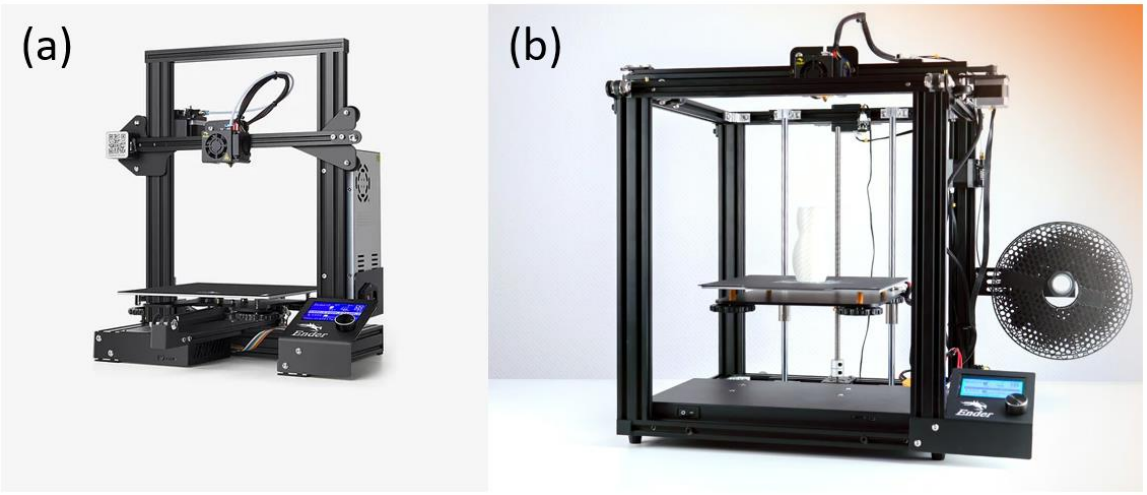

Figure 17: *The Creality Ender 3 (a)* [57] *and the Creality Ender 5 (b)* [58].

The Ender 5 differs from the Ender 3 because the bed moves up and down along the z-axis instead of back and forth along the y-axis like the Ender 3. Moving the bed along the z-axis prevents sloshing of the support gel, which could influence the quality of the printed part. This sloshing has been noted by Zhao *et al.* in their decision to use an H-bot motion system, which, like the Ender 5, only moves the bed along the z-axis [28].

4.4. Firmware

Several firmware solutions, like Klipper, Marlin, and Repetier, work well for FDM 3D printing. The author has experience working with FDM 3D printer firmware, including configuring Marlin and Klipper-based systems. An argument could be made for several firmware solutions to be adapted for use in embedded 3D printing and can be heavily swayed by preference. With this in mind, Klipper has been selected for this project.

Klipper has some benefits but also some drawbacks:

Benefits:

- It is an easy-to-use web interface for interacting with the printer.
- It supports an extensive range of hardware.
- Configuration edits can be done quickly without re-flashing the microcontroller.
- Offloads processing to an external Linux-based computer.

Drawbacks:

- Initial setup and configuration can be challenging.
- Requires another Linux-based computer, increasing cost and complexity.

Marlin is similarly capable, but configuration edits do require re-flashing the microcontroller. Re-flashing would slow development, but ultimately, if a user were to switch to Marlin or another competent firmware solution, with foreknowledge of how to configure that firmware, they would likely be able to create a similarly capable embedded 3D printer.

4.5. Microcontroller

Knowing the firmware selected, one may begin selecting a microcontroller board that supports that firmware based on the processor of the microcontroller board. Happily, dozens of processors are supplied by several brands [59].

Knowing that many options for a microcontroller may work with Klipper leaves the requirement for a board that may support tool change functions. This includes needing five or more stepper driver slots, 3 for the X, Y and Z motion axes and a motor for each required pump/extruder. Some systems do have the ability to use one extruder motor that is shared between all the extruders, but they are rare, experimental and require complexity outside the scope of this project. Another motor will likely be needed for the tool change functionality, although this may also be done without stepper motors [60]. The author was already familiar with the microcontroller offerings from BigTreeTech (BTT), having used them in some previous 3D printing-related projects.

Several offerings in BTT's catalogue would work, but ultimately, the BTT SKR Pro Control Board was chosen since it had six stepper motor driver slots and support for up to three print heads [61]. Having six stepper motor slots gave some peace of mind, which paid off throughout this project. It is recommended when trying to replicate the prototype built that one should aim to have at least six stepper motor driver slots if one wants to avoid buying more than one board and running them in parallel, which can also be easily done using Klipper. The SKR Pro board also supports using a display, which was helpful during all project stages involving the embedded 3D printer.

The user typically can choose from a number of appropriate stepper motor drivers and install them into sockets on the microcontroller board. TMC2209 stepper motor drivers are ubiquitous throughout the consumer 3D printing market and are compatible with Klipper and the SKR Pro board [61]. For these reasons, they were selected for this project.

4.6. Replistruder testing

A modified Replistruder v5 extruder [3] was investigated in the initial stages of the project. An investigation of the performance of the Replistruder was done to inform the design of the extruder used later in the project. The Replistruder is a proven extruder used in embedded 3D printers where a syringe plunger is depressed by a screw driven by a NEMA17 motor to extrude ink out of the syringe needle. The modified Replistruder is shown mounted on the Ender 5 in Figure 18. An initial print test is shown in Figure 19.

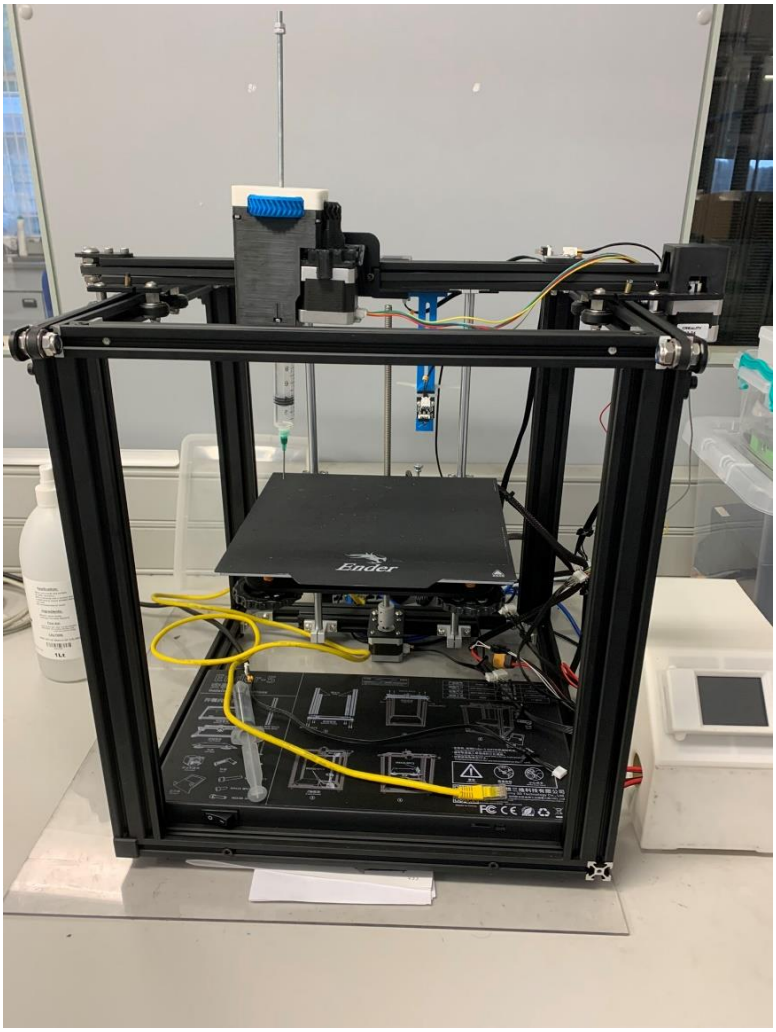

Figure 18: *The Creality Ender 5 in the BISRU Laboratory with the Replistruder v5 print head attached.*

The modifications were mainly done to make the extruder compatible with metric hardware, to accommodate 20 cc syringes, and to mount the design to the Creality Ender 5 toolhead carriage in place of the original tool. Otherwise, little was done to change the core functionality of the Replistruder extruder.

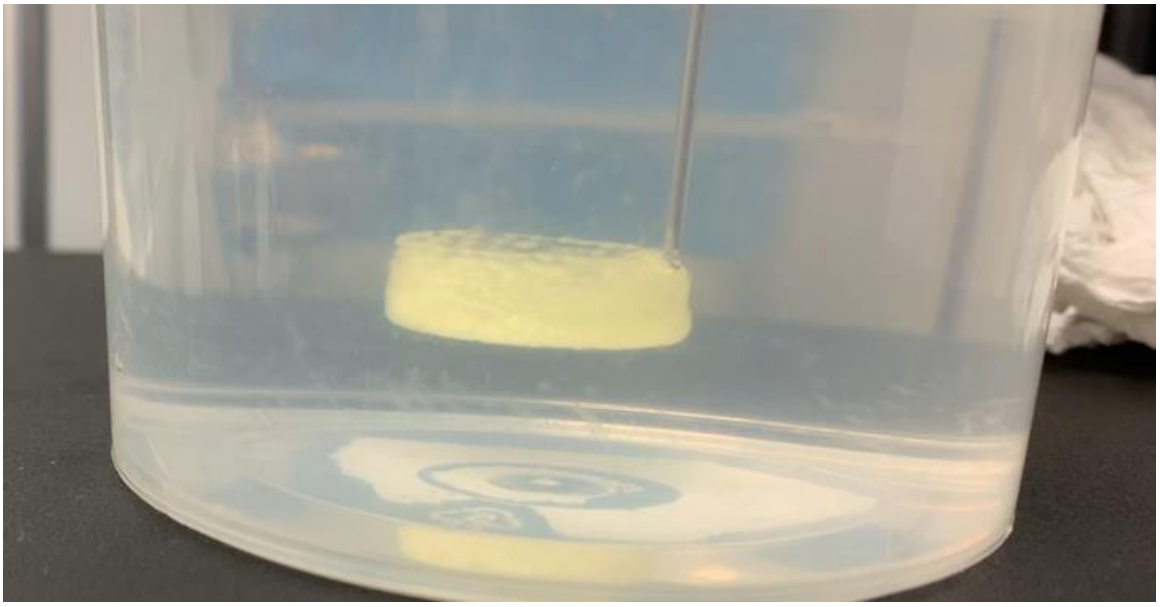

Figure 19: *Part being printed by the Replistruder Extruder on the Ender 5 using custard.*

Using the modified Replistruder extruder allowed the beginning of the development of much of the software configuration of the printer. Another essential aspect of testing the Replistruder design was troubleshooting hardware issues before compounding them with a new toolhead design. Issues such as microcontroller configuration, Klipper firmware refinements, and extending wiring for the new extruder motor locations were resolved while testing the Replistruder syringe pump. The Department of Electrical Engineering at the University of Cape Town aided in the troubleshooting of the often confusing faults related to the end-stops and motor wiring, which were discovered to be more sensitive to wiring faults and interference than initially thought.

Some other important lessons were how vital avoiding some of the instabilities can be to print quality. These initial tests used custard as a substitute printed ink, rather than a silicon ink, in a support bath of 3 g/l Carbopol gel. As custard's "pot life" at room temperature is many times greater than any silicon ink, it allowed for a less rushed system preparation while learning the various controls. The custard was less dense than the gel, which caused it to float upwards over the print. The already printed part would then collide with the needle as it was depositing the next layer of custard, negatively affecting the printed part's quality. This instability is shown in Figure 20.

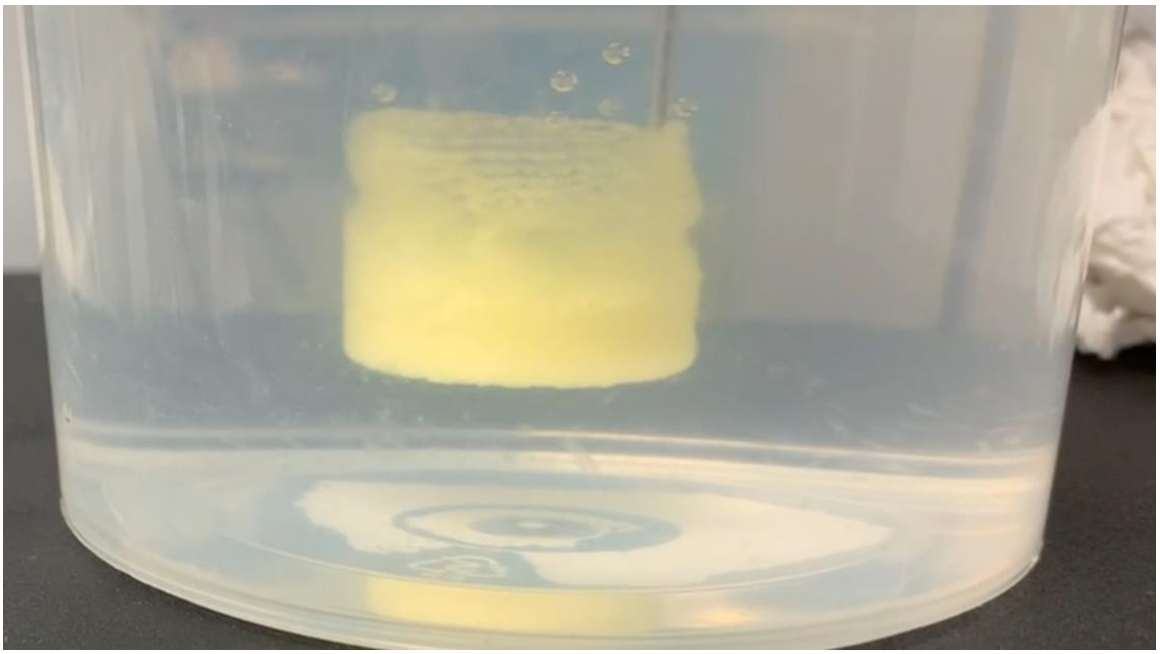

Figure 20: *Parts being printed using custard in Carbopol 980 can show poor printing quality as the custard floats upwards to the needle.*

4.7. Dual-Extrusion design

In Section 3.3.1, seven options were listed for tool changers to switch from ink-mode extrusion to gel-mode extrusion. A comparison can be made of the toolhead weight, compactness, mechanical simplicity, cost, ease of configuration, extrusion quality of the ink and gel, likelihood of bubbles, tool change speed and flexibility of each tool changer methodology to aid in the selection. This comparison is made in Table 1.

Table 1: *Comparing different dual extrusion designs using a number of variables with a focus on the suitability of printing inks and gels. Scores or ranking given were between one (best property) and seven (worst).*

	Toolhead weight	Compactness	Mechanical simplicity	Cost	Ease of configuration	Ink Extrusion quality	Gel Extrusion quality	Likelihood of voids	Tool change speed	Flexibility	Total
Tool changer	2	7	7	7	7	1	1	1	5	1	39
Switching head	4	2	3	3	4	3	3	4	2	4	32
Mixing head	3	3	2	2	2	7	7	5	1	7	39
Dual extruder	6	4	4	5	3	5	4	3	3	3	40
Independent dual extruder	7	5	5	6	5	4	2	2	4	2	42
Recoating blade	5	6	6	4	6	2	6	6	6	5	52
Reservoir feed	1	1	1	1	1	6	5	7	7	6	36

Each compared property of the tool changing method was ranked from one to seven in Table 1, with one being the best and seven being the worst. The "Total" column shows the total of each tool changer ranked, with the lowest total being best. The switching head tool change method scored best and was used for the tool changing method in the project.

The switching head design has some benefits that helped in this comparison. A switching head can be very compact inside the build volume. It also has the advantage of rapid tool changing since both tools are already on the same carriage. It reduces the tool changing operation to one very short move instead of an operation where, like the tool changer or independent dual extruder, the other tool must make a large move to be in place.

It does, however, come with a significant drawback, namely the toolhead weight. Since the switching hardware is on the same carriage, it will limit the maximum nozzle translation rate compared to designs using a tool changer or reservoir feed, which keeps the other tools off the carriage and any gantries that move. The design must keep the total weight within reason to maintain the nozzle translation speed in the 10-100 mm/s range as outlined in Section 3.3.3.

Switching toolheads work by moving one tool into place while moving others out of the way. This differentiates switching toolheads from dual extruders, where each tool is adjacent to the other on the same carriage, and the entire carriage moves along the x or y-axis, reducing the maximum build volume available to dual extruders. The switching toolhead achieves tool changing by rotating the carriage or linearly moving the tools relative to the other tools on the head along the z-axis, as is shown in Figure 21. If the tools are only kept adjacent on switching head designs, dual extruder and switching head designs have nearly the same profiles on the gantry, and the switching head will similarly reduce the maximum build volume.

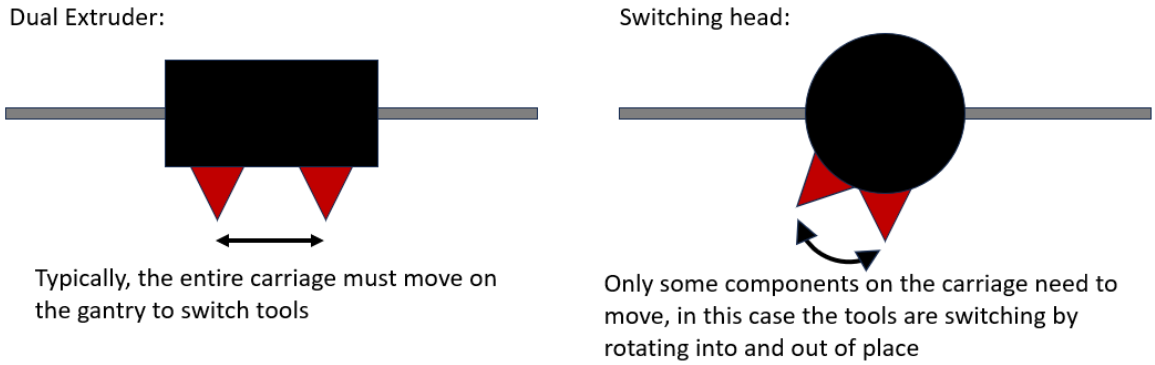

Figure 21: *Some differences in tool changing between dual extruders and switching head tool changers.*

Since the resolution of the gel extrusion compared to the ink extrusion is so low, the gel nozzle may be large enough to be coaxial with the ink needle. This comes with several benefits:

- Both nozzles being coaxial instead of taking up their separate volumes makes the overall design more compact.
- Coaxial nozzles may allow shared hardware related to motion, reducing weight.
- Complexity in configuration is reduced since only one small linear move can be used for a tool change to occur.

Switching between the ink and gel extrusion modes will be handled by Klipper macros, which are detailed in Appendix C.2. These macros will be triggered by some lines of code inserted by the Python script shown in Appendix C.3. This will automatically switch between the modes as needed during the print job and allow a user to switch between the modes on command, as well as automatically perform several operations required during 3D printing.

The developed tool change system uses a motor driving a sheathed cable that pulls the coaxial gel nozzle up into a sealed position for the ink extrusion mode, as shown in Figure 22. A tension spring was used to pull the gel nozzle back down, allowing the motor to release a specified length of cable, which would return the coaxial gel nozzle to an open position and change to the gel extrusion mode. The motor used in this application was a NEMA17 stepper motor, and the cable was a 1.1 mm sheathed cable.

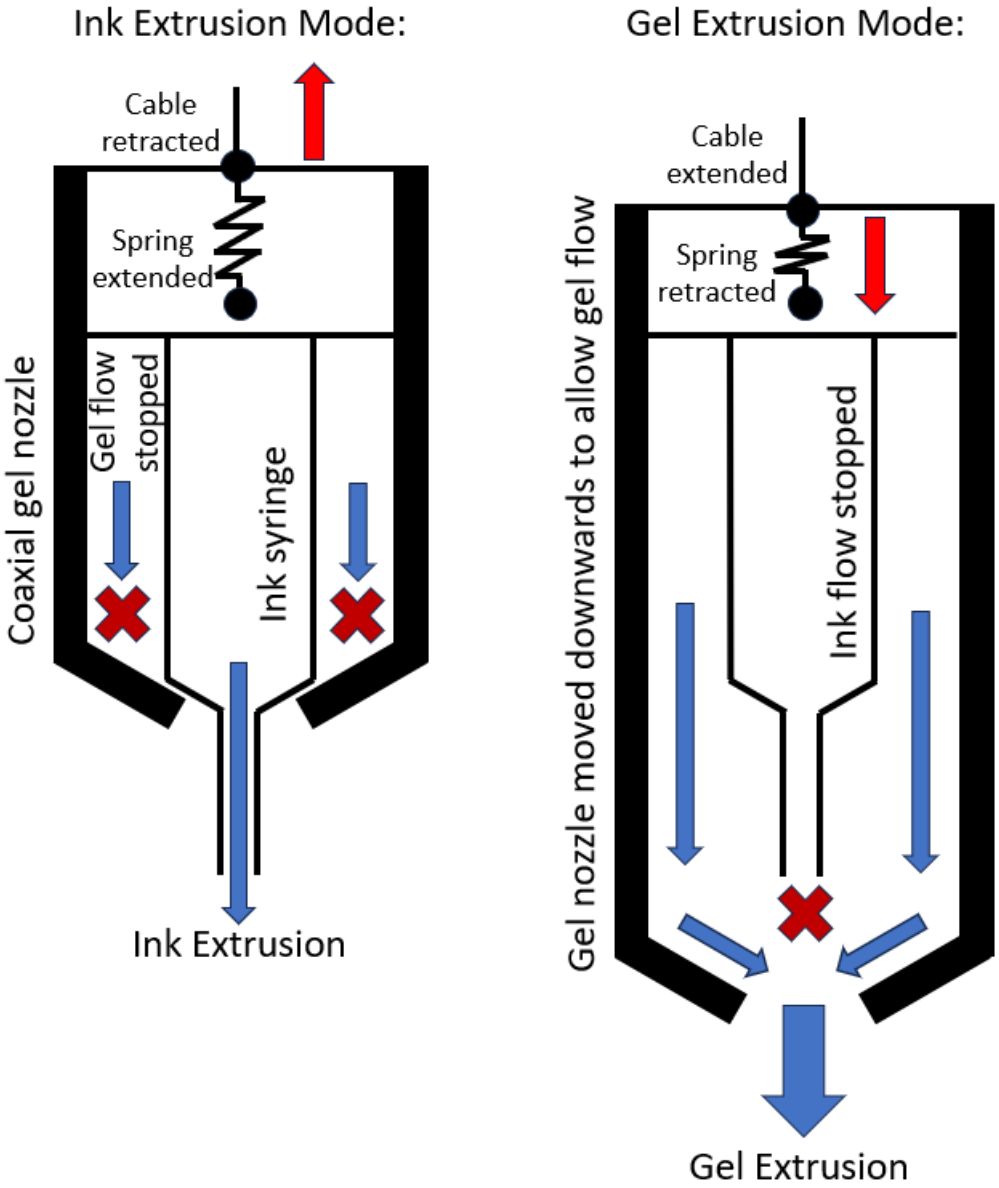

Figure 22: *How the coaxial ink-gel nozzle design may switch from ink mode to gel mode.*

4.8. Ink extrusion

Knowing the requirements of the resolution and nozzle translation rates, found in Section 3.3.3, along with the restrictions of keeping the tool head assembly lightweight and compact, a small, consistent, and accurate pumping method is recommended. Of the options of pumping methods referred to in Section 3.3.2, piston pumps have been used most often in ink extrusion in embedded 3D printing. The piston pump meets the prototype design requirements and is well understood as some guidance is provided on how to implement the pumps in embedded printer designs by Pusch et al. [37].

The variation of piston pumps used in this application is called a "syringe" pump. Using a syringe in a piston pump keeps the weight and cost of the pump down. Syringes can use exchangeable tips like those used in the Luer-lock system. Quick change syringe tips allow easy swapping between plugs and needles of various gauges as required. Additionally, one can ensure initial sterility in the syringe body for applications like bio-printing, where that may be important. An example of a syringe pump is the Replistruder extruder, shown in Figure 23.

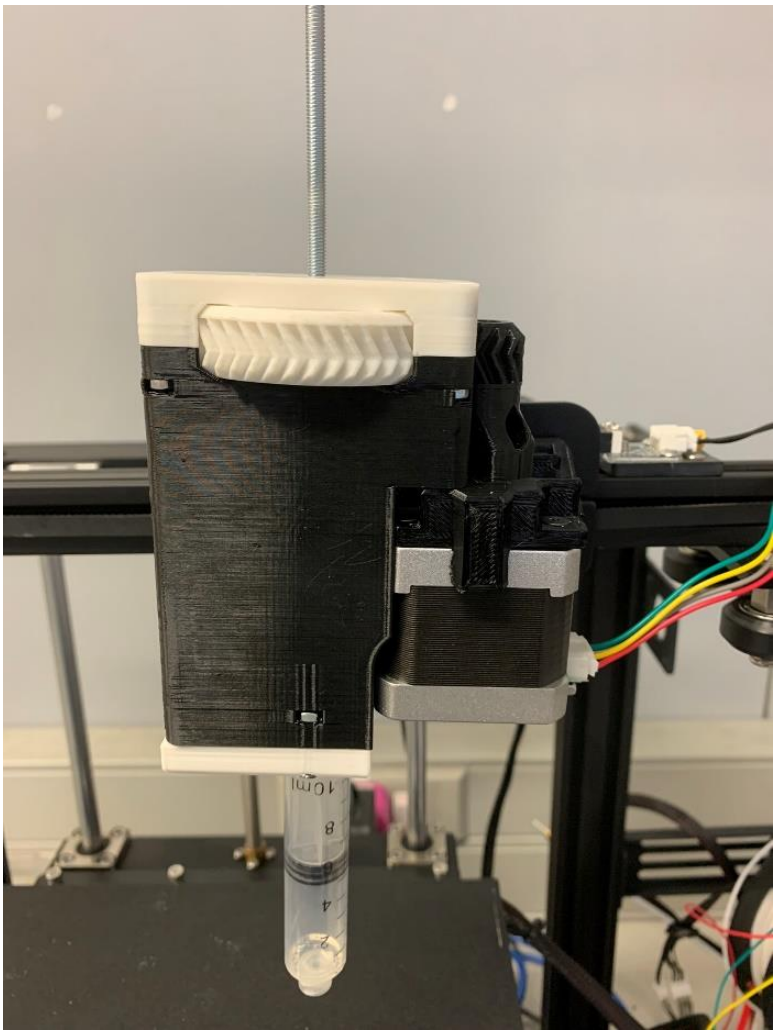

Figure 23: *Replistruder mounted on Ender 5.*

When analysing sliced G-code files generated in previous work using the Replistruder design of embedded 3D printer syringe pump extruder [25], it was found that no linear movement of the plunger was made that was smaller than about 2 microns. Hinton *et al.* used a set of gears with a ratio of 48:13 to achieve this resolution. This gear arrangement is relatively large compared to typical extruders. With this in mind, it was decided to design and test the use of a planetary gearbox due to the compact volume of a planetary gear set.

This planetary gearbox was designed to closely match the capabilities of the combination of gears used by Hinton *et al*. The gear ratio of 48:13 translates to a ratio of 3.692:1. To this end, the planetary gearbox used 16 teeth for the planet gear, 20 for the sun gear, and 56 for the ring gear. The sun gear was driven by a stepper motor with the ring gear fixed as shown in Figure 24.

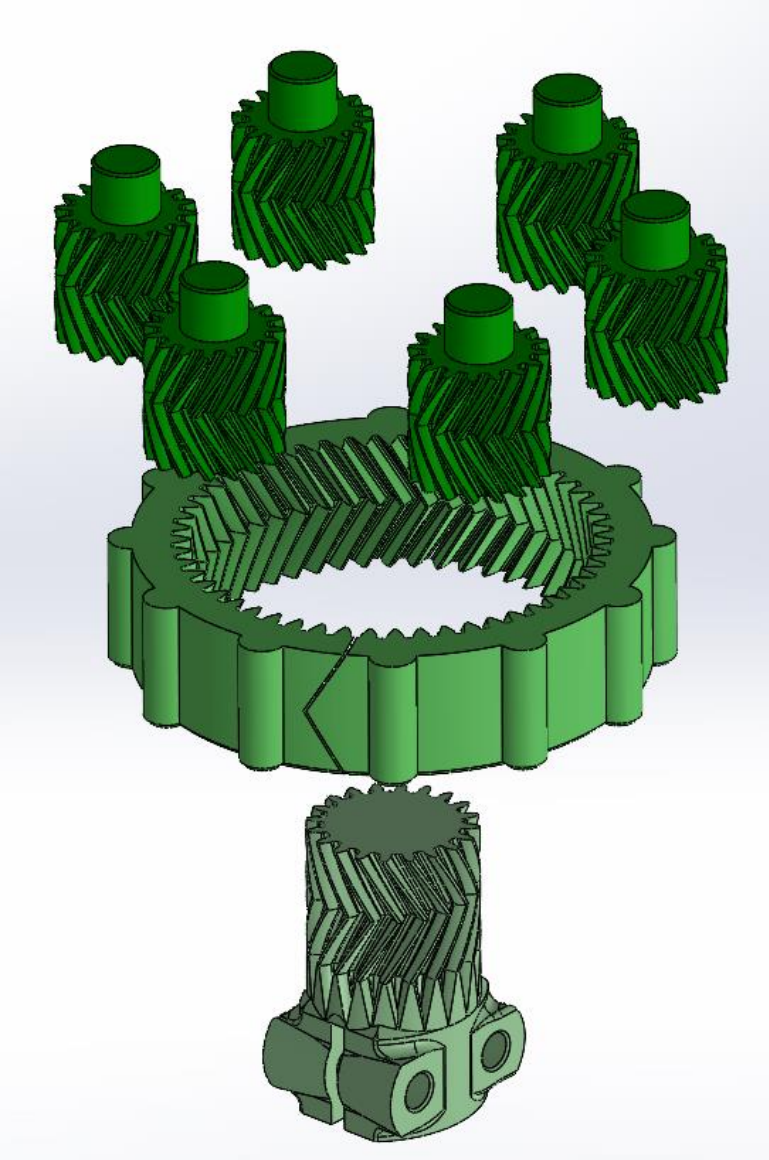

Figure 24: *An exploded view of the planetary gearbox designed for ink extrusion with double helical gears. The 6 planet gears on top each have 16 teeth, the ring gear in the middle has 56 teeth and the sun gear on the bottom has 20 teeth.*

Knowing the tooth counts and using Equation 6.12 from Shigley's Mechanical Design, page 121 [62]:

$$r = 1 + \frac{N_R}{N_S} \tag{4-1}$$

Where r is the gear ratio, N_R is the number of teeth of the ring gear, N_S is the number of teeth of the sun gear. Substituting the known values for the gears into Equation 4-1:

$$r = 1 + \frac{52}{20}$$

$$r = 3.6$$

This gives a gear reduction of 3.6:1, closely matching the ratio of 3.692:1 from the Replistruder extruder. The stepper motor itself has 200 steps. If a 4 mm threaded rod with a pitch of 0.7 mm is used, Equation 4-2 can be used to determine the final resolution.

$$R = \frac{p}{s \cdot r} \tag{4-2}$$

Where R is the resolution, p is the pitch of the threaded rod, s is the steps of the stepper motor per revolution, and r is the gear ratio of the planetary gearbox. Substituting in all the specified values into Equation 4-2 gives:

$$R = \frac{0.7}{200 \cdot 3.6}$$

$$R = 0.972\ \mu m$$

This gives a resolution of 0.972 µm, below the maximum desired resolution of 2 microns for the syringe pump attained from the g-code used for creating parts with the Replistruder syringe pump.

The gears in the gearbox utilise a double helix or herringbone design. The helical design allows multiple teeth to be engaged at any point, reducing backlash and theoretically allowing the design to withstand higher torques before the 3D-printed gears break. However, single helical gears have a significant axial force, which a thrust bearing must support. The herringbone gear geometry substantially reduces the resulting axial force, simplifying the support bearing arrangements. Six planetary gears distribute torque, protecting the teeth and reducing backlash.

The ability of the motor and gearbox combination to apply enough pressure on the syringe pump plunger/piston to extrude ink was investigated. Since 10 cc syringes are readily available, they were used in the syringe pump. Twenty-one gauge general application needles (0.57 mm internal diameter) at 20 mm long provide a good balance between detail, speed, and stiffness of the needle, as shown below:

Volumetric Flow Rate:

$$Q = \pi v {R_s}^2 \tag{4-3}$$

Where Q is the volumetric flowrate, v is the velocity of the syringe pump plunger and R_s is the internal radius of the syringe. Assuming a maximum velocity, v, is 0.33 mm/s (Appendix D.8) and the inner radius of the syringe used, R_s, is 7.285 mm, yields:

$$Q = \pi(0.33)(7.285^2)$$

$$Q = 55.02\ mm^3/s$$

Hagen-Poiseuille Equation [42]:

$$\Delta p = \frac{8\mu L Q}{\pi {R_n}^4} \tag{2-1}$$

μ is 3 Pa·s for Ecoflex 00-30 [63], L is 20 mm for the needle, and R_n is 0.285 mm, which yields:

$$\Delta p = \frac{8(3)(20)(55.02)}{\pi(0.285)^4}$$

$$\Delta p = 1274185\ Pa$$

From Appendix D.1, the 10 cc syringe plunger could have a maximum force of about 460 N applied to it before buckling. To determine the force required to depress the plunger and determine whether the syringe pump would extrude material or would instead buckle the plunger, one needs Equation 4-4.

$$F = \Delta p \cdot A \tag{4-4}$$

Where F is the force applied to the top face of the plunger, Δp is the difference in pressure required to extrude material out of the needle, and A is the area of the top face of the plunger. In this case, the area equation is:

$$A = \pi r^2 \tag{4-5}$$

Where r is the radius of the top face of the plunger. The radius of the top face of the syringe plunger used in the tests was 7.5 mm. The force applied to the top of the plunger is determined as:

$$F = (1274185)(\pi(0.0075)^2)$$

$$F = 225.2\ N$$

Comparing a force required of 225.2 N against the 460 N that would buckle the plunger calculated in Appendix D.1, we can see that the 20 mm, 21 GA needle should be safe to print with. Using the steps presented above, one would need to shorten the needle further if using a larger gauge. The 22 GA needle at 15 mm long would require a force of 398.2 N to extrude material, and at 20 mm long, would need 531 N, which would buckle the plunger.

4.9. Gel Extrusion

Gel extrusion has not been used extensively in embedded 3D printing, although some work has been done using gel extrusion[64][41]. More investigation should be done to determine an appropriate pumping method for moving gel. This investigation will evaluate low-cost, relatively low-effort methods of pumping gels for embedded 3D printing so as not to outgrow this project's scope.

Two pumping methods, piston pumping and peristaltic pumping, where investigated in this project. Piston pumping can easily be applied similarly to the ink extrusion syringe pump, and peristaltic pumping can continuously pump in both directions quite accurately.

They both have disadvantages that complicate gel extrusion. Piston pumps have limited extrusion and suction strokes. This means the pump must "refill" the piston in large parts or even large layers. The pump should execute a refill move between layers to get around this. Refilling between layers does not entirely solve large layers potentially needing piston refill moves mid-print. Peristaltic pumps do not have this issue, but they display sinusoidal flow behaviour, which could become an issue since layers may be too inconsistent for ink extrusion.

An essential first step to designing a pump in a new use case, such as embedded 3D printing, would be to determine an appropriate volumetric flow rate. To this end, the printing speed, gel layer height, and nozzle diameter were used to determine an initial estimate for a proper volumetric flow rate.

$$\dot{V} = v_n h_l d_n \tag{4-6}$$

Where $\dot{V}$ is the volumetric flowrate, v_n is the nozzle translation speed, h_l is the layer height and d_n is the nozzle diameter.

Figure 25 provides a cross-sectional view of the gel nozzle configuration. Accessing the tip of the syringe is useful when changing needles or stoppers before, after or even during printing. The inner diameter of the gel deposition nozzle must accommodate the user's fingers as they tighten and loosen the needle tip onto the ink deposition syringe to allow the user access to the syringe tip. Having a larger gel nozzle diameter will also result in better coverage to the edge of the gel container as with a traditional nozzle, a "dead zone" is formed around the edge of the build volume where it is impossible to deposit material as the nozzle cannot possibly reach there without the print head colliding with the container or the frame. The desire for a larger nozzle should be balanced with the desire not to lose the ability to seal the gel nozzle when closed as the gel nozzle becomes so wide that the opening extends under the inlet tube openings, making sealing them impossible using the current design.

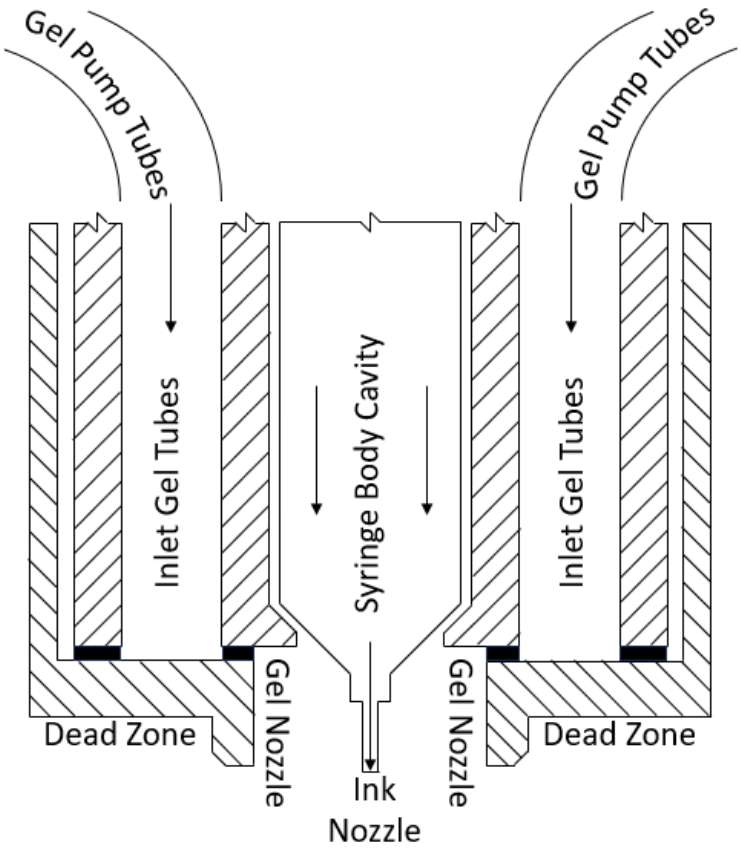

Figure 25: *A cross-sectional view of the lower gel nozzle configuration.*

Using an inner gel deposition nozzle diameter of 24 mm, a target translation speed of 10 mm/s, and a layer height of 1.6 mm gives:

$$\dot{V} = (10)(1.6)(24)$$

$$\dot{V} = 384\, mm^3/s$$

One can design either the peristaltic pump or the syringe pump with this target volumetric flow rate in mind, though each will present its own challenges as outlined in Sections 4.91 and 4.9.2.

4.9.1. Peristaltic pump design

A peristaltic pump is a positive displacement pump where rollers depress a soft tube. The rollers are on arms driven by a motor so that the circular motion of the arms causes fluid flow in the tube. This fluid flow pulsates sinusoidally since flow is pushed through the pump in individual "packets" between the rollers.

Previous work done at the University of Cape Town regarding embedded 3D printing has attempted to develop a peristaltic pump for pumping support gel [41][65]. A previous design for a peristaltic pump was adapted for this project [66], shown in Figure 26. The prior work at the University of Cape Town left some 5 mm soft tubing and 625RS radial ball bearings. These were easily integrated into the design of the peristaltic pump as they were initially intended for peristaltic pumps with similar purposes. A NEMA17 motor was used to drive the pump.

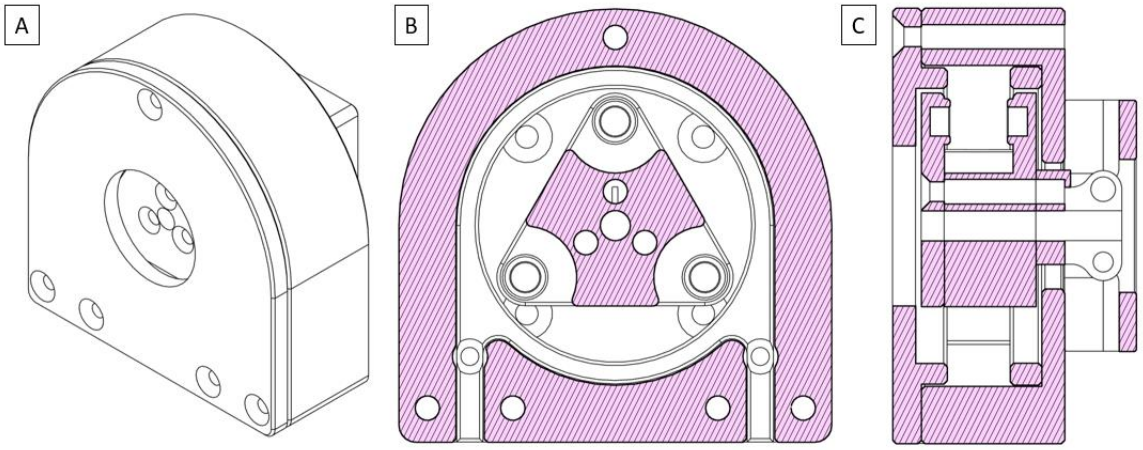

Figure 26: *The printed components of the PattysLab peristaltic pump. A shows an isometric view, B shows a sectioned front view and C shows a sectioned side view.*

The pump was designed to draw gel from a reservoir on command and pump it to the gel nozzle, where it may be deposited in the build volume of the 3D printer. Ideally, the pump would mount to the frame of the 3D printer, so some consideration was given to limiting the size of the peristaltic pump to make this practical.

A method was developed to calculate the theoretical volumetric flowrate of this peristaltic pump in Appendix D.4. Using this method, the theoretical volumetric flowrate of the pump is 913 mm^3/s. This flowrate was compared in Section 6.2 against the actual flowrate to determine if the built peristaltic pump should be used over a piston pump for the gel deposition system.

Two methods were selected to calculate the torque required to pump gel using the peristaltic pump as designed to determine if a NEMA17 stepper motor is appropriate for the peristaltic pump.

Knowing the gel rheological properties shown in Section 6.1 allows one to be informed of whether or not the size of the stepper motor is adequate for driving the peristaltic pump. One may calculate an answer for the required torque using the result derived by Masters [41]:

$$T = \frac{\pi R^2 \theta N}{5}\left(\frac{\rho {r_t}^2}{160}\left(\frac{{r_t}^4 - {r_n}^4}{{r_n}^4}\right)(R\theta N) + 2L\mu\right) \tag{4-7}$$

Where T is the required torque, R is the radial distance from the motor axis to the centre of the tube in the peristaltic pump, θ is the angle between the rotor arms, N is the angular velocity of the rotor arms in rpm, ρ is the fluid density, r_t is the inner radius of the tube, r_n is the outlet nozzle radius, L is the length of the pipe, and μ is the dynamic viscosity of the fluid.

Knowing R is 25.5 mm, θ is $2\pi/3$ radians, N is the independent variable, ρ is 1026 kg/m^3, r_t is 2.5 mm, r_n is 12 mm, L is 1 m, and μ can be determined by Equation 4-8 [67]:

$$\mu = \frac{\tau_w}{\dot{\gamma}} \tag{4-8}$$

As determined previously for Herschel-Bulkley fluids:

$$\tau_w = \tau_0 + K(\dot{\gamma}_w)^n \tag{4-9}$$

$$\dot{\gamma}_w = \frac{3n+1}{4n} \cdot \frac{8V}{D} \tag{4-10}$$

Since $\dot{\gamma}_w$ is dependent on the velocity of the fluid, this shows that μ is also dependent on the velocity of the fluid. To convert N in rpm to V in m/s, Equation 4-11 can be used:

$$N = \frac{60V}{2\pi R} \tag{4-11}$$

To change V to a volumetric flow rate, which will be helpful in later comparisons, one may use Equation 4-12:

$$\dot{V} = V \cdot 2\pi {r_t}^2 \tag{4-12}$$

Figure 27 presents the torque required for a peristaltic pump driving 3 g/L Carbopol 980 gel:

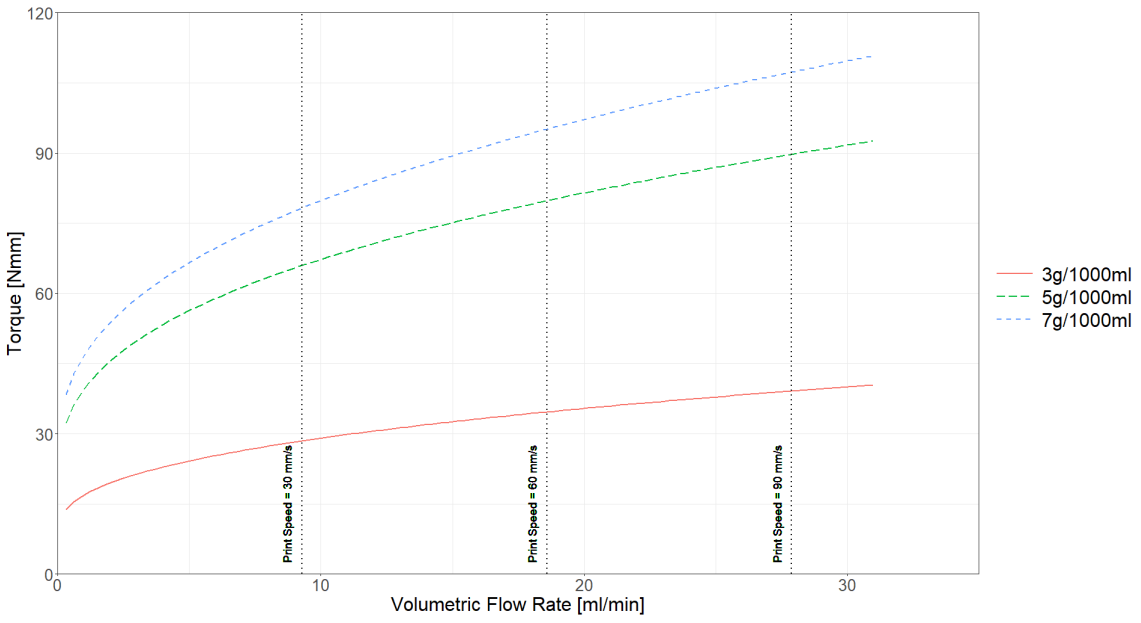

Figure 27: *The torque required by the peristaltic pump to pump Carbopol 980 gel over a range of volumetric flow rates at various concentrations using Masters' equation.*

In Figure 27, the required torque for the most viscous gel at printing speeds of 90 mm/s (well above what this project aims to achieve) is about 107 Nmm. As a NEMA17 stepper motor has a rated maximum torque of 0.4 Nm, which should be ample to drive the peristaltic pump at lower printing speeds.

To do an additional check to see if the torque should be enough, one can do a force balance where the pressure difference over the length of the tube is equal to the losses due to the shear stresses acting on the fluid in contact with the walls of the tube. For further details on the derivation of Equation 4-13, see Appendix D.9.

$$T = \pi D_t L_t R \left(\tau_0 + K \left(\left(\frac{3n+1}{4n} \right) \left(\frac{8V}{D_t} \right) \right)^n \right) \tag{4-13}$$

Using Equation 4-13 and the same variables as was used to generate Figure 28 based on the author's equation yields:

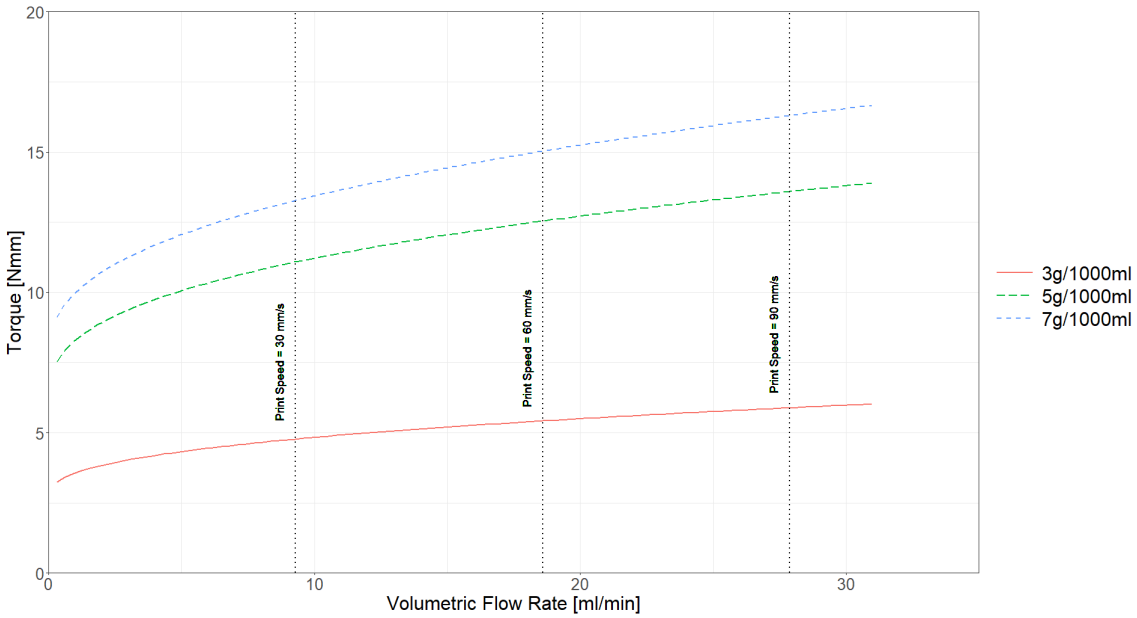

Figure 28: *The torque required by the peristaltic pump to pump Carbopol 980 gel over a range of volumetric flow rates at various concentrations using the author's relation.*

These results show that using this method for the most viscous gel, printing at 90mm/s, the required torque would be less than 0.02 Nm, which should be well within the ability of the NEMA17 stepper motor.

Note that neither one of these methods considers the torque required to compress the tube as is necessary in a peristaltic pump. Still, since both methods gave results well below the maximum torque of a NEMA17 stepper motor, it was determined that building and testing could commence.

4.9.2. Piston pump design

A syringe was used to keep the cost down of the piston pump, with the plunger being driven by a screw attached by a coupler to a NEMA 17 stepper motor, similar to the ink extrusion syringe pump.

The syringe should be large enough to print at least one layer of support gel without performing a refilling suction stroke to avoid prints taking too long and causing the ink to cure before the print is completed. Using this criterion, it becomes essential to calculate the volume of support gel to fill the volume that may be printed within a single layer on the Ender 5.

$$V = \pi \left(\frac{w}{2}\right)^2 h_l \tag{4-14}$$

In Equation 4-14, V is the volume of a single printed layer, w is the width of the build plate, and h_l is the height of the printed layer. The square build plate on the Ender 5 has a width of 220 mm, and in this case, the layer height was 1.6 mm. This yields:

$$V = \pi \left(\frac{220}{2}\right)^2 1.6$$

$$V = 60821.234mm^3 = 60.8\ cm^3$$

A volume of about 60 cc is needed if using a cylindrical container with a diameter of 220 mm, the same as the width of the build plate of the Ender 5. In the gel extrusion syringe pump, a 60 cc Catheter tip syringe was used, as this tip has less restriction of flow in comparison to Luer tip syringes. The Ender 5 does have a square build plate. It was thus determined if 60 cc would be sufficient to fill a container with a footprint the same size as the build plate:

$$V = w^2 h_l \tag{4-15}$$

Using the same variables as was just used to calculate the volume of a layer printed in a cylindrical container; V would be 77.44 cc, which is greater than what can be delivered by a 60 cc syringe. If the layer height, h_l, is reduced to 1.2 mm, this yields a volume of 58.08 cc. Knowing this, one could reasonably use a 60 cc syringe in this application, but one should consider reducing the layer height as needed.

The Equation 4-16 may be used to achieve the required volume flow rate of 384 mm^3/s:

$$\dot{v_p} = \frac{\dot{V}}{\pi {r_s}^2} \tag{4-16}$$

Where $\dot{v_p}$ is the piston depression speed, $\dot{V}$ is the required volume flowrate and r_s is the internal radius of the syringe being depressed by the piston. With the 60 cc syringes used in this case, the inner radius is 14.3 mm. This yields:

$$\dot{v_p} = \frac{384}{\pi(14.3)^2}$$

$$\dot{v_p} = 0.598\ mm/s$$

This piston depression speed can be used to determine how effectively the piston pump performs compared to the peristaltic pump by seeing how well the piston pump performs when the piston is being depressed at 0.6 mm/s.

One should note that the flow out of the gel piston pump is not directed like the flow out of the peristaltic pump. The tip of the syringe is both an inlet and an outlet. This is not ideal since there is a desire to send controlled small amounts of gel towards the gel nozzle. Choosing not to direct the flow would result in unexpected fluctuations in performance as the gel is allowed to flow back from the nozzle during retraction moves of the gel syringe plunger, and the gel is allowed to flow back towards the gel reservoir when depressing the plunger.

Non-return valves were configured, as shown in Figure 29, to direct the gel flow through the syringe pump. On the retraction stroke, valve A would shut, stopping flow from the gel nozzle, and valve B would open, allowing flow from the gel reservoir. On the extrusion stroke, valve A would open, allowing flow to the gel nozzle, and valve B would shut, stopping flow to the reservoir. Ball check valves should suffice in this application.

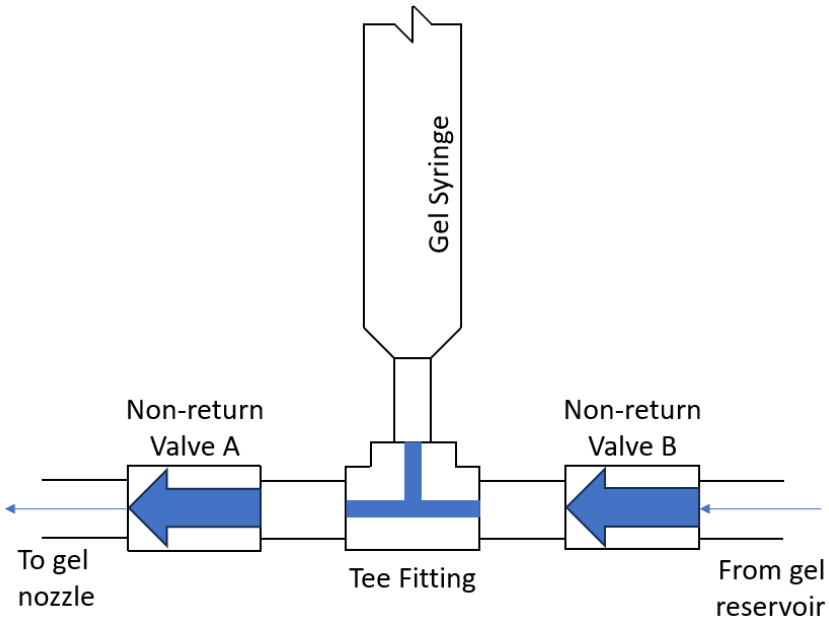

Figure 29: *Gel syringe pump configuration.*

Some investigation into whether an M4 threaded rod being driven by a NEMA17 stepper motor was appropriate for the gel syringe pump in Appendix D.10. It was found that the M4 threaded rod being driven by a NEMA17 stepper motor should be able to output 882 N. In Section 6.3.1, it was measured that this was more than 10 times more than what was required to extrude support gel through 1 m of tubing. The M4 threaded rod and the NEMA17 stepper motor should be adequate for use in a piston pump. With this knowledge, one can proceed confidently in building and testing the syringe pump design for gel delivery.

Figure 30 shows the initial mounting location of the syringe pump on the printer frame, which performed poorly. The gel flow suffered from significant air inclusion, attributed to the gel reservoir and valves being located below the delivery point, causing significant sub-atmospheric pressures in the line. The pump and gel reservoir were moved above the printhead, shown in Figure 31, to avoid this, which improved the pump's performance.

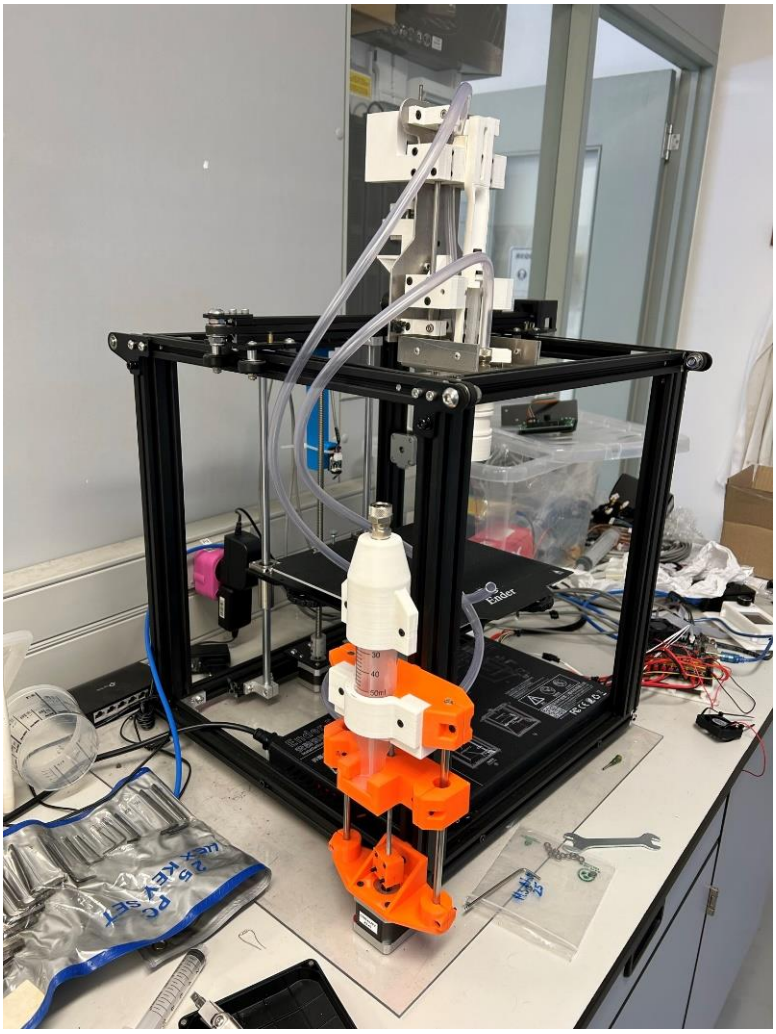

Figure 30: *Initial orientation of the gel syringe pump below the DIGEX print head.*

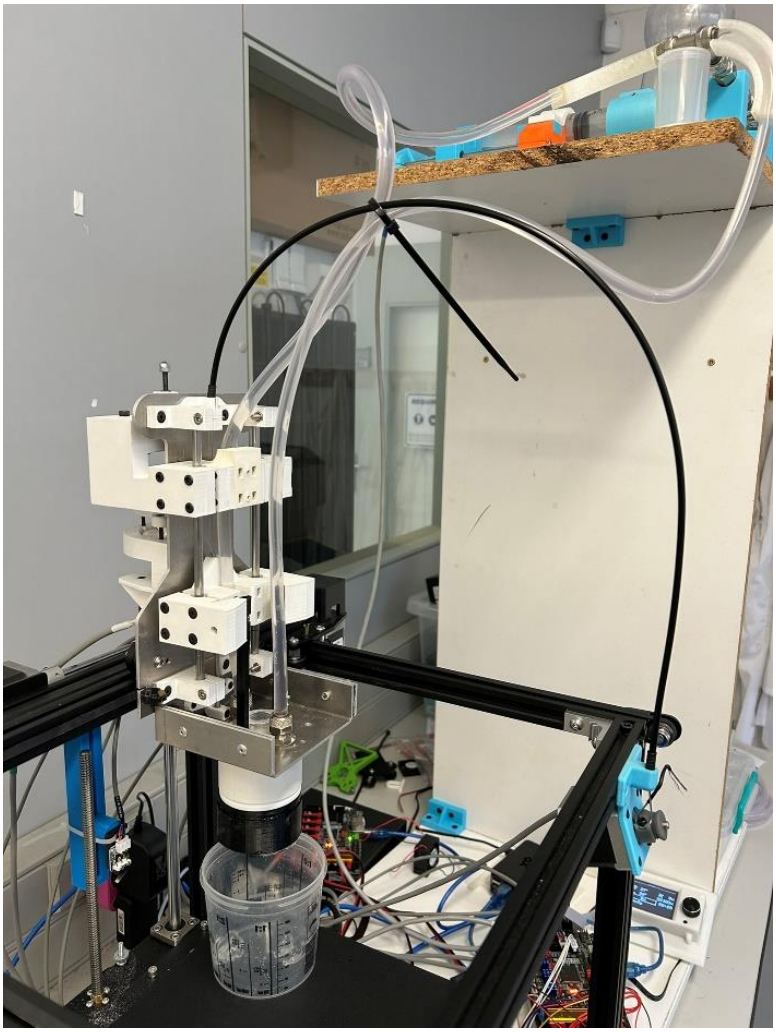

Figure 31: *New orientation and location of the gel syringe pump above the DIGEX print head.*

4.10. DIGEX print head design

Knowing that the ink syringe pump would be mounted on the print head and the gel extrusion pump would be mounted elsewhere, work could be done on the design of the print head. It had been determined that a co-axial ink-gel deposition system would be used whereby an ink and gel could be deposited on demand for the sake of compactness of the print head. The result of this is shown in Figure 32.

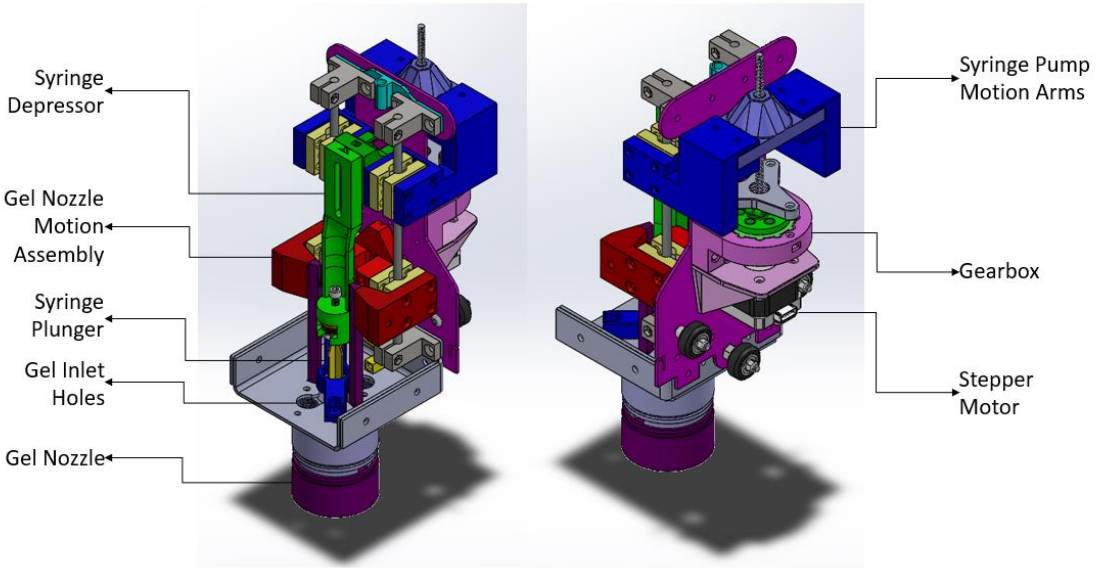

Figure 32: *Print head design of the DIGEX print head.*

The syringe pump is mounted on both sides of the backplate, with the heavy stepper motor mounted behind the backplate above the X-axis gantry along with the planetary gearbox. Moving these heavier components over the gantry should reduce vibrations during print head moves and the print head size in the X-Y plane.

The syringe pump motion arms transfer the stepper motor and gearbox's rotational motion to linear motion along two linear rods and use the syringe depressor to move the syringe plunger to extrude material from the ink syringe. Figure 33 shows a closer view of the upper sub-assemblies of the print head, specifically how the stepper motor's movement is connected to the movement of the syringe plunger.

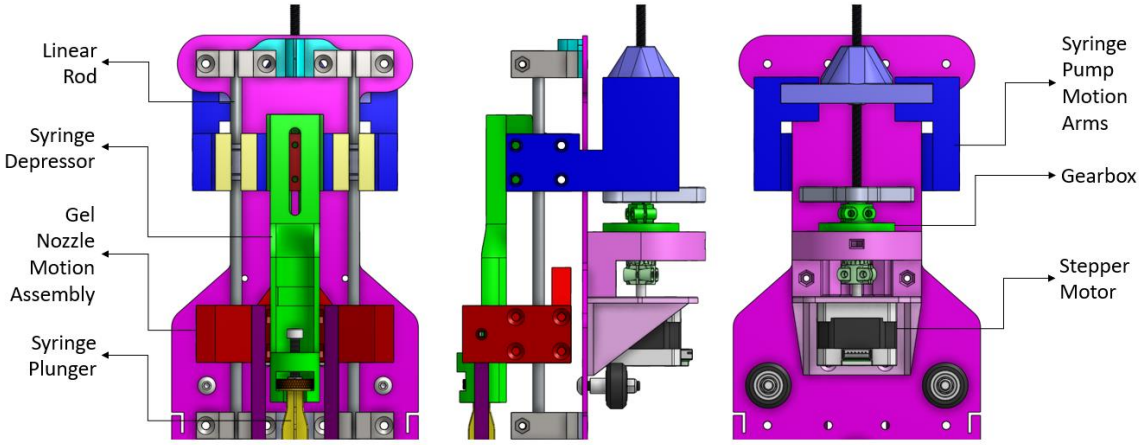

Figure 33: *Closer views of the DIGEX upper print head assembly*

The gel nozzle is moved up and down using the gel nozzle motion assembly that uses the same linear rods to move the syringe depressor up and down. Using the same linear rods in the syringe pump and with the gel motion assembly further reduces the size and mass of the print head. Figure 34 shows how the gel nozzle connects to the gel nozzle motion assembly in a partial sectional view of the lower assemblies.

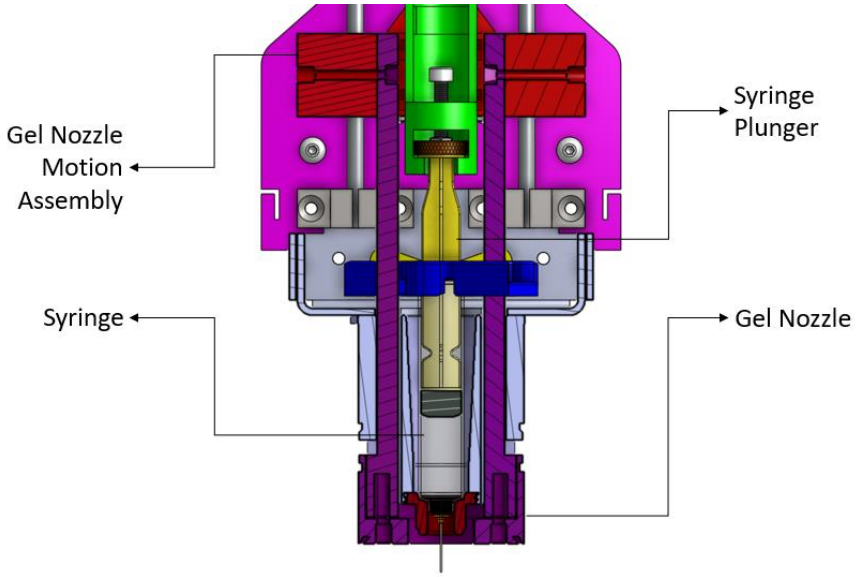

Figure 34: *Partial section view of the DIGEX lower print head assembly*

More detailed drawings are provided in Appendix I if the reader needs further clarification on the assembly and individual components.

4.11. Instability management

Flow instabilities that affect the printing of liquid inks in gel supports include recirculating wakes, static crevasse formation, ink sagging, ink droplet break up and needle extrusion pressure. Sylgard 184 is used instead of Ecoflex 00-30 in these equations. This was based on the reasoning discussed in Section 6.6.

To avoid recirculation wake instabilities, the minimum nozzle depth during printing may be found in Section 2.2.5.5.1:

$$L > \frac{v_n \eta}{\rho g d} \tag{2-3}$$

Knowing the relationship between the length of the needle submerged in the gel and the velocity at which the needle is translating allows for the safe avoidance of recirculation wake instabilities. Using representative nozzle geometry (outer diameter 1.27 mm, depth of printing 10 mm) and Carbopol 980 and Sylgard fluid properties (density 1026 kg/m^3, viscosity 3.5 Pa·s), we can calculate that print speeds should be kept to below 35 mm/s.

The next instability to consider would be static crevasse formation. Static crevasse formation is defined by:

$$h = \frac{\sigma_y}{\rho g} \tag{2-5}$$

Using the yield stress from each gel using the data from Appendix F and a density of 1026 kg/m^3, the heights from each gel at 22 °C would be 3.4 mm, 7.8 mm and 9.6 mm for 3, 5 and 7 g/L concentration Carbopol 980 respectively. Noting this, in this case, avoiding recirculation wake instabilities should also avoid static crevasse formation.

Sag, due to gravity, is caused by a mismatch in density between the ink and the gel. The gel was measured to have a density of 1026 kg/m^3, and the manufacturer cites a density of 1030 kg/m^3 for Sylgard 184. Most silicon elastomers considered for inks in this project have densities between 1020 kg/m^3 and 1050 kg/m^3. The small density difference between the gel and inks means that the inks should be close to neutral buoyancy in a support bath of Carbopol 980.

Interfacial tension was not tested for this project, meaning the critical feature diameter in interfacial tension-driven droplet breakup could not be determined using Equation 2-6 in Section 2.2.5.5.4. It is helpful to know what droplet breakup looks like and how one may avoid it, which is also detailed in Section 2.2.5.5.4.

Needle extrusion pressure was dealt with in Section 4.9.2, and it was concluded that the current ink piston pump setup is more than adequate to provide enough pressure to extrude Sylgard 184 and avoid inconsistencies in extrusion due to needle extrusion pressure issues.

5. Material preparation and testing methodologies

Evaluating the embedded 3D printing system included sub-system and function testing. This involved common tasks, such as preparing the ink and support gel. The flow characteristics of the support gel also needed to be measured to inform various design and performance calculations. These procedures are briefly described in this chapter. Finally, a brief description of the process of preparing a part file for embedded 3D printing is given, as well as a description of using the embedded 3D printer. Many of the chemicals used in this work required personal protective equipment and an awareness of the safety requirements of those substances. More detailed step-by-step instructions are given in Appendix A.

5.1. Silicone ink preparation and testing

Much of the testing used PDMS silicon elastomers as the ink. These were prepared by thoroughly mixing the component parts per the manufacturer's ratio. The mixed ink was degassed in a vacuum chamber. A syringe was filled with the ink with the aid of a funnel. The syringe was inverted to allow any small bubbles entrapped during filling to accumulate at the nozzle before the plunger was depressed till the nozzle flow was free of visible bubbles. Refer to Appendix A.2 for more details.

A determination of whether the silicone ink was extrudable out of the desired syringe needles was first done to avoid damaging the ink syringe pump. After preparing the ink as detailed above, the ink was loaded tip down into a stand, and an Instron Universal Loading Frame with a 1000 N load cell attached was used to depress the syringe plunger at a constant velocity. As the material was extruded out of the needle tip, the force-displacement data was recorded for later analysis. Refer to Appendix A.4 for more details.

5.2. Gel preparation and testing

The support gels used in this project were exclusively made using Carbopol 940 powder. These were prepared by thoroughly mixing the dry carbomer powder in demineralised water in the desired concentration, ranging from 1.2 to 7 g/l. After mixing, the pH of the gel was measured and adjusted by adding 1 N Sodium Hydroxide solution until the desired pH range of 6.9 - 7.1 was reached. Once the mixed gel met the pH requirement, it was degassed in a vacuum chamber. Refer to Appendix A.1 for more information.

Some testing was done to investigate the rheological properties of the support gel. After the support gels were mixed to the desired pH and concentration, as detailed above, the gels were loaded into a Rheolab QC rheometer using a concentric cylinder geometry. The rheometer performed a logarithmic shear rate sweep while keeping the temperature constant using the included Peltier temperature control system. Refer to Appendix A.3 for more information.

The extrudability of the support gels from a 60 cc catheter tip syringe was investigated in a similar manner to the extrusion of the silicon inks, described in Section 5.1. After the gels had been prepared as explained above, a gel-filled syringe was loaded into a stand, and an Instron Universal Loading Frame with a 1000 N load cell was again made to depress the syringe plunger at a constant velocity, and the force-displacement data was recorded. This test was also done with various lengths of tubing attached to the tip of the syringe. Refer to Appendix A.5 for more information.

5.3. Pump testing

The flow performance of the peristaltic pump and large volume syringe pumps were assessed similarly. The inlet side of the pump being tested was connected to a reservoir filled with the desired test fluid. After the pump had been primed to remove as much air as possible, a G-code command was sent to the pump motor to extrude a desired volume of test fluid. The fluid output of the pump was weighed, and its mass was converted to volume, given the density of the test fluid. As both pumps were driven by the same NEMA 17 extruder motor, with the relevant "Steps/Extrusion Length" factor changed in the firmware, allowing direct comparison of the accuracy of the material delivered. Refer to Appendix A.6 and Appendix A.7 for more information.

5.4. Hardware preparation for embedded printing

A methodology was developed for embedded 3D printing part preparation. The multi-material portion of Cura was not used to ensure better flexibility and control of the output. The gel part was sliced normally, but the ink part needed prime and dwell towers offset from the part to increase part quality. After the ink and gel parts had been sliced separately, the two files were knit together using an external python script provided in Appendix C.3. Refer to Appendix B for more information.

Using the embedded printer is a non-trivial process and will be detailed here. The reservoir was filled with support gel up to a day beforehand while trying not to introduce air bubbles into the gel. The ink syringe was removed shortly before printing and filled with the ink material. While preparing the ink material and filling the syringe, the gel pump was made to prime and fill the entire gel deposition system with gel. Once the ink syringe and the gel deposition system were prepared, the ink syringe could be placed back into the ink deposition system and the container holding the print was prepared. After the container had been prepared, it was placed in the middle of the build plate. The gel nozzle was prepared, and the ink needle was attached to the ink syringe before commencing the print job.

6. Testing, results and discussion

Testing was needed to determine the design's efficacy and improve the prototype's design iteratively. Gel extrudability testing was done to determine the relevant properties for other design and testing work. Testing was also done to assess the efficacy of the two pumping methodologies regarding gel extrusion. Finally, testing was done to improve the design of the prototype using analysis of tests and print results.

6.1. Gel extrudability testing

Knowing the rheological properties of the pumped liquids is useful when designing pumping mechanisms. The inks being pumped come with manufacturer data sheets that can be referenced. Still, the gels are non-Newtonian fluids with behaviour that may depend on several factors, including temperature, pH, shear rate and concentration.

To this end, the rheological properties were tested using an Anton Paar Rheolab QC rheometer, with the methodology detailed in Appendix A.1. Carbopol 980 powder at concentrations of 3, 5 and 7 grams mixed with 1 litre of distilled water was used as the gel mixture. Each sample was pH balanced to a pH = 7.0 +/- 0.1. Each concentration was tested at 18, 22 and 30°C. The resultant shear stress from a logarithmic sweep between 0.001 and 500/s was measured. Figure 35 shows the average data from these tests; see Appendix E for the full results.

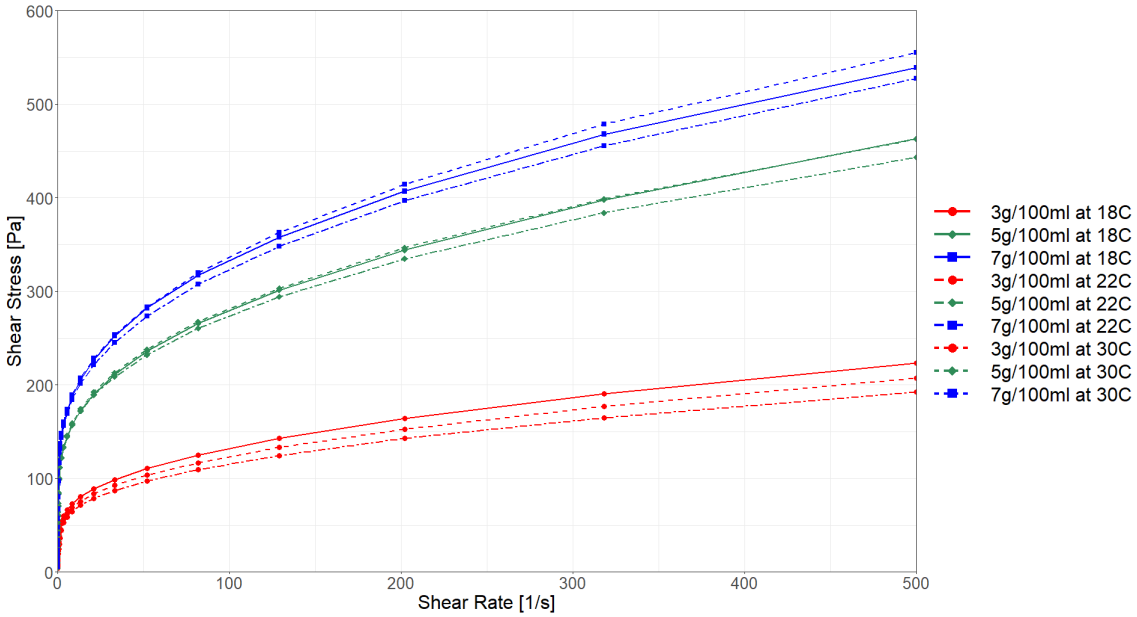

Figure 35: *Averaged Shear Stress and Shear Rate behaviour of Carbopol 980 gel at various temperatures and concentrations.*

Figure 35 shows that the required shear stress at a given shear rate increases non-linearly as that shear rate increases. This non-linearity confirms that Carbopol 980 is a non-Newtonian fluid showing typical yield stress fluid properties, only flowing significantly after exceeding the yield strength. Carbopol 980 is a Herschel-Bulkley fluid, which is defined by the following law [68]:

$$\dot{\gamma}_w = 0 \quad if\ \tau_w < \tau_0 \tag{6-1}$$

$$\tau_w = \tau_0 + K(\dot{\gamma}_w)^n \quad if\ \tau_w \geq \tau_c \tag{4-9}$$

Where τ_w is the wall shear stress, τ_0 is the yield stress, K is the consistency, n is the flow index, and $\dot{\gamma}_w$ is the wall shear rate. If the constants τ_0, K and n are known, one can calculate the shear stress causing yielding when $\tau_w \geq \tau_c$. Calculating the shear rate is done using the following relation from Metzner and Reed [69]:

$$\dot{\gamma}_w = \left(\frac{3n+1}{4n}\right)\frac{8V}{D} \tag{4-10}$$

Where additionally, V is the velocity of flow and D and is the diameter of the pipe through which the fluid flows. Combining Equation 4-9 and Equation 4-10, we get:

$$\tau_w = \tau_0 + K\left(\left(\frac{3n+1}{4n}\right)\frac{8V}{D}\right)^n \tag{6-2}$$

Equation 6-2 can be used in pressure drop and head loss equations that were used later in this project when discussing the gel pumps.

Figure 35 also shows that the shear stress at a given shear rate is not significantly affected by the temperature in the range being tested in this series of tests. If the gel already has the required rheological properties at room temperature, it is unlikely that normal room temperature fluctuations will make the gel unusable. These results indicate that this project does not need temperature control while using Carbopol 980.

6.2. Peristaltic pump variability testing

The results shown in Table 2 were gathered using the methodology detailed in Appendix A.6:

Table 2: *Performance of the peristaltic pump*

Test #	Concentration [g/l]	Distance [mm]	Velocity [mm/s]	Theoretical Mass [g]	Measured Mass [g]	Mass Output Fraction [%]
1	3	5000	100	121.07	3.78	3.12
2	3	15000	100	363.20	11.37	3.13
3	1.2	2000	100	48.43	33.01	68.16
4	1.2	2000	50	48.43	33.96	70.13
5	1.2	2000	110	48.43	29.09	60.06

For details on the number of tests and how all the values are calculated, consult Appendix G.1. The key observations from these experiments can be seen in the last column of Table 2, showing that the measured output of the peristaltic pump was much lower than predicted by the theoretical relationships.

The peristaltic pump was consistent between tests 1 and 2, which were conducted with a higher viscosity gel. Still, those results showed how poorly the pump performed at this concentration, with the pumped material being 30 times smaller than the theoretical amount. Test 2 increased the extruded distance requested to test if the pump's performance was affected by the amount extruded, with no change seen. It was then decided to try pumping a much lower gel concentration, but the pump was still performing poorly despite testing at different velocities to test how performance changed with the extrusion rate.

Additionally, the flow showed a high degree of pulsation. The tube would also wander over time and required collars to be installed to keep the tube in place. Finally, the pump would occasionally seize up, ruining the test.

Improving the performance of the peristaltic pump could be achieved by adjusting many variables. These variables include tube thickness and stiffness, roller geometry, lubricant, number of rollers, sprung rollers and flow dampers, among other variables. Noting the impending scope creep, it was decided to test the piston pump's performance before any more refinement should be done to the peristaltic pump's design.

6.3. Piston pump performance testing

6.3.1. Piston pump tube force testing

To determine if it was feasible to build a piston pump based on a 60 cc syringe, a simple test was done as detailed in Appendix A.5. This test involved measuring the force required to extrude Carbopol gel out of the syringe, with varying lengths of 10 mm diameter tubes attached to the syringe to simulate different levels of flow resistance.

The results can be seen in Figure 36 and Appendix G.2. One can note that the maximum force seen generally increases with the tube length attached to the syringe's end. The maximum force seen with no tube was 7.1 N, while the maximum for all the tests was 53 N, with the longest tube tested being 1 m long.

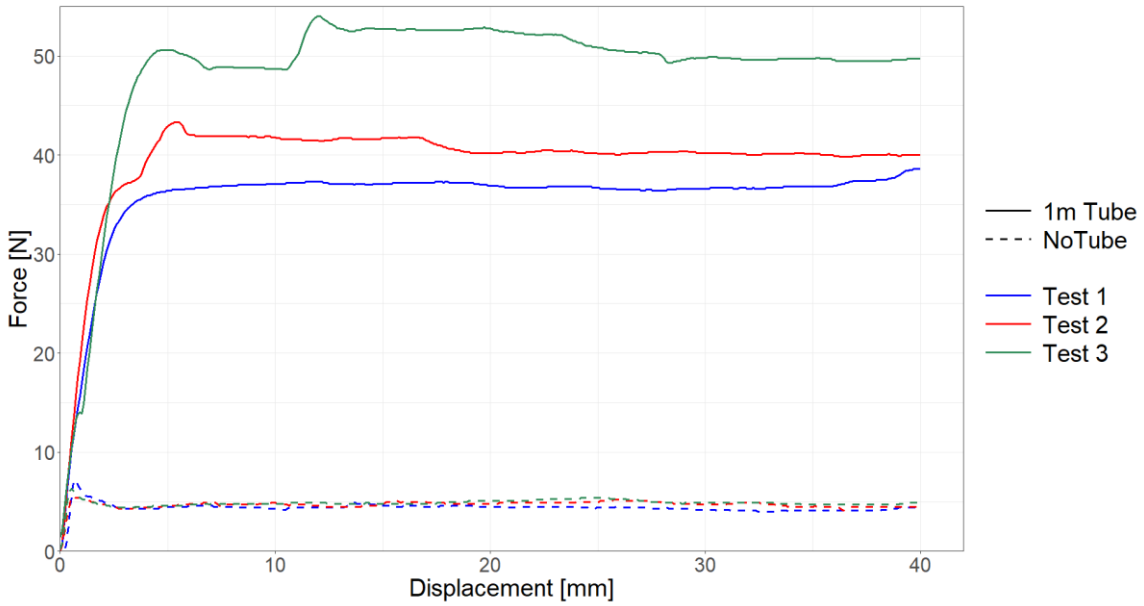

Figure 36: *Force-displacement behaviour of the 60 cc syringe extruding gel through one meter of tube (above) and without a tube (below).*

6.3.2. Piston pump hardware and methodologies refinements testing

Tests were done according to the methodology detailed in Appendix A.7, and the data is shown in Table 3. All the data collected may be seen in Appendix G.2. The concentration of Carbopol gel was varied to investigate if performance reduced as the concentration increased, and the speed of extrusion was varied to see if extrusion speed also positively affected pump performance like the case in the peristaltic pump was. Any modifications and refinements made were also tested; their results are also shown in Table 3.

Table 3: *Performance of the gel syringe pump*

Test #	Concentration [g/l]	Extrusion speed [mm/min]	Average Measured Weight [g]	Theoretical Expected Weight [g]	Percentage [%]
1	0	180	145.64	173.46	83.96
2	0	90	94.20	173.46	54.31
3	0	24	11.66	173.46	6.72
4	1.6	180	146.88	173.46	84.68
5	3	180	114.87	173.46	66.22
6	3	90	159.63	173.46	92.03
7	3	90	162.64	173.46	93.76

The first three tests were done with water, showing how speed affects the pump's output. As one can see, the output reduced with reduced extrusion speed despite the same volume of gel being requested to be pumped. The one-way valves in the system just before and after the syringe were likely responsible for this behaviour. Unless sufficient back pressure is developed, the one-way valves can remain closed or allow flow back towards the reservoir, which shouldn't be allowed. As back pressure would be proportional to flow rate, this suggested that slowly pumping support gel should be avoided.

Test 4 investigated how the pump reacted to more viscous fluid. To this end, Carbopol 980 gel with a concentration of 1.6 g/l was used. This test showed that the pump was indifferent to this change in viscosity, delivering about the same volume of gel as would have been delivered with water.

However, it was noted that the M4 threaded rod was becoming heavily worn down from rubbing against the steel M4 nut required to convert the threaded rod's rotational movement into linear movement on the syringe plunger. The lead screw was increased to M8 nominal diameter, and the corresponding M8 nuts changed from steel to brass. This offered lower friction of the nut on the lead screw and meant that the nut would be the wearing part. These modifications are shown in Figure 37.

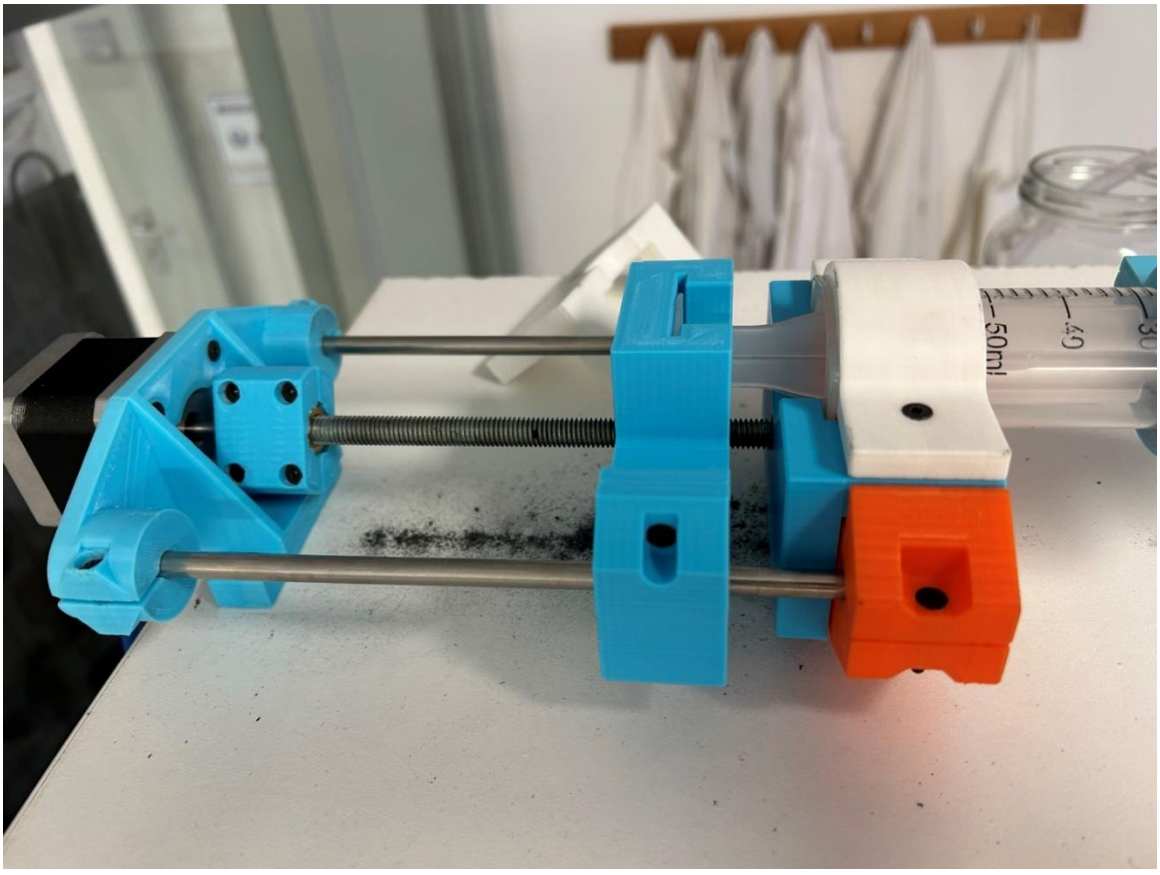

Figure 37: *Gel syringe pump assembly with M8 hardware. Note black dust below the screw from damaged M4 hardware.*

Tests 5 through 7 moved on to the more viscous 3 g/l Carbopol gel. The higher viscosity required a more considerable pressure difference, resulting in a significant vacuum pressure on the inlet hose during suction strokes. The magnitude of the suction was severe enough that the flexible tubing between the pump and the reservoir collapsed to a nearly flat ribbon on suction strokes, negatively affecting the quality of pumping. Any fitting joints that may not have allowed air in previously could also have allowed air into the pump under such a vacuum, negatively affecting pumping. These negative factors are shown in Figure 38.

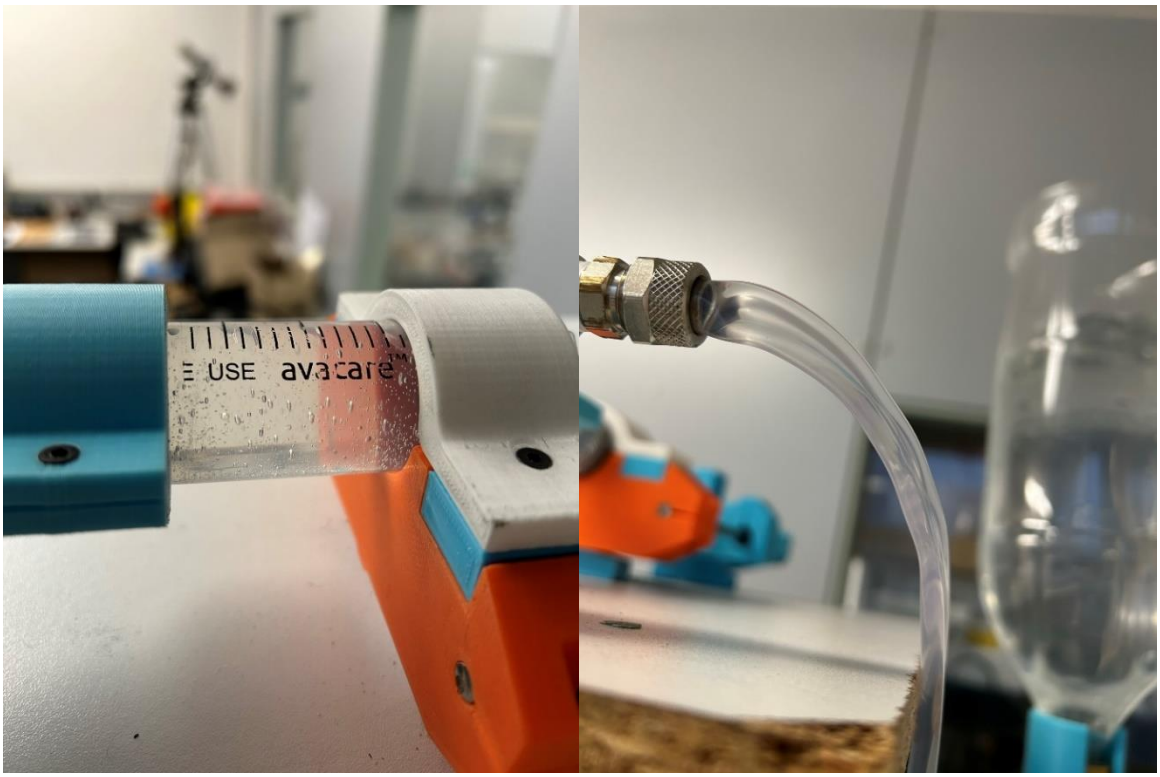

Figure 38: *Void formation in the pump and the flexible tubing "ribboning" in the gel syringe pump.*

After disassembling and rebuilding the pump to ensure all fittings were more resistant to leaking and replacing the 8 mm internal diameter flexible tubing with 10 mm internal diameter reinforced hose between the pump and the reservoir, Test 6 performed the best of all the tests so far, even exceeding the results from Test 1 which was using water.

The tests showed that more viscous gels are more likely to retain their shape and make an empty "funnel" to the tube's inlet to the pump, allowing air to flow into the pump. The possibility of air being sucked into the required diligent monitoring of the gel reservoir and moving the inlet periodically to avoid the pump sucking air. Monitoring the pump became impractical for longer prints, so the decision was made to refine the reservoir to the current design. The old reservoir consisted of a glass jar containing the support gel, with the inlet tube entering the jar through the top and the tube's inlet placed at the bottom. The old design can still be seen in the top right of Figure 37. In Test 6, a new reservoir was used, consisting of a 2-litre soft drink bottle, as shown in Figure 39. Switching to a bottle was done since the tall, thin shape and the bottle's narrow neck allowed most of the gel to flow out of the reservoir before air would be drawn into the pump.

Figure 39: *The new gel reservoir.*

Test 6 still showed some air bubbles in the syringe barrel. These bubbles were theorised to be coming from the air in the gel already before entering the pump and expanding under the vacuum inside the syringe. After every suction stroke, a 10-second dwell command was inserted to equalise pressure in the syringe. This modification yielded the best result yet and removed most of the bubbles in the syringe before every extrusion stroke.

A minor recurring issue is the plunger sometimes moving in small discrete movements on suction strokes instead of one consistent stroke. The cause of the small movements appears to be the flexible rubber plunger end sticking and unsticking to the inside of the syringe body instead of the stepper motor skipping, as the stepper motor is silent during these moves instead of making the loud clicking indicative of skipping.

Considering how well the syringe pump was performing at this stage. It was decided that gel extrusion would be handled by the syringe pump instead of the peristaltic pump.

6.3.3. Gel syringe pump low flow rate compensation

At low flow rates, the gel syringe pump was found to under-extrude. Testing was done to investigate a more appropriate flow multiplier at low flow rates. Since the non-return valves in the flow path heavily affect the gel deposition rate, it was thought that it would be acceptable to measure the gel output directly after the outlet non-return valve. As will be seen, this was not sufficient.

A digital scale was used to measure the gel output mass of the pump after each test run. To calculate a more appropriate flow rate based on the weight measured by the scale, the relation between the distance the syringe plunger moves and the weight measured was determined. Equation 6-3 was used to relate the mass extruded and the distance the plunger was depressed:

$$m = \rho D \pi \frac{{d_s}^2}{4} \tag{6-3}$$

Where m is the weight of the extruded material, ρ is the density of the extruded material, D is the distance the syringe plunger moves, and d_s is the internal diameter of the syringe. In this case, the density of the gel is 1027 kg/m^3, and the internal diameter of the syringe is 28.6 mm. A range of values for the plunger distance was used from 5 to 30 mm in increments of 5 mm. Table 4 was generated using the information stated previously:

Table 4: *Theoretical output weight against the extrude distance of the piston pump.*

Distance [mm]	Theoretical output weight [g]
5	3.3
10	6.6
15	9.9
20	13.2
25	16.49
30	19.79

Knowing this, the real outputs from the tests were compared, and the pump performance was assessed, as shown in Table 5. Tests were put in order of theoretical output mass since they showed a relationship demonstrating the pump's performance dependence on the mass output per an extrusion command.

Table 5: *Comparison of the theoretical and the real output of the piston pump*

Test #	Real output mass [g]	Theoretical output mass [g]	Output fraction [%]	Notes
1	0.35	3.3	10.61	
4	0.3	3.3	9.09	Increased flow rate
2	2.61	6.6	39.56	
5	2.16	6.6	32.74	Small initial extrusion
3	5.13	9.9	51.84	
6	7.66	13.2	58.05	
7	10.5	16.49	63.66	
8	13.1	19.79	66.18	

From Table 5, it may be seen that the pump performs better as the demanded output mass increases, and therefore, the plunger stroke distance increases. The varying output fraction shows that a flat flow multiplier is insufficient to correct the real output of the pump at low flow rates.

All the results, apart from Tests 4 and 5, only tested the effects of increasing the plunger distance. Test 4 investigated the effect of increasing the extrusion rate, which showed little difference in the extrusion amount at the tested rates. Test 5 investigated whether extruding an initial amount before extruding the rest of the material would improve performance by giving the non-return valves in the pump more chance to open. Unfortunately, the resulting pump's performance was 6.82% worse, and that line of inquiry was abandoned.

Knowing from previous tests that no material was generally extruded below a plunger distance of about 3 mm and that over a 90 mm plunger distance, the pump extruded 91.27% of the expected amount, the plot in Figure 40 was generated.

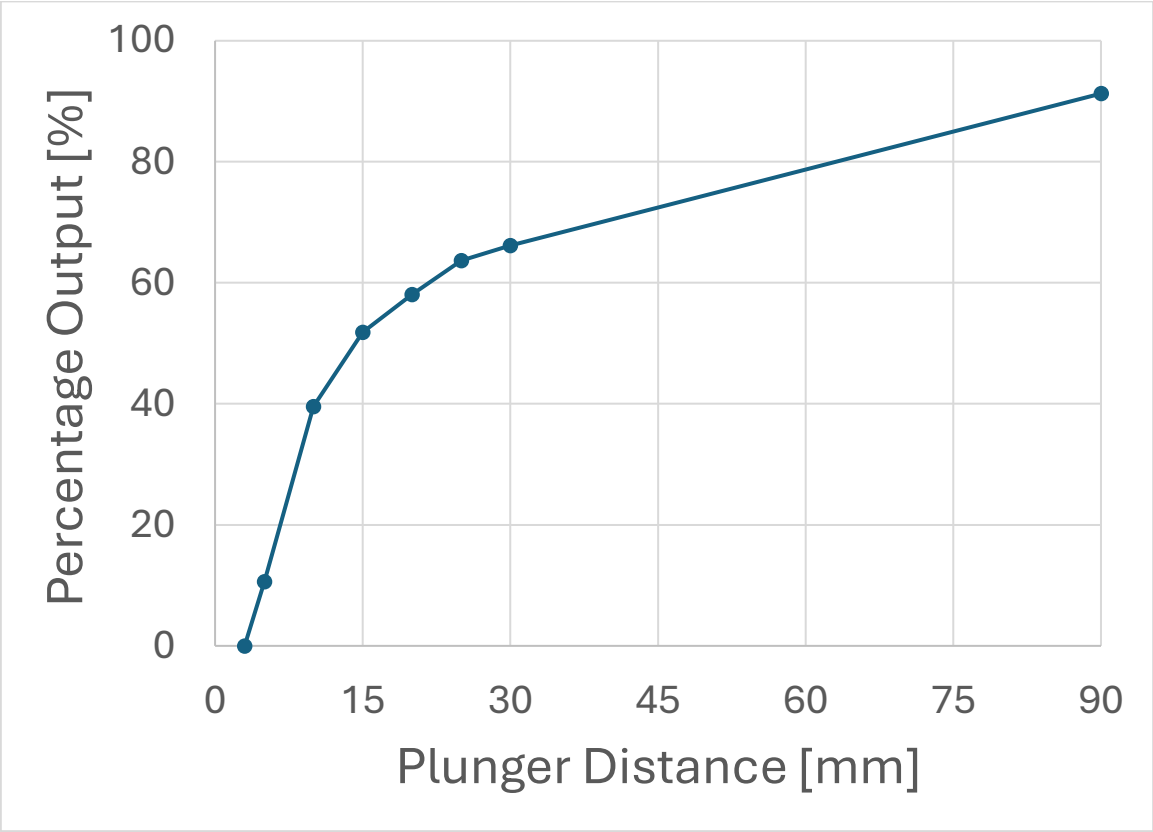

Figure 40: *The real output of the piston pump as a percentage of the theoretical output plotted against the extrude distance of the pump.*

Figure 40 shows that a simple flow multiplier would not work for this gel for all extrusion amounts. To make a relation that would work for extruding gel at a low flow rate, it was necessary to alter the equation for the mass of material extruded for a given plunger distance and make the plunger distance the subject of the equation as has been done in Equation 6-4:

$$D = \frac{4m}{\rho \pi {d_s}^2} \tag{6-4}$$

Using Equation 6-4 to calculate equivalent output plunger distances from the real output distances, Table 6 was generated:

Table 6: *Comparison of the requested distance against the equivalent real output extrude distance of the piston pump.*

Requested Distance [mm]	Real output weight [g]	Equivalent output Distance [mm]
5	0.35	0.53
10	2.61	3.96
15	5.13	7.78
20	7.66	11.61
25	10.5	15.91
30	13.1	19.86

With this data, Figure 41 was created:

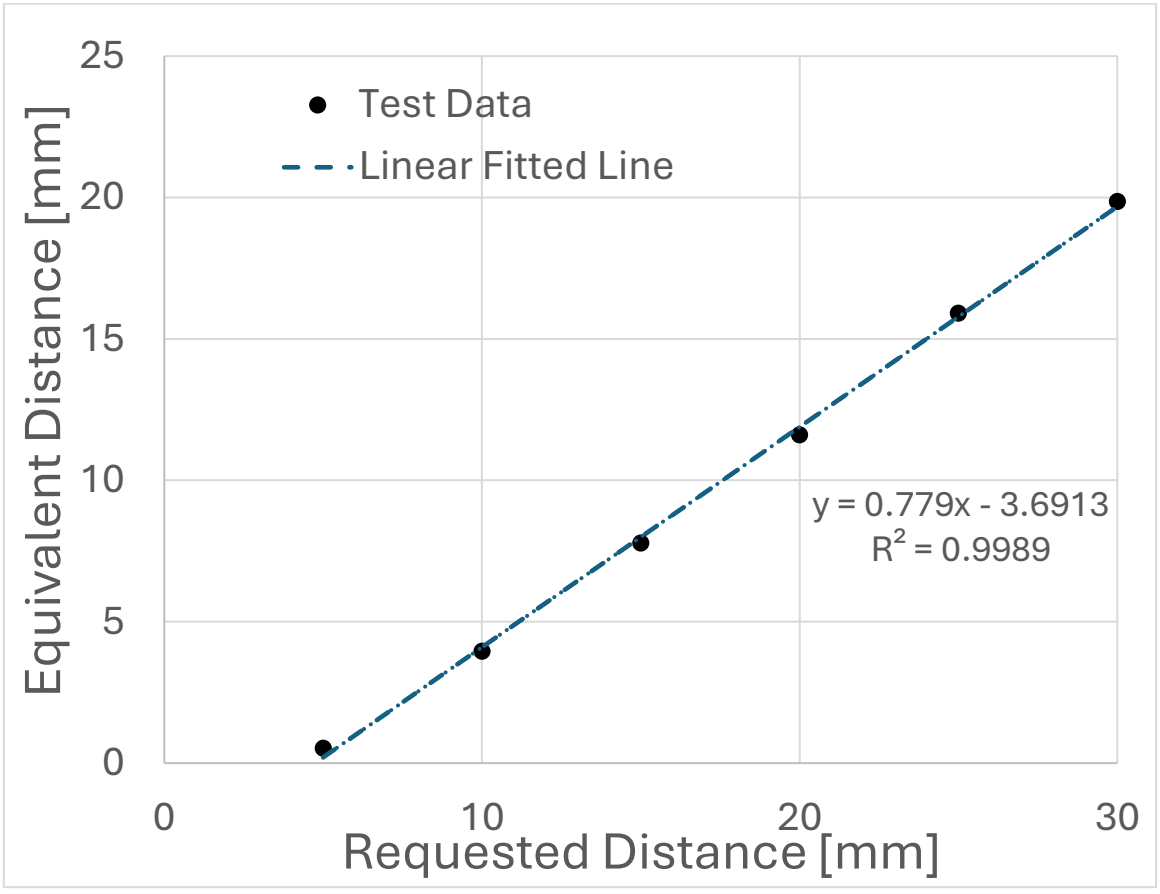

Figure 41: *The relationship between the equivalent extrusion distance and the requested extrusion distance of the piston pump.*

Figure 41 includes a linear fitted line with an R^2 value of 0.9989, which shows that in the range of 5 to 30 mm of plunger distance, one may use this equation representing the line to predict the output of the pump if given a requested distance. Noting that the x-axis on the above plot is the requested distance and the y-axis is the equivalent distance, making the x variable in the equation, the subject will give an equation for adjusting a desired distance to a required distance:

$$d_r = 1.2837 d_d + 4.7385 \quad For\ 5\ mm \leq d_d \geq 30\ mm \tag{6-5}$$

d_r and d_d, in this case, are the required and desired distances, respectively. Note that a positive intercept on the requested or required distance axis shows that the syringe pump must extrude some distance to open the non-return valve. With all this known, this equation for the required distance may be used to adjust the pump output accurately to deposit gel as needed.

The gel pump's output was adjusted by the required distance equation as defined above, with some improvement in the quality of the gel extrusion. Still, some under-extrusion was observed. The under-extrusion was significant enough that another round of testing was performed, this time measuring the output of the complete gel deposition system as it would be assembled during printing. Testing with the full assembly yielded the data in Table 7:

Table 7: *The new piston pump output results after considering the entire gel deposition system.*

Requested Distance [mm]	Real output weight [g]	Theoretical output weight [g]	Equivalent output Distance [mm]
5	0.088	3.3	0.13
10	1.64	6.6	2.49
15	3.73	9.9	5.65
20	5.65	13.2	8.56
25	7.57	16.49	11.47
30	9.52	19.79	14.43

Poorer performance resulted from the full assembly tests when compared to the gel pump output data set. The new data shows that one should consider the entire system as it would be during printing. Similarly to before, the data can be shown to be linear between the requested distances of 5 and 30 mm. A new equation for the desired and required distance was generated:

$$d_r = 1.7268 d_d + 5.2029 \quad For\ 5\ mm \leq d_d \geq 30\ mm \tag{6-6}$$

A comparison of the two output curves was done to determine if the new equation was significant enough to have caused the under-extrusion, as shown in Figure 42:

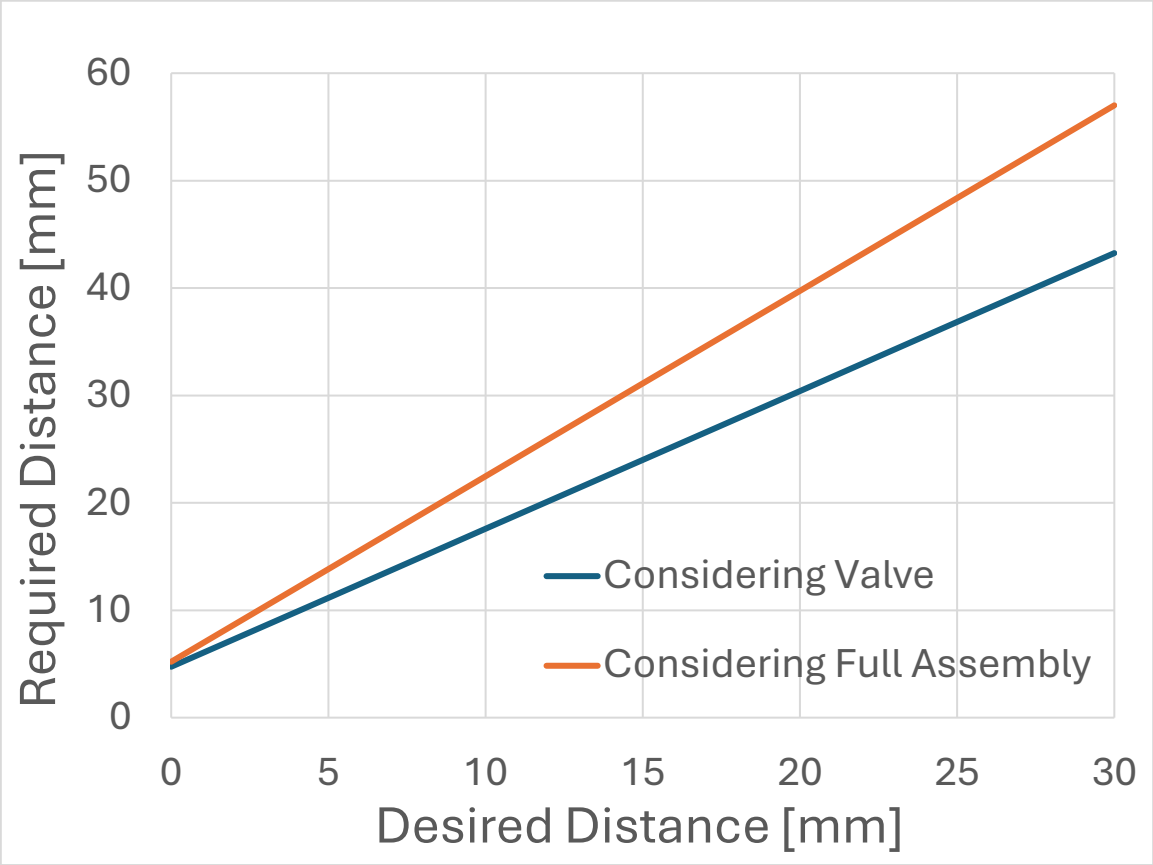

Figure 42: *Comparison of the lines fitted for the piston pump output considering just the valve and the full gel deposition system.*

Note that at a desired distance of 10 mm, the difference between the required distances is 21.8%. Thus, the two equations differ significantly. With this known, the extrusion should improve with the equation considering the entire assembly.

At a later testing date, while printing, the gel pump was found to be over-extruding gel. This was traced to the latter batch of gel having a lower viscosity due to its being made using de-ionised water instead of distilled water.

The switch from distilled water to de-ionised water was due to a brief period in which the water distiller was non-functional, and de-ionised water was a readily available alternative. The pH between the distilled water and the de-ionised water differed subtly. The gel was prepared using the quantity of neutraliser from a previous bath without confirming the pH, which resulted in the later batch having a different final pH and viscosity. This small change seemed to have changed the rheological properties enough that the effects were noticeable over a print taking more than an hour.

New data was collected in the same manner as previously collected and is shown in Table 8:

Table 8: *The new piston pump output results after using the de-ionised-water-based gel deposition system.*

Requested Distance [mm]	Real output weight [g]	Theoretical output weight [g]	Equivalent output Distance [mm]
10	1.23	6.6	1.86
20	5.82	9.9	8.82
30	10.76	13.2	16.31

As has been done previously, a new desired versus the required distance equation can be generated:

$$d_r = 1.384 d_d + 7.548 \quad For\ 5\ mm \leq d_d \geq 30\ mm \tag{6-7}$$

One may then generate Figure 43 comparing this equation against the previous one using the gel prepared from distilled water instead of de-ionised water:

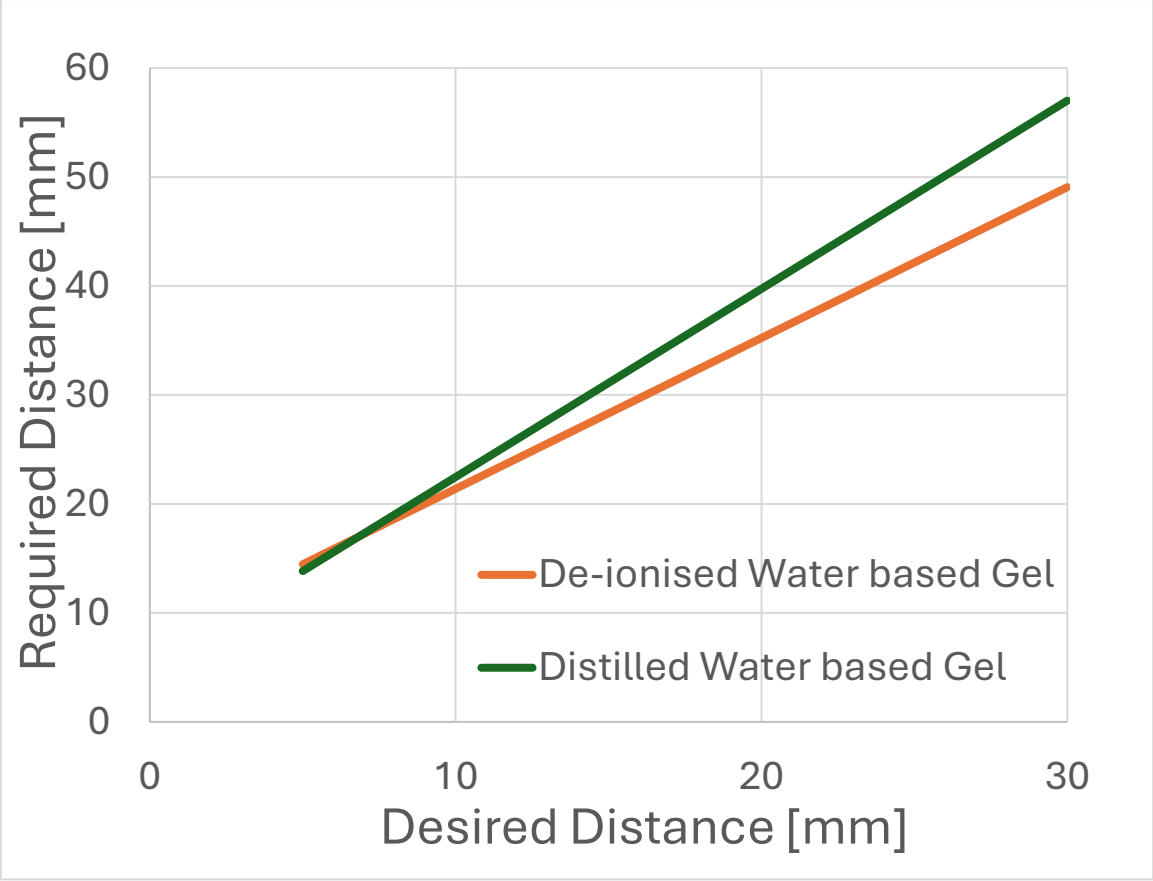

Figure 43: *Comparison of the lines fitted for the piston pump output comparing the use of de-ionised and distilled water in the making of the gel*

From Figure 43, at a desired distance of 10 mm, a difference of 4.82% can be observed. A typical layer of gel can easily require extrusion distances of gel closer to 20 mm. A difference of 11.35% can be seen when comparing the two required distances at a desired distance of 20 mm, which can explain the over-delivery seen.

In summary, it has been found that when one is extruding support bath material using a syringe pump, some consideration must be made to adjust the flow rate depending on the length of the stroke. On longer strokes, little compensation is required; on shorter strokes, much more compensation is needed. The entire flow path of the support material and any subtle changes in the properties of the support material will also affect the amount of compensation.

6.4. Co-axial gel nozzle design

Initially, the gel nozzle's design was a simple nozzle that took the gel from the tubes coming from the gel piston pump and funnelled that gel out the centre of the nozzle onto the already deposited support gel. A problem with this design became evident when attempting to fill a container with gel. The nozzle could not deposit gel all the way to the edges of the container for each layer.

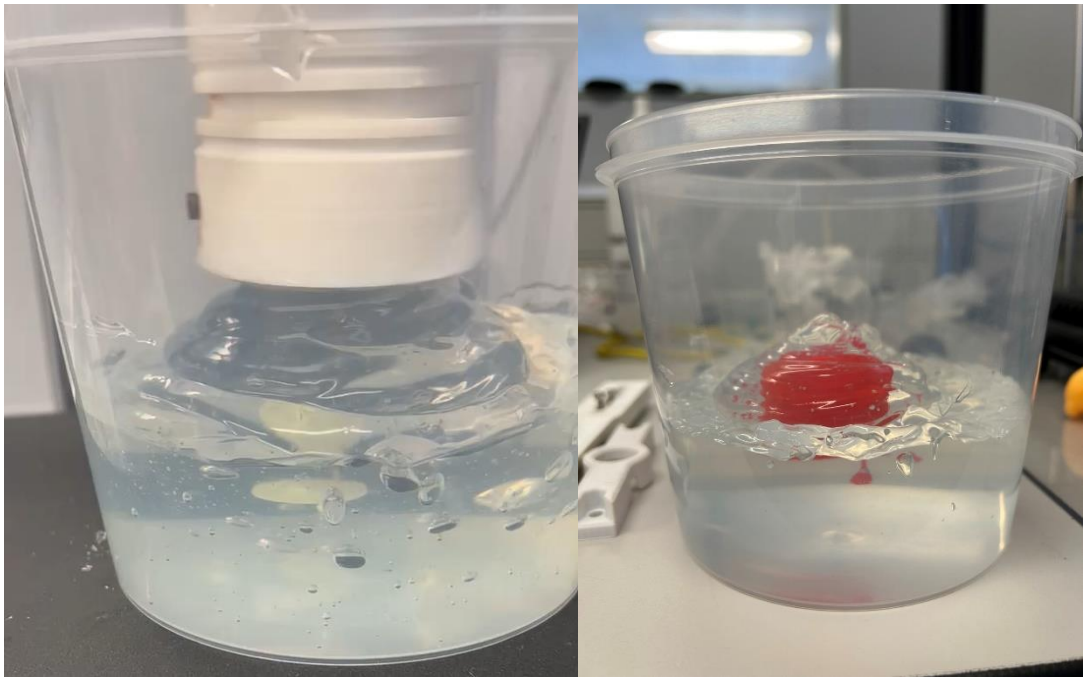

Figure 44: *The initial nozzle design and the resulting domed shape of the deposited support gel*

To solve this problem, updating the gel nozzle design became necessary. To this end, considerations were made to a few different options, as shown in Figure 44. One could enlarge the nozzle to the point where the bottom of the lower ink-gel extrusion assembly was entirely open. Another consideration would be to remove the nozzle and perforate the bottom of the lower ink-gel assembly, similar to a salt and pepper shaker. Both these options would remove the ability to shut the nozzle when gel deposition was not desired. A perpetually open gel nozzle would pose a problem for thinner support gels, which would be able to evacuate the tubes into the support bath unpredictably, unlike thicker gels, which will remain in the tubes without a seal.

Another solution would be to use an annular nozzle. An annular nozzle would allow the gel to be deposited all the way to the edge of any container the nozzle could fit within. However, some difficulty arises when configuring the software required to operate 3D printers. This software assumes a more conventional nozzle, meaning one must be mindful of this during configuration. The nozzle options detailed here are shown in Figure 45.

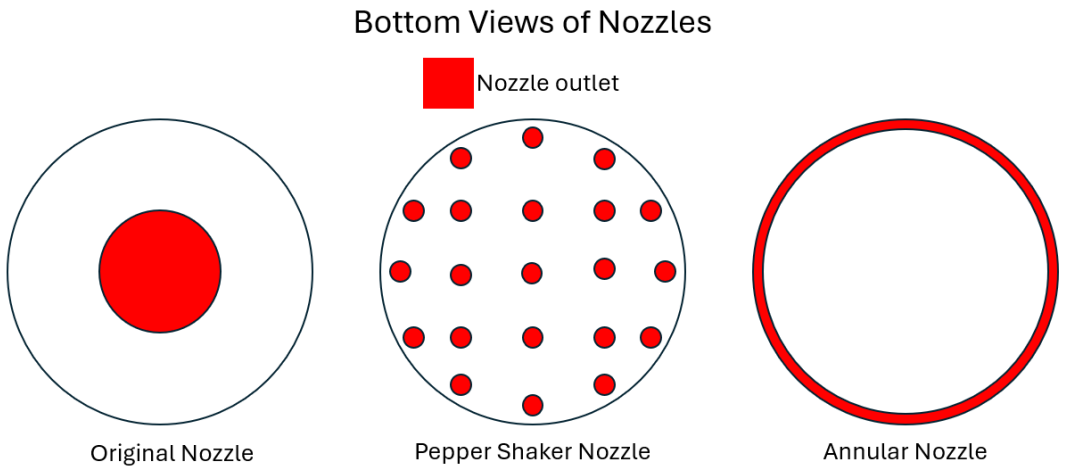

Figure 45: *Some possible nozzle designs as seen from the bottom*

In the slicer and other software, one can configure the annular nozzle as a large conventional nozzle with the same diameter as the lower ink-gel assembly. In this project, that would be 60 mm. Since one is not using a traditional 60 mm nozzle, the flow rate must be reduced to match the appropriate flow rate for a conventional nozzle with the same cross-sectional area of the outlet of the annular nozzle.

Some calculations were done, as detailed in Appendix D.11, to calculate the required flow modifier to implement in the slicer software to deliver gel in a manner that best suits an annular nozzle. This modifier was calculated to be 15.9%.

6.5. Accounting for the non-cylindrical print volume

While printing gel within a container, it became apparent that filling that container to the edge is essential. The printed gel will eventually become dome-like if the container is not filled to the edge. The printed material may begin to sag as the dome flattens out to fill the container within which the gel is printed.

Simple plastic containers usually do not have walls perpendicular to their bases. These containers often have what is called a "draft angle" to aid in their removal from moulds. This draft angle further complicates filling the container as the cross-sectional area that must be filled with each layer increases.

There are two ways (illustrated in Figure 46) to address the issue of the increasing cross-sectional area. The more complicated way is to automatically detect the dimensions of the printed layer and adjust the printed amount accordingly. The more straightforward but less accurate way is to print the same amount for each layer to fill out an unchanging area, hoping that the amount lost to fill the edges will not affect the overall quality of the print.

Automatic detection is done in FDM printing, where the printed plastic is solid until it melts at the nozzle and can be extruded accurately enough for that application. 3D printing gels have proven somewhat more challenging than initially thought. Automatic detection requires small amounts to be extruded as needed. Trying to do this with the current assembly of the syringe pump, non-return valves, tubing and nozzle has shown that this is ineffective and leads to severe under-extrusion. With this in mind, the more straightforward approach was tried first.

An approach of extruding all the material needed for a given layer at the beginning of the layer and then spreading it to deposit gel was tried. Simply taking the radius of the bottom of the container and the layer height and extruding enough material to fill out a cylinder with that radius and layer height had some success.

However, some issues were still experienced with the flatness of the top layer of the gel since the container required increasingly more material to fill out each layer as it had a draft angle, as mentioned before. Not accounting for the draft angle made the gel's dome shape progressively worsen as printing continued.

The gel could be modelled as a truncated cone like the inside of the container being used and extruding enough gel, just like the automatic solution requires. Modelling the truncated cone was done, but it was tested to see if an average amount of gel would work well enough to ensure good print quality. The logic behind this approach was that the errors would cancel one another out by the end of the print by initially over-delivering gel and under-delivering gel towards the end of the print job.

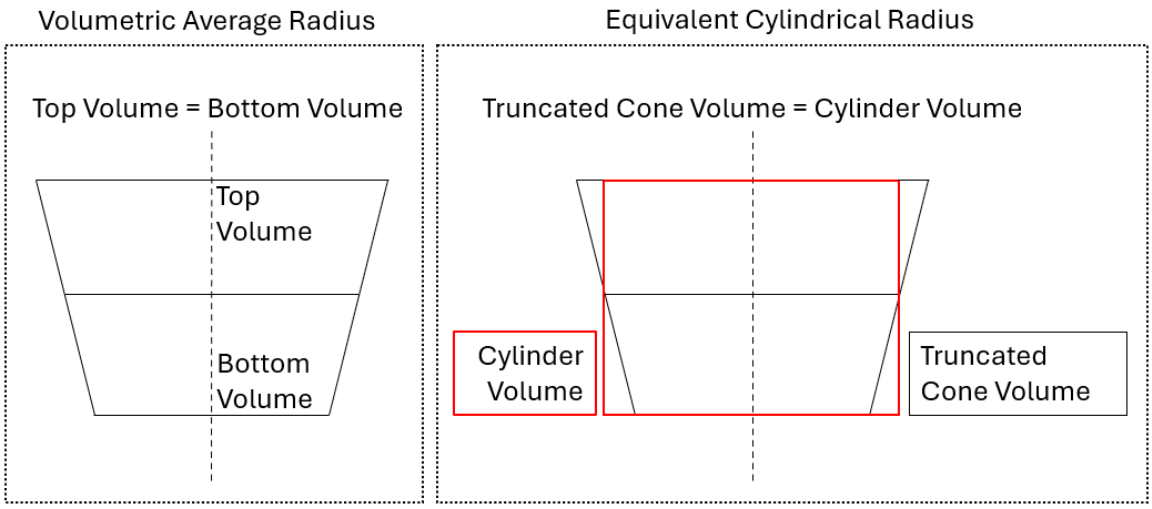

Figure 46: *The two different methods for finding the radius for calculating the required amount of gel to be extruded per layer.*

The first method investigated was the volumetric average radius method. This method calculates the point at which the volume above and below that point would be equal if one were to split the truncated cone being printed. The second method investigated is called the equivalent cylindrical radius method. This method makes the volume of the truncated cone being printed equal to the volume of a cylinder with the same height as the cone.

The calculation of the volumetric average radius and the equivalent cylindrical radius methods are investigated further in Appendix D.6.

Of the two methods, the equivalent cylindrical radius method is most likely to best suit this application. The equivalent cylindrical radius method will ensure that the gel support material should end with a flat top surface, albeit with some over-extrusion before then. This conclusion was borne out in testing, resulting in even top gel layers, as seen in Figure 47.

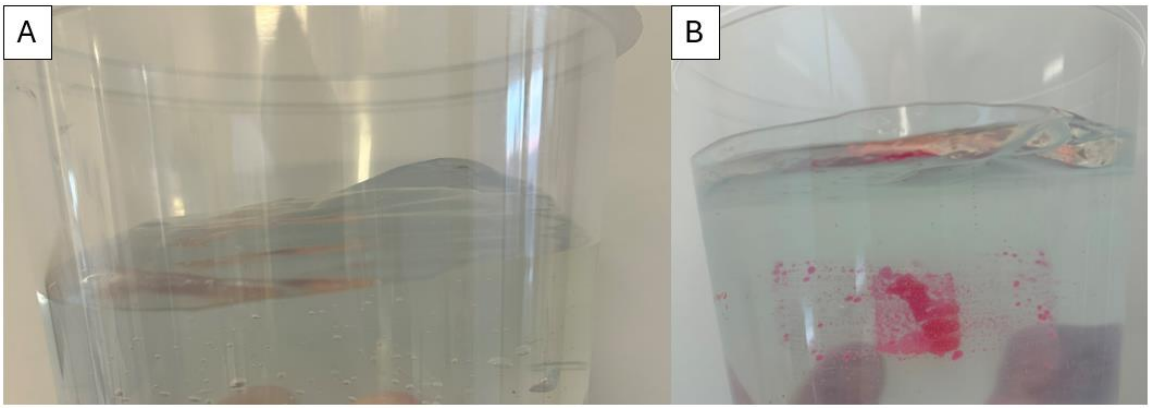

Figure 47: *Before the equivalent cylindrical radius method (A) and after it had been used (B). Note the domed top layers in A against B, where gel has been deposited all the way to the edge.*

6.6. Embedded 3D printing results

Much of the work discussed in Sections 6.2, 6.3 and 6.4 was done concurrently with the testing done in this section. This section focussed on resolving the issues related to the delivery of the support gel as results from testing were generated from embedded 3D printing using the DIGEX print head, seen in Figure 48.

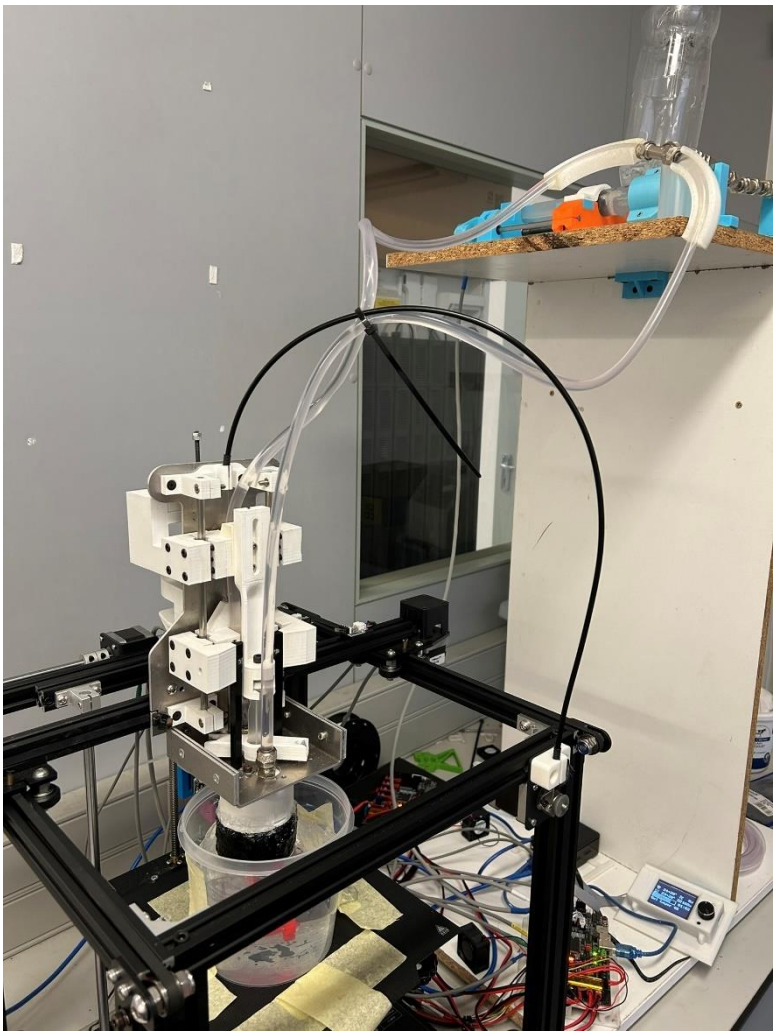

Figure 48: *The DIGEX print head and gel syringe pump in use on the embedded 3D printer.*

A cylinder with a height and a diameter of 20 mm was decided on for the tests as it could feasibly be printed within 90 minutes while being tall enough to test if the gel deposition system was performing adequately over the whole printing process.

Initial testing was done with generic store-bought custard for the reasons stated in Section 4.1. These tests went well, although custard does not cure in the way silicone does. The parts printed using custard would begin diffusing through the print volume and distort the part's shape, as seen in Figure 49, making further analysis much more difficult. The distortion of the custard part indicates that it may be essential to deposit even layers of support gel, as uneven layers may settle over time and distort the part underneath.

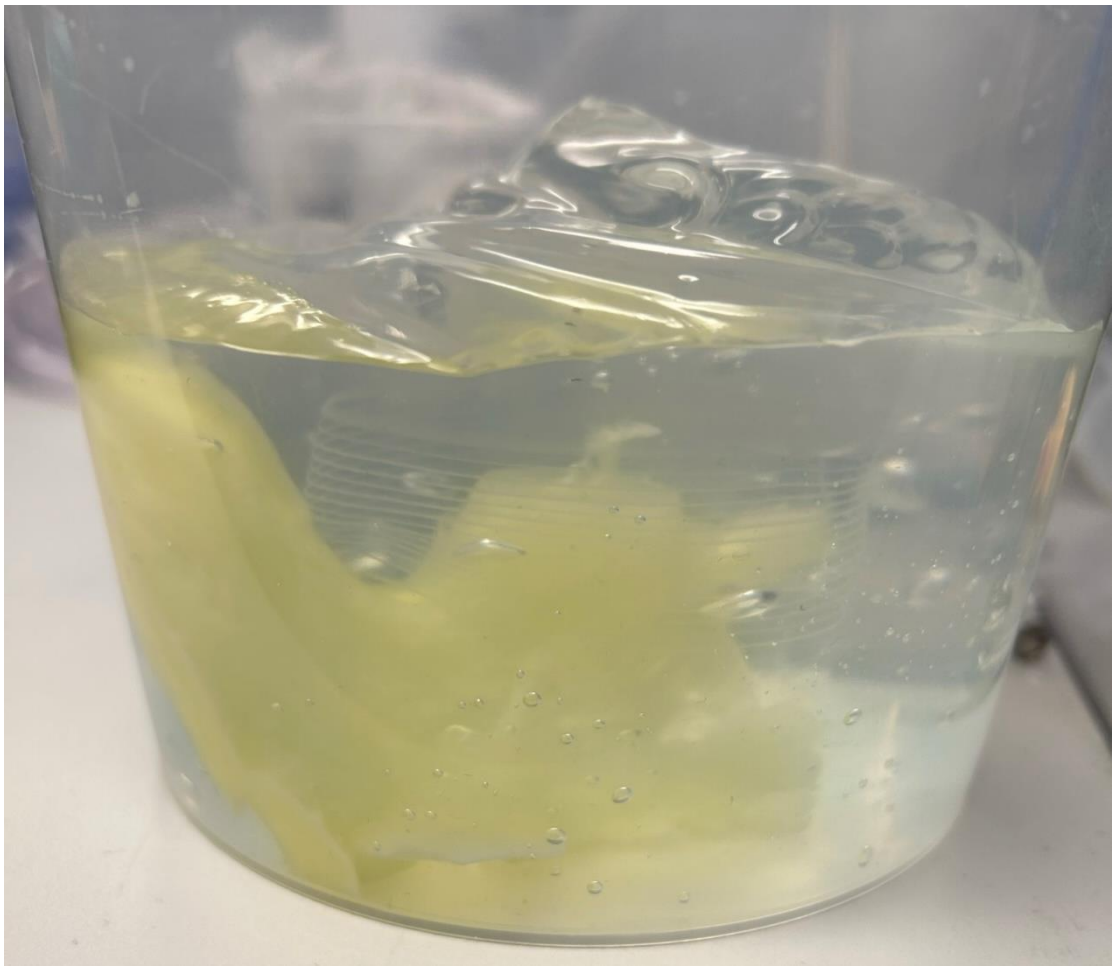

Figure 49: *The custard failed to maintain its as-printed shape after printing*

The behaviour of custard in the support gel meant that curing ink material should be used to truly investigate the output of the embedded 3D printer so that the printed part can be extracted and inspected. Initial testing was conducted with Ecoflex 00-30, but a working time of 45 minutes for this material made testing difficult. A switch to Sylgard 184 was made since it had double Ecoflex 00-30 working time with similar properties.

Initially, the ink deposition system appeared to perform well, while the gel deposition system appeared to underperform. An investigation was conducted to determine the causes of this poor performance. The most probable causes were nozzle shape, void and bubble formation in the pump and inconstant flow.

The solution for the nozzle shape was to switch to an annular nozzle to deposit material throughout the print volume in a way that could not be done with a traditional nozzle design. The second cause of poor performance required some time to allow pressure to be equalised in the pump after extrusion and retraction strokes so that any voids could collapse and the non-return valves could be in a predictable state. The final cause required testing of the low flow rate behaviour of the pump when pumping through the entire flow path the gel would take during regular embedded 3D printing.

Once the gel pump performance was improved, a critical eye could be turned to the ink deposition system. Since the ink deposition system is much simpler than the gel deposition system, any non-mechanical problems can likely be attributed to chemical or slicer issues. At this late project stage, the decision was made to focus on slicer issues.

Initially, an ugly scar was formed where the needle would leave the printed part to begin printing the next layer of the support gel. The gel layers' start locations were randomised to reduce this 'seam' on the walls of the printed part. The trade-off was made for lighter strings, leaving the printed part instead of one large, stretched seam. The seam scar and the lighter stringing can be seen in Figure 50.

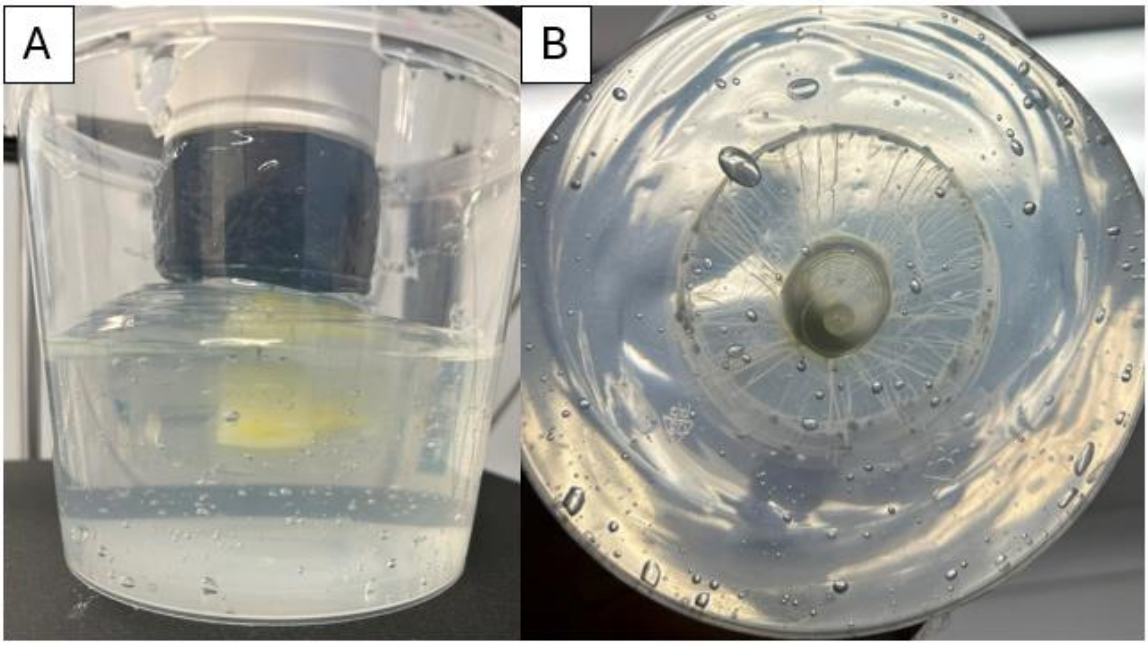

Figure 50: *A shows the seam on the right side of the part because the layer starts and ends always in the same place. B shows fine stringing of the part material during printing but lacks the large seam.*

Reducing the seam made another problem even more apparent. This problem was the tendency of the ink to form droplets instead of discrete lines during printing. From the literature [40], it was recommended that one should increase the feature size to avoid droplet breakup. First, the layer height was increased with little effect. To further increase the feature size, a 17-gauge was used instead of an 18-gauge needle, which resulted in some improvement.

Testing was done to see if increasing the flow rate of ink would yield better results. After each ink layer was printed, the ink's flow rate was increased by 1% in the slicer software, sweeping from 100% to 139%. The increase in flow rate did not ultimately yield a noticeable improvement.

A switch was then made to a 14-gauge needle. The larger gauge needle immediately yielded improvements, but the printed lines would still slowly break up in the seconds following deposition. An attempt was made to print multiple adjacent walls to increase the features' size before droplet breakup. These adjustments, coupled with some other improvements like a small, thin tower offset from the printed part, where the ink needle could dwell immediately after an ink layer has been printed while waiting for the gel layer to begin and printing a small skirt around the bottom of the part, significantly improved printed part quality, see Figure 51.

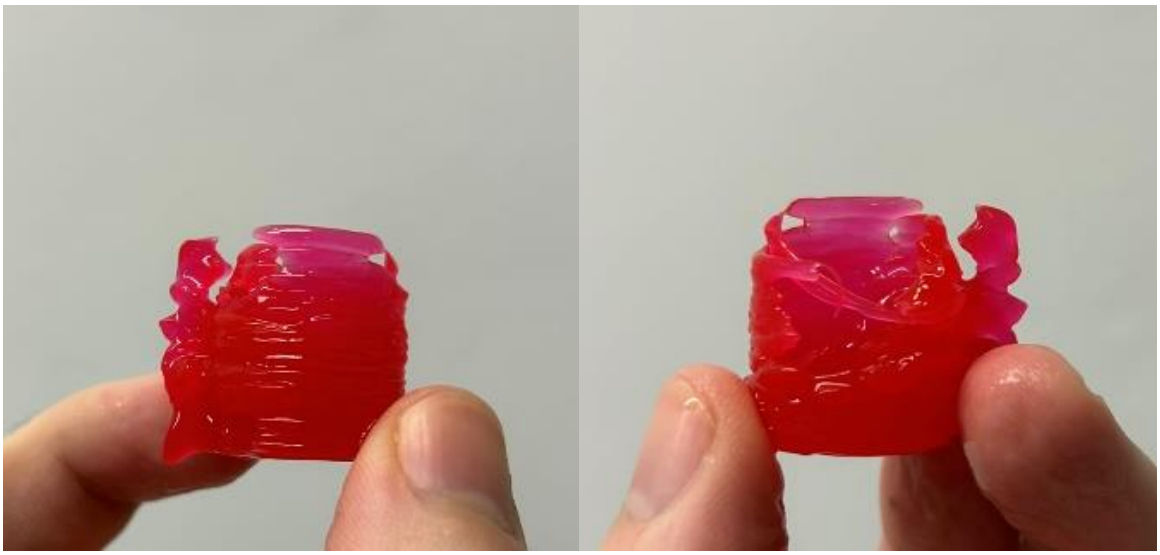

Figure 51: *Extracted embedded print with multiple printed walls and the dwell tower still attached.*

Considering that the deposited material tends to form a circular cross-section instead of the ideal rectangular cross-section, a layer height equal to the printed line width was investigated. However, poor interlayer fusion resulted with a step backwards in overall part quality when tested.

In hindsight, one may say that the result shows that consideration should be given to the neutral buoyancy of the ink in the gel. It is standard practice in FDM 3D printing to print layers at a height of half their nozzle diameter to ensure overall good part quality. One of the benefits of this is that the molten plastic material is forced onto the previously printed material. The complication in embedded 3D printing is that neither the support gel nor printed ink are rigid, so there is insufficient resistance when trying to "squeeze layers together". In the case of 3D printing material with a circular cross-section, using traditional slicer techniques, only a tiny portion of the edges of the printed material will touch adjacent part material, ensuring poor inter and intralayer adhesion in this case. To provide better adhesion in the part, one is tempted to over-extrude a small amount and force more overlap between layers. An attempt at this was made by increasing the flow multiplier by the ratio of a square over a circular cross-section, $4/\pi$, which equals 127.3%.

It was also observed that some under-extrusion occurred at the beginning of each ink layer due to the oozing of ink out of the needle tip between printing ink layers. An attempt was made to fix this by printing a 'draft shield' around the printed part. A draft shield is often used in FDM 3D printing to maintain a more homogeneous air temperature around the printed part during printing to avoid warping due to uneven heat distribution through the part. In practice, it looks like a skirt around each printed layer.

Testing these two modifications to the slicer configuration unveiled that although better adhesion could be seen in the printed part, the draft shield highlighted the need to manage the twisting of the support gel. As the printed ink and gel were always deposited clockwise, the subsequent printed layer exerted clockwise torque on the previous layer. This resulted in a visible twist of the part after several layers. The amount of twist was roughly proportional to printing speed. The ink printing speed was reduced, and the walls were printed in alternating directions to minimise twisting. The draft shield was replaced with a prime tower to refill the needle nozzle with ink before each layer. These adjustments resulted in a good, albeit rather bumpy part, as seen in Figure 52. Unfortunately, after curing, the part did not survive extraction from the support bath.

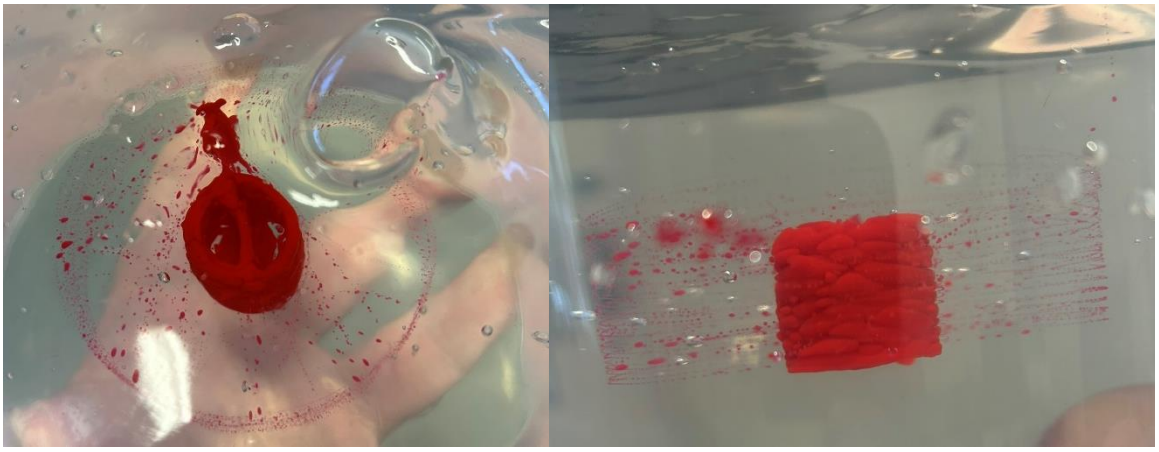

Figure 52: *Top and side view of the printed part with random layer starts and alternating wall printing directions*

Since many of the part defects were related to extrusion issues, an attempt was made to investigate the effects of retraction distance on the quality of the print. To this end, a retraction tower was printed (Figure 53), which increased the retraction distance by 0.2 mm for every ten layers of ink printed, starting at a distance of 0.1 mm and ending at 0.9 mm.

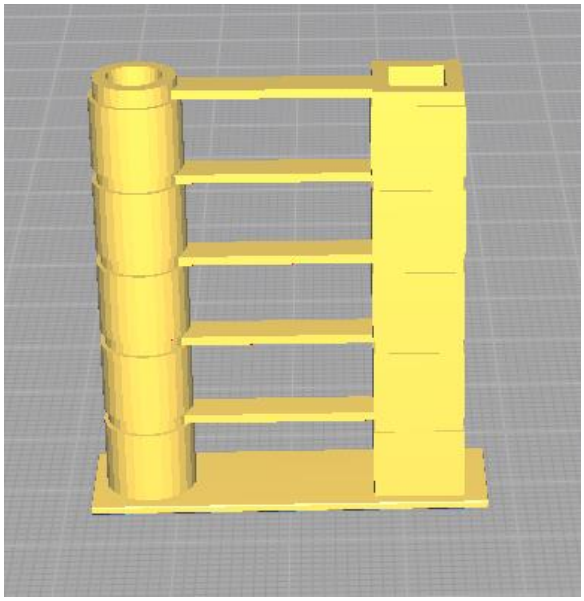

Figure 53: *A retraction tower, as seen in Cura, a 3D printing program*

This part was printed well enough that almost the entire part could be extracted and inspected, as shown in Figure 54. The part seemed to have retained the bumpiness as was seen before but was still recognisably a retraction tower. The round and square shape of both sides of the tower, the bridges between the two sides, and the base are all recognisable in the final part. The printed part also seemed to have a minimal twist up its length, showing that alternating the direction in which the walls are printed helped immensely in keeping the part stable. The previously mentioned bumpiness made it challenging to ascertain if any improvements were made by changing the retraction distance.

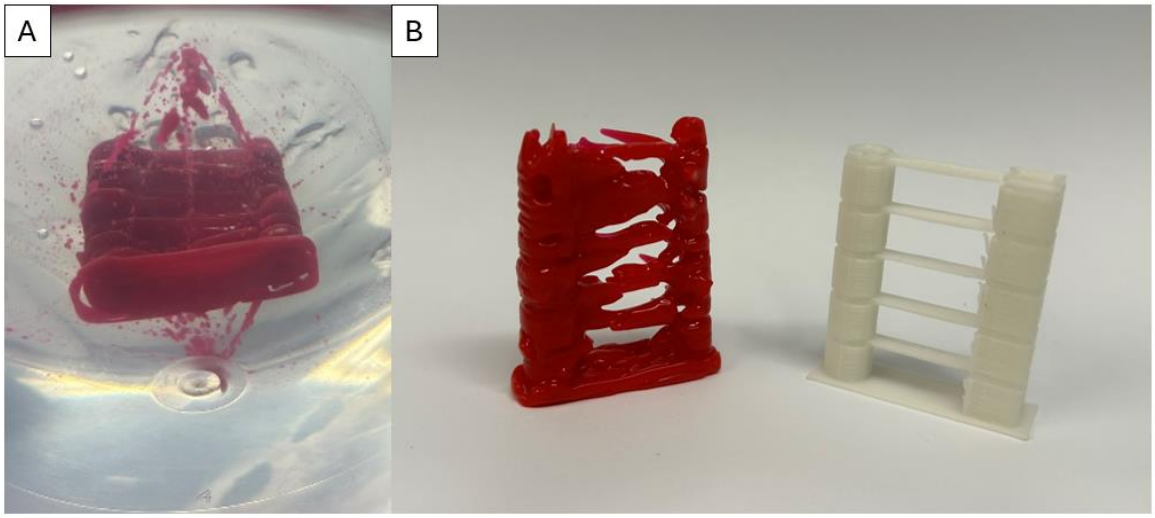

Figure 54: *The first attempt at printing a retraction tower. A shows the part in the support gel. B shows the extracted part next to an FDM printed part.*

Interestingly, the prints could display over-extrusion with the bumpiness seen but also under-extrusion with poor inter and intra-layer fusion. To investigate if this was a hardware issue related to inconsistent extrusion, two simple cylinders were printed as continuous spirals, and the extrusion flow rate was reduced to 100%. These prints can be done in less than 15 minutes and quickly show extrusion issues while depositing material quickly enough to prevent some droplet breakup.

The two cylinders printed well, as seen in Figure 55, with the difference being that one was printed with a solid base and one without. Despite the two cylinders showing poor inter-layer adhesion and droplet breakup, both could be extracted and inspected.

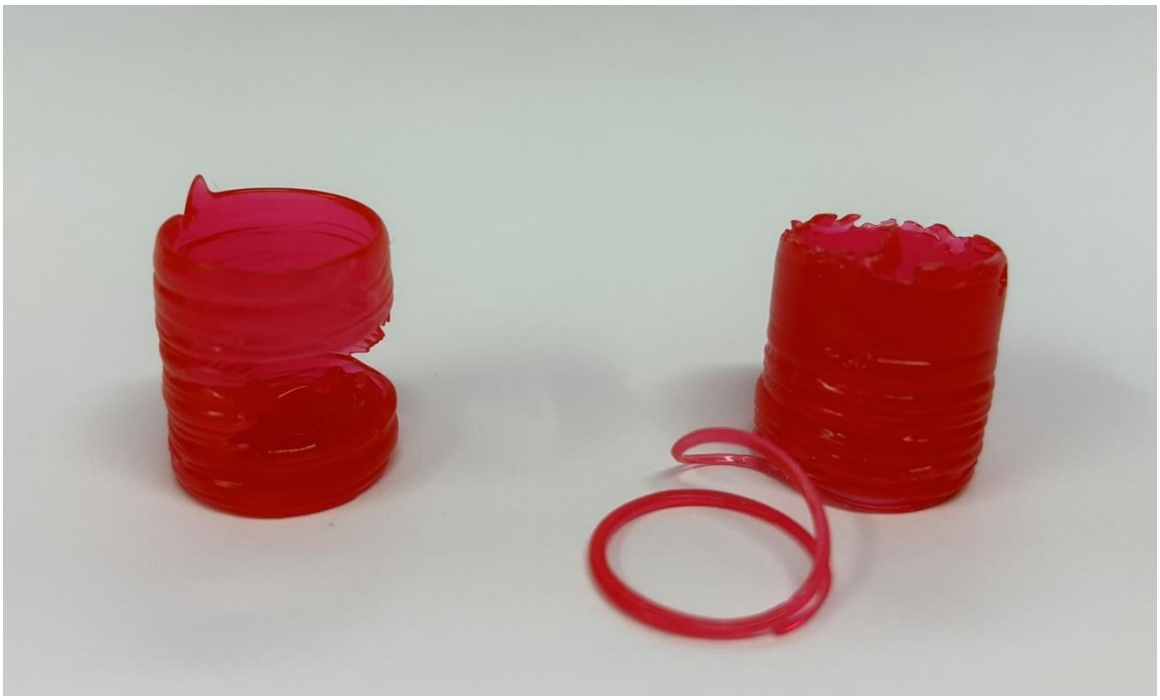

Figure 55: *The two spiralised cylinders. The cylinder on the left was printed with a base, and the cylinder on the right without.*

During printing, an interesting phenomenon was observed that seemed to explain the under and over-extrusion. In the trailing wake of the ink nozzle, the deposited ink would briefly stick to the side of the needle tip. This brief sticking to the needle tip left a thin ridge of ink that collided with the needle if it travelled over that deposited material and created blemishes, strings and the bumpiness previously seen. Additionally, as the material was drawn away from the recently deposited ink, the amount of ink pressed into the previous layers was reduced, resulting in poorer inter and intra-layer adhesion, shown in Figure 56.

Figure 56: *The wake behind the needle draws up material just printed and then forces that material down again when it next passes.*

Since the previous retraction tower was inconclusive in finding the best retraction and the spiralised cylinders printed well at 100% flow rate, another retraction tower was printed with the same settings but the flow rate also at 100%, shown in Figure 57. A larger prime tower was also placed in front of the print to ensure the nozzle was full for every layer. This print job was recorded, and the videos may be found in the following Google Drive:

https://drive.google.com/drive/folders/1mXSRrU1Rug7xi4EunPfRDUiUuODyCZJ4?usp=drive_link

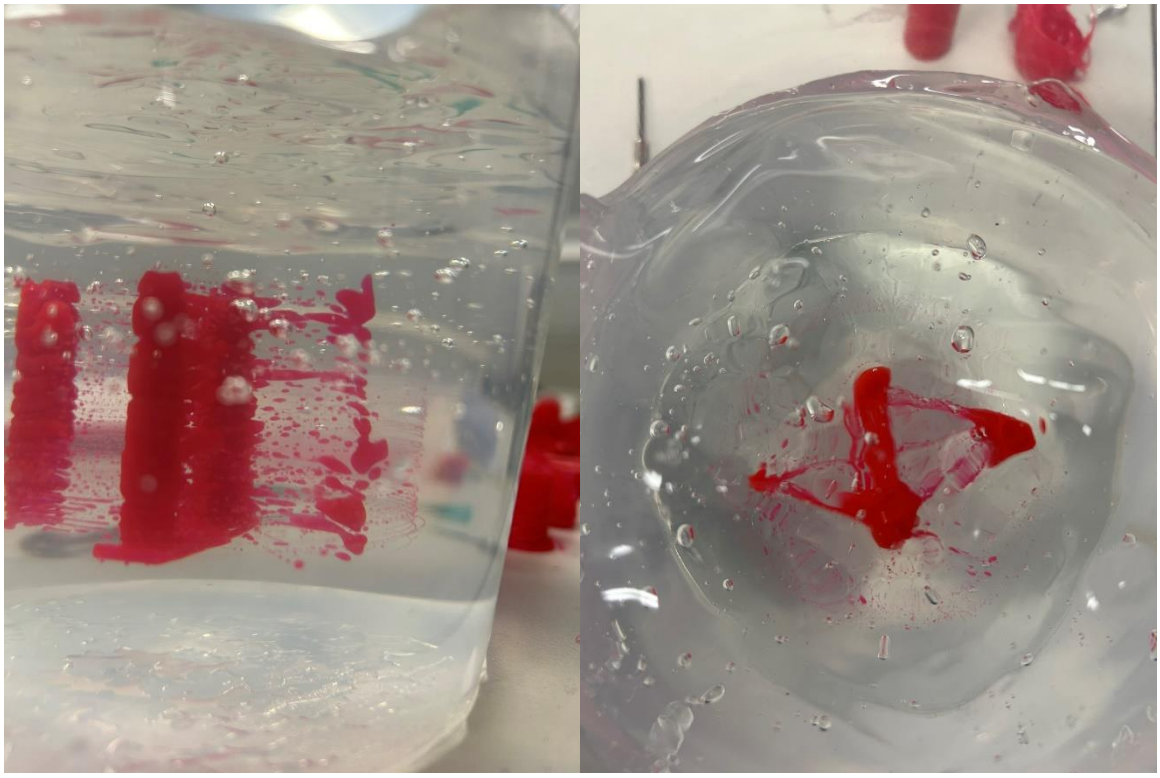

Figure 57: *The second retraction tower, with the thicker prime tower in front and the thinner dwell tower behind the part.*

The second retraction tower could be extracted, and some additional under-extrusion could be observed. It was decided that further experimentation with 3D printer settings and slicer variables was best left to another project to limit the impending scope creep.

One should note that better results may be had with different ink-gel pairings. The silicone ink used is highly immiscible in the Carbopol gel, which is water-based. Initially, having an ink-gel pairing that does not mix at all seems ideal, but after investigating these results, that may not be the case. This can be likened to trying to pour long chain, non-polar molecule filled fatty oils into a liquid like water with highly polarised molecules and the oil breaking up into droplets that float on the water's surface. It is outside this project's scope, but some investigation into whether allowing some mixing between the ink and gel may make for smaller minimum feature sizes, allowing the use of finer ink needles.

7. Conclusion

Referring to Section 1.1, this project aimed to alleviate the size constraints plaguing previous embedded 3D printer prototypes while maintaining the ability to achieve print quality similar to previous printers. The DIGEX print head has been demonstrated to effectively increase the build volume to nearly the entire printer build volume. Less success was had in achieving high print quality, but this may be attributed to the selection of the ink-gel pairing rather than the performance of the printer itself.

As steps along the way to achieving the aims laid out in Section 1.1, this project aimed to build a first prototype of an embedded 3D print system that could print larger parts by using alternating support gel/ink deposition. Additionally, this project aimed to overcome specific issues that previous embedded 3D printers have demonstrated. Namely, those issues are a reliance on bed-slinger type 3D printer designs and a need for long needles as ink extrusion nozzles. Further investigation was also made into the ink-gel pairing and optimization of the slicer configuration when preparing a part to be printed using an embedded 3D printer.

The first issue was easily solved using a Creality Ender 5 as the base to build the embedded 3D printer. Using an Ender 5 eliminates any disturbance of the support gel due to large bed movements in the X or Y-axis, as the bed in the Ender 5 only moves along the z-axis.

Moving away from long needles for ink extrusion to print large parts was more challenging. Previous designs required the user to select a needle at least as long as the shortest axis of the part being printed. To this end, the Dual Ink-Gel Extruder (DIGEX) was designed and tested to eliminate the need to consider the part's dimensions and allow the user to select a needle size that best suits the accuracy required by the part. The DIGEX embedded printing system prints gel on-demand as one prints a liquid ink part. The system could reliably alternate between ink and gel deposition after some iterative improvements in the hardware, software, and firmware. The DIGEX system can deposit ink and gel using a co-axial nozzle arrangement, with the ink needle centred in the annular gel nozzle. The annular nozzle reduced the size of the print head assembly and allowed the gel to be deposited to the edge of the container being printed within. The weight of the print head was also considered, and the modified printer was found to be more than capable of printing at speeds of 50 mm/s, well beyond the speeds expected during embedded 3D printing.

Several investigations were undertaken for the gel deposition system to ensure the best chances of consistent on-demand gel deposition. These included measuring the rheological properties of Carbopol 980 gel at several concentrations and temperatures and designing and testing an appropriate pump to extrude gel as required. Over the temperature range of 18-30°C (typical for Cape Town without air conditioning), the rheological properties of the gels showed minimal variation. Gels with a concentration of 3 g of Carbopol 980 and one litre of distilled water were found to best suit the needs of embedded 3D printing of the concentrations tested.

A prototype of a peristaltic pump and a piston pump were designed and tested with the various concentrations of support gels, and the piston pump was consistently found to perform best. The gel deposition system was improved iteratively and performed adequately, but it still presented some challenges.

Operating the printer is non-trivial. From starting the printer to starting a print job, one can conservatively expect to spend 20-30 minutes setting up the 3D printer. If one needs to prepare an ink as well, that time can be increased to nearer an hour.

Initially, poor inter- and intra-layer adhesion in the ink part and the dominance of the droplet breakup of the ink due to unoptimized slicer profiles and the ink-gel pairing resulted in disappointing prints. Additionally, it was discovered that the gel syringe pump performed poorly at the low volumes of gel requested during typical printing jobs. Iterating on the slicer configuration and investigating and making a model that accounts for the gel syringe pump's low-flow behaviour significantly improved the printed parts' quality. The printed parts are imperfect, but they validate that it is possible to print both ink and gel on demand during embedded printing. Further iterations of this design and slicer setup will allow future users of this technology to print much larger prints than have been possible.

8. Recommendations

Although the dual extruder demonstrates that simultaneous ink-gel deposition is possible, some notable high points in the design are the ink deposition system and the gel deposition nozzle. The ink deposition system performs well, depositing ink material on-demand while generally keeping the assembly's weight down. Of note, the planetary gearbox sub-assembly has shown little degradation while performing well for dozens of hours despite being 3D printed. Another high point is the gel deposition nozzle, which serves its purpose well by depositing even gel layers right to the container's edge.

However, improvements on several aspects of this project are still needed, especially the gel deposition system. Some things may be done concerning the number of fittings used and the compromises that must be made in a project such as this that uses a large amount of 3D printed parts. Some more broad avenues of research are also suggested at the end of this section.

8.1. Design issues

8.1.1. Gel extruder

8.1.1.1. Gel nozzle

The gel nozzle motion assembly was not entirely reliable in pushing the gel nozzle down when required. Some problems with the gel nozzle motion assembly design and the gel nozzle have inflated this issue. A spring was attached to the bottom of the motion bracket to pull down on it and move it down when required, moving the gel nozzle down. Unfortunately, that spring was not strong enough to overcome the suction forces present in the gel nozzle when it was full of gel and the friction between the components of the lower gel nozzle assembly.

8.1.1.2. Gel Pump

The gel syringe pump had some trouble with void formation and retention. These voids are seen as air bubbles that are trapped within the syringe. These voids diminish or disappear if pressure is allowed to equalise in the syringe using 10-second dwell commands after every retraction move the gel syringe pump makes. Still, if larger bubbles form and are retained in the pump, performance noticeably drops.

8.1.2. General issues

8.1.2.1. Fittings

A more general issue of this project that could have been avoided is the number of different fittings required to build this prototype. A decision was not made until later in the project to standardise the sizes and lengths of fittings used to assemble all the parts. The variety of different fittings made it somewhat complex to assemble the entire assembly in a single sitting. Retroactively fixing this issue was not prioritised since the parts required to be upgraded are still working well on the embedded 3D printer.

Another issue related to the number of fittings is the use of nuts instead of threaded heat inserts. Threaded inserts are designed to be heated by a soldering iron and pressed into plastic parts to give them a durable metal thread. Using threaded heat inserts increases the lifetime of that printed part by allowing fittings to screw into the metal thread instead of cutting into softer plastic. It also makes assembly much easier since nuts inserted into a pocket may become misaligned, fall out of their pockets, or deform the softer plastic around them when over-tightened.

8.1.2.2. Printed part limitations

Most custom parts for this design were manufactured using FDM 3D printing to save on costs and time associated with machining metal parts. However, FDM polymer parts have inherent limitations.

Depending on the materials being used, the part may be prone to warping and creeping as it is exposed to stresses and elevated temperatures over the hours that embedded 3D printing may take over several tests of the embedded 3D printer. These properties became particularly problematic on parts holding motors or linear rods in place.

The motors get hot as they are given commands during a regular print job, causing creeping in the 3D-printed plastic parts in contact with those motors. The author recommends considering using steel or aluminium, if possible, instead of 3D printing those plastic parts.

The printed parts securing the linear or threaded rods also showed poor performance over time. This poor performance was due to the printed parts' exposure to stresses over long periods. Eventually, cracks began forming in the parts after retightening the fittings in these parts securing the rods many times during testing. Since these parts are not exposed to elevated temperatures, perhaps improvements in the designs of these parts to avoid crack propagation or using a different material that is less prone to creep may help.

8.2. Recommendations

8.2.1. Ink deposition system

A practised hand should not take longer than a minute or two to exchange the syringe in the ink deposition system. For a system that may need the syringe replaced before every print and potentially multiple times mid-print, the process should be less complicated and expose the user less to getting ink or gel on their hands. Making a less awkward design was difficult with the space available. Still, one may be able to fit something like a collet in the lower assembly, similar to those found in drills or lathes, to secure the syringe in a less awkward and toolless manner.

Changing the shape of the needle tip to suit ink deposition better may be worth investigating. Adding a slight bend in the needle tip or tilting the printhead may improve ink deposition. To this end, separating the gel and ink deposition systems may work well if a tool change system is used instead of the current switching head system. One may even consider using a robotic arm tipped with the ink deposition system mounted off to the side of the printer, printing at the required angle while the gel deposition system remains on the x-axis gantry or potentially on another robotic arm.

A final minor issue on the ink deposition needle side was the use of steel nuts on the threaded rod to transfer rotational movement from the motor-gearbox assembly to linear movement of the syringe depressor assembly. After observing how a similar arrangement degraded on the gel syringe pump, the author would recommend using brass nuts instead for this use case since steel rubbing on steel can abrade the fine teeth of the threaded rod and render it useless.

8.2.2. Gel deposition system

A few updates to the design can be done to aid in moving the gel nozzle on command. The most apparent update would be to use a more appropriate spring, although the small space the current spring occupies makes this problematic. Another solution is to use an upgraded cable, similar to that used in gear shift mechanisms, capable of pushing the nozzle down and pulling the nozzle up. However, using a more rigid cable may make it more challenging to move the print head. One may also consider moving multiple smaller springs into the lower gel nozzle assembly and using their compounded force to push the gel nozzle down, which could neatly fix the above issues. If one disregards the weight requirement of the print head and added complexity, a solenoid or hydraulics could also be used to solve these issues.

One should consider reducing the size of the lower gel nozzle assembly since such a large nozzle limits how small a container can be used to print within and reduces the total height of the build volume of a printer. Note that reducing the length of the lower assembly also reduces the total height of a potential print because the x-axis gantry or the print head will collide with the container being printed in at the beginning of the print job if the print head cannot reach low enough into the container. The limit in print height related to the length of the lower assembly is inherent to this design but is an improvement on extending the needle to print larger parts, as had been done up to this point.

One could mount the syringe pump vertically, tip upwards, instead of horizontally, making it easier for the pump to purge air trapped inside it to deal with the void formation in the pump. Another solution would be to change the reservoir to allow it to be put inside a vacuum chamber before a print to remove the remaining trapped air before taking it out of the chamber and reconnecting the reservoir to the gel pump. A further improvement would be to investigate using more appropriate valves for this application. Non-return valves with faster reaction times, solenoid valves or even tesla valves may reduce the vacuum formed in the pump, leading to less bubble formation. The gel degassing process could be improved by using a centrifuge over a vacuum chamber since there is a worry that the vacuum formed during degassing may be causing the gel to boil. Finally, the adapter between the tubing and the syringe is 3D printed. This part, being 3D printed, causes some issues under pressure where the tightness required by the fittings to keep air ingress during suction strokes can damage the 3D print, allowing air into the pump anyway. Changing this design to use aluminium or resin-printed parts could improve the performance of the part.

A peristaltic pump could be optimised for the gel delivery, but the sinusoidal flow typical of these pumps would need to be minimised. However, the design and proving of a suitable peristaltic pump would be a significant task on its own. A peristaltic pump would hopefully display less tendency to trap air in the pump and perform better when delivering small volumes of gel than the syringe pump.

8.2.3. Broad changes to the design

A design improvement to consider would be to, in some way, allow a user to automatically expand the height of the container throughout a print job. This modification could look like an extension that the user attaches to the existing container or an automatic mechanism that can increase the height of a container with telescopic sides. This idea would enable the DIGEX system to not only use the entire x-y dimensions of a given 3D printer but also increase the available z-axis height to print within. Care should be taken in this design to remove any "draft angles" in this container since container walls perpendicular to the print bed simplify print preparation in the slicer software.

Some slicer optimisations could be found and implemented in the slicing process through further testing. Optimising for reduced stringing could be done, for example, in the slicer by testing different retraction settings, noting that this will need to be done separately for each ink-gel combination. Another optimisation would be to increase the wall overlap percentage to ensure better intra-layer adhesion. Similarly, offsetting every other printed wall except the outer-most walls could improve inter-layer adhesion.

Further research could be done to determine optimal ink-gel pairings regarding interfacial tension, miscibility and droplet breakup. Droplet breakup has been a consistent issue for this work, pushing for the use of larger needle sizes than may be initially desirable to keep the feature size large enough to mostly avoid droplet breakup. A broader investigation into this topic, with a wide range of ink-gel pairing candidates, could be helpful in further research in embedded 3D printing. Also, investigating if a small amount of miscibility may be desirable to decrease the minimum feature size and improve inter- and intra-layer adhesion by reducing the interfacial tension may be interesting.

8.2.4. Assessing print quality

As the basic concept of dual ink-gel deposition has been demonstrated, the next phase of this research would include the refinement of procedures and print parameters to improve print quality. Establishing a framework for quantitatively assessing print quality after each run would be helpful. This data would be beneficial when experimental variables and print parameters interact complexly.

Bibliography

[1] J. Zhao and N. He, 'A mini-review of embedded 3D printing: Supporting media and strategies', *Journal of Materials Chemistry B*, vol. 8, no. 46. Royal Society of Chemistry, pp. 10474–10486, Dec. 14, 2020. doi: 10.1039/d0tb01819h.

[2] C. Brinkley, '3D Printing with Resins and Pastes: Investigation of the Interactions between Support Bath and Ink Materials for Freeform Reversible Embedding', Final Year Report, Univ. of Cape Town, Cape Town, South Africa, 2019.

[3] T. J. Hinton, 'Rapid Prototyping Tissue Models of Mammary Duct Epithelium', Dissertation, Carnegie Mellon University, Pittsburgh, United States of America, 2017.

[4] 'When Was 3D Printing Invented? The History of 3D Printing', BCN3D. Accessed: Jan. 26, 2024. [Online]. Available: https://www.bcn3d.com/the-history-of-3d-printing-when-was-3d-printing-invented

[5] S. S. Crump, 'Apparatus and method for creating three-dimensional objects', U.S. Patent 5 121 329, Jun. 09, 1992.

[6] '7 Types of Additive Manufacturing', Applied Engineering. Accessed: Mar. 27, 2024. [Online]. Available: https://www.appliedengineering.com/blog/2021/1/22/7-types-of-additive-manufacturing

[7] T. D. Ngoa, G. Imbalzanoa, A. Kashania, K. T. Q. Nguyen, and D. Huib, 'Additive manufacturing (3D printing): A review of materials, methods, applications and challenges', *Composites Part B*, no. 143, pp. 172–196, 2018.

[8] N. Shahrubudina, T. C. Lee, and R. Ramlana, 'An Overview on 3D Printing Technology: Technological, Materials, and Applications', *Procedia Manuf*, no. 35, pp. 1286–1296, 2019.

[9] R. Lawless, 'Stereolithography: SLA 3D Printing Simply Explained | All3DP', All3DP. Accessed: Jan. 26, 2024. [Online]. Available: https://all3dp.com/2/stereolithography-3d-printing-simply-explained/

[10] 'Guide to Stereolithography (SLA) 3D Printing | Formlabs', Formlabs. Accessed: Jan. 26, 2024. [Online]. Available: https://formlabs.com/blog/ultimate-guide-to-stereolithography-sla-3d-printing/

[11] P. Piszko, 'What is SLS 3D printing?', Sinterit. Accessed: Jan. 26, 2024. [Online]. Available: https://sinterit.com/blog/sls-technology/what-is-sls-3d-printing/https:/sinterit.com/blog/sls-technology/what-is-sls-3d-printing/

[12] J. J. Beaman and C. R. Deckard, 'Selective Laser Sintering with Assisted Powder Handling', U.S. Patent 4 938 816, Jul. 03, 1990.

[13] '9 Best FDM 3D Printers in 2024 (All Budgets) - 3DSourced', 3DSourced. Accessed: Jan. 26, 2024. [Online]. Available: https://www.3dsourced.com/rankings/best-fdm-3d-printer/

[14] L. Carolo, 'What Is FDM 3D Printing? – Simply Explained | All3DP', All3DP. Accessed: Jan. 26, 2024. [Online]. Available: https://all3dp.com/2/fused-deposition-modeling-fdm-3d-printing-simply-explained/

[15] '3D Printers with Different Kinematics: Comparison, Advantages and Disadvantages', Top 3D Shop. Accessed: Jan. 26, 2024. [Online]. Available: https://top3dshop.com/blog/3d-printer-kinematics-explained

[16] G. Ang, 'Bed Slinger (3D Printing): What Is It Exactly? | All3DP', All3DP. Accessed: Jan. 26, 2024. [Online]. Available: https://all3dp.com/2/bed-slinger-3d-printing-simply-explained/

[17] D. Ahlers, '3D Printing of Nonplanar Layers for Smooth Surface Generation', M.S. thesis, Dept. Computer Science, Univ. of Hamburg, Hamburg, Germany. [Online]. Available: https://www.researchgate.net/publication/335542650

[18] I. Kauppila, 'The Best Pellet 3D Printers in 2024 | All3DP Pro', All3DP. Accessed: May 14, 2024. [Online]. Available: https://all3dp.com/1/cheaper-3d-printing-with-pellets/

[19] M. Reichenbach, 'The Ultimate Guide to Concrete 3D Printing in 2023 - 3DSourced', 3DSourced. Accessed: May 08, 2024. [Online]. Available: https://www.3dsourced.com/guides/concrete-3d-printing/

[20] V. Martinho, 'The Best Ceramic / Pottery 3D Printers in 2024 | All3DP', All3DP. Accessed: May 08, 2024. [Online]. Available: https://all3dp.com/2/ceramic-3d-printer-ceramic-3d-printing/

[21] A. Lalani, 'Mycusini Chocolate 3D Printer Review: A Real Treat | All3DP', All3DP. Accessed: May 08, 2024. [Online]. Available: https://all3dp.com/1/mycusini-chocolate-3d-printer-review-a-real-treat/

[22] Y. Choi, Y. Jun, D. Y. Kim, H. Yi, S. Chae, J. Kang, J. Lee, G. Gao, J. Kong, J. Jang, W. K. Chung, J. Rhie, D. Cho, 'A 3D cell printed muscle construct with tissue-derived bioink for the treatment of volumetric muscle loss', *Biomaterials*, 2019, doi: 10.1016/j.biomaterials.2019.03.036

[23] G. M. Gratson, M. Xu, and J. A. Lewis, 'Microperiodic structures', *Nature*, vol. 428, p. 386, Mar. 2004.

[24] M. S. Mannoor, Z. Jiang, T. James, Y. L. Kong, K. A. Malatesta, W. Soboyejo, N. Verma, D. H. Gracias, M. C. McAlpine, '3D printed bionic ears', *Nano Lett*, vol. 13, no. 6, pp. 2634–2639, Jun. 2013, doi: 10.1021/nl4007744.

[25] T. J. Hinton, Q. Jallerat, R. N. Palchesko, J. H. Park, M. S. Grodzicki, H. Shue, M. H. Ramadan, A. R. Hudson, A. W. Feinberg, 'Three-dimensional printing of complex biological structures by freeform reversible embedding of suspended hydrogels', *Sci Adv*, vol. 1, no. 9, Oct. 2015, doi: 10.1126/sciadv.1500758.

[26] J. T. Muth, D. M. Vogt, R. L. Truby, Y. Mengüç, D. B. Kolesky, R. J. Wood, J. A. Lewis, 'Embedded 3D Printing of Strain Sensors within Highly Stretchable Elastomers', *Advanced Materials*, 2014, doi: 10.1002/adma.201400334.

[27] M. Wehner, R. L. Truby, D. J. Fitzgerald, B. Mosadegh, G. M. Whitesides, J. A. Lewis, R. J. Wood, 'An integrated design and fabrication strategy for entirely soft, autonomous robots', *Nature*, vol. 536, no. 7617, pp. 451–455, Aug. 2016, doi: 10.1038/nature19100.

[28] J. Zhao, M. Hussain, M. Wang, Z. Li, and N. He, 'Embedded 3D printing of multi-internal surfaces of hydrogels', *Addit Manuf*, vol. 32, Mar. 2020, doi: 10.1016/j.addma.2020.101097.

[29] N. Noor, A. Shapira, R. Edri, I. Gal, L. Wertheim, and T. Dvir, '3D Printing of Personalized Thick and Perfusable Cardiac Patches and Hearts', *Advanced Science*, vol. 6, no. 11, Jun. 2019, doi: 10.1002/advs.201900344.

[30] O. Jeon, Y. B. Lee, T. J. Hinton, A. W. Feinberg, and E. Alsberg, 'Cryopreserved cell-laden alginate microgel bioink for 3D bioprinting of living tissues', *Mater Today Chem*, vol. 12, pp. 61–70, 2019.

[31] 'Organ Donation and Transplantation'. Accessed: Jan. 26, 2024. [Online]. Available: https://data.hrsa.gov/topics/health-systems/organ-donation

[32] W. Wu, A. DeConinck, and J. A. Lewis, 'Omindirectional Printing of 3D Microvascular Networks', *Adv Healthc Mater*, vol. 23, pp. H178–H183, 2011.

[33] R. L. Truby, M. Wehner, A. K. Grosskopf, D. M. Vogt, S. G. M. Uzel, R. J. Wood, J. A. Lewis, 'Soft Somatosensitive Actuators via Embedded 3D Printing', *Advanced Materials*, 2018.

[34] Y. Zhang, B. Wang, J. Hu, T, Yin, T. Yue, N. Liu, Y, Liu, '3D Composite Bioprinting for Fabrication of Artificial Biological Tissues', *Int J Bioprint*, vol. 7, no. 1, pp. 7–20, 2021, doi: 10.18063/ijb.v7i1.299.

[35] T. J. Hinton, A. Hudson, K. Pusch, A. Lee, and A. W. Feinberg, '3D Printing PDMS Elastomer in a Hydrophilic Support Bath via Freeform Reversible Embedding', *ACS Biomater Sci Eng*, vol. 2, no. 10, pp. 1781–1786, Oct. 2016, doi: 10.1021/acsbiomaterials.6b00170.

[36] Y. Jin, K. Song, N. Gellerman, and Y. Huang, 'Printing of Hydrophobic Materials in Fumed Silica Nanoparticle Suspension', *ACS Applied Materials & Materials*, 2019, doi: 10.1021/acsami.9b07433.

[37] K. Pusch, T. J. Hinton, and A. W. Feinberg, 'Large volume syringe pump extruder for desktop 3D printers', *HardwareX*, vol. 3, pp. 49–61, Apr. 2018, doi: 10.1016/j.ohx.2018.02.001.

[38] E. Miramadi, J. W. Tashman, D. J. Shiwarski, R. N. Palchesko, and A. W. Feinberg, 'FRESH 3D Bioprinting a Full-Size Model of the Human Heart', *ACS Biomaterials Science & Engineering*, pp. 6453–6459, Nov. 2020, doi.org/10.1021/acsbiomaterials.0c01133.

[39] R. G. Budynas and J. K. Nisbett, *Shigley's Mechanical Engineering Design, Tenth Edition in SI Units*, 10th ed. New York: McGraw-Hill Education, 2015.

[40] C. S. O'Bryan, T. Bhattacharjee, S. R. Niem, S. Balachandar, N. Baldwin, S. T. Ellison, C. R. Taylor, W. G. Sawyer, T. E. Angelini, 'Three-dimensional printing with sacrificial materials for soft matter manufacturing', *Materials Research Society Bulletin*, vol. 42, pp. 571–577, 2017, doi.org/10.1557/mrs.2017.167.

[41] J. S. S. Masters, 'SUPPORT BATH DEPOSITION FOR EMBEDDED 3D PRINTING', Final Year Report, Univ. of Cape Town, Cape Town, South Africa, 2019.

[42] J. Pfitzer, 'Poiseuille and his law', *Anaesthesia*, vol. 31, pp. 273–275, 1976.

[43] B. Rugara, 'Investigation of support bath materials for embedded 3D printing of liquid inks', Final Year Report, Univ. of Cape Town, Cape Town, South Africa, 2019.

[44] D. Kolesky, R. L. Truby, A. S. Gladman, T. A. Busbee, K. A. Homan, and J. A. Lewis, '3D Bioprinting of Vascularized, Hetergeneous Cell-Laden Tissue Constructs', *Advanced Materials*, 2014, doi: 10.1002/adma.201305506.

[45] K. Ioannidis, R. I. Danalatos, S. C. Tsaniras, K. Kaplani, G. Lokka, A. Kanellou, D. J. Papachristou, G. Bokias, Z. Lygerou, S. Taraviras, 'A Custom Ultra-Low-Cost 3D Bioprinter Supports Cell Growth and Differentiation', *Front Bioeng Biotechnol*, vol. 8, Nov. 2020, doi: 10.3389/fbioe.2020.580889.

[46] 'GT2 Pulley (6.35mm Bore / 20 Tooth / 6mm Belt)', DIYElectronics. Accessed: Jan. 26, 2024. [Online]. Available: https://www.diyelectronics.co.za/store/pulleys/1045-gt2-pulley-635mm-bore-20-tooth-6mm-belt.html.

[47] D. Papp, 'Get A Better Look At E3D's Tool-changing 3D Printer Kit | Hackaday', Hackaday. Accessed: Jan. 26, 2024. [Online]. Available: https://hackaday.com/2021/03/20/get-a-better-look-at-e3ds-tool-changing-3d-printer-kit/.

[48] 'Dual Switching Hotend v2.1 – Makertech Store', Makertech 3D. Accessed: Jan. 26, 2024. [Online]. Available: https://www.makertech3d.com/products/dual-switching-hotend-v2-non-proforge?variant=40409454149791.

[49] 'Sovol SV02 Dual Extruder 3D Printer with Touch screen, Creality Silent Board', Sovol. Accessed: Jan. 26, 2024. [Online]. Available: https://www.sovol3d.com/products/sovol-sv02-dual-extrusion-3d-printer.

[50] '3DSWAY Improved E3D Chimera 2 In 2 Out Hotend Kit Dual Heads Extruder For 3D Printer – Alexnld.com', Alexnld.com. Accessed: Jan. 26, 2024. [Online]. Available: https://alexnld.com/product/3dsway-improved-e3d-chimera-2-in-2-out-hotend-kit-dual-heads-extruder-for-3d-printer/.

[51] ‘Sovol SV04 Review: Large Format IDEX 3D Printer | 3D Print Beginner’, 3DPrintBeginner. Accessed: Jan. 26, 2024. [Online]. Available: https://3dprintbeginner.com/sovol-sv04-review-large-format-idex-3d-printer/.
[52] A. Amado, K. Wegener, M. Schmid, and G. Levy, ‘Advances in SLS powder characterization’, 2011. [Online]. Available: https://www.researchgate.net/publication/268434379.
[53] ‘ELEGOO Jupiter 6K Resin 3D Printer’, Elegoo. Accessed: Jan. 26, 2024. [Online]. Available: https://www.elegoo.com/products/elegoo-jupiter-resin-3d-printer-6k-mono-msla-3d-printer.
[54] M. Iyas, ‘Different Types of Pumps Explained [Pictures & Uses] PDF’, The Engineer’s Post. Accessed: Jan. 26, 2024. [Online]. Available: https://www.theengineerspost.com/types-of-pumps/.
[55] N. Bessler, D. Ogiermann, M. Buchholz, A. Santel, J. Heidenreich, R. Ahmmed, H. Zaehres, B. Brand-Saberi, ‘Nydus One Syringe Extruder (NOSE): A Prusa i3 3D printer conversion for bioprinting applications utilizing the FRESH-method’, *HardwareX*, vol. 6, Oct. 2019, doi: 10.1016/j.ohx.2019.e00069.
[56] D. J. Shiwarski, A. R. Hudson, J. W. Tashman, and A. W. Feinberg, ‘Emergence of FRESH 3D printing as a platform for advanced tissue biofabrication’, *APL Bioengineering*, vol. 5, no. 1. American Institute of Physics Inc., Mar. 01, 2021. doi: 10.1063/5.0032777.
[57] ‘Ender-3 3D Printer’, Creality. Accessed: Jan. 26, 2024. [Online]. Available: https://www.creality.com/products/ender-3-3d-printer.
[58] A. Locker, ‘Creality Ender 5 Review: Great 3D Printer Under $500 | All3DP’, All3DP. Accessed: Jan. 26, 2024. [Online]. Available: https://all3dp.com/1/creality-ender-5-review-3d-printer-specs/.
[59] ‘Features - Klipper documentation’, Klipper3D. Accessed: May 09, 2024. [Online]. Available: https://www.klipper3d.org/Features.html.
[60] D_P_R, ‘3D Printed Magnetic Toolchanger : 6 Steps (with Pictures) - Instructables’. Accessed: Jul. 09, 2024. [Online]. Available: https://www.instructables.com/Magnetic-3D-Printed-Toolchnager/.
[61] ‘BIGTREETECH SKR PRO V1.2 32 Bit Control Board – Biqu Equipment’, Biqu. Accessed: May 09, 2024. [Online]. Available: https://biqu.equipment/collections/control-board/products/bigtreetech-skr-pro-v1-1-32-bit-control-board.
[62] P. R. N. Childs, *Mechanical Design, Second Edition*, 2nd ed. Oxford: Elsevier Butterworth-Heinemann, 2004.
[63] ‘Ecoflex™ 00-30 Product Information | Smooth-On, Inc.’, Smooth-On. Accessed: Jan. 26, 2024. [Online]. Available: https://www.smooth-on.com/products/ecoflex-00-30/.
[64] J. W. Tashman, D. J. Shiwarski, B. Coffin, A. Ruesch, F. Lanni, J. M. Kainerstorfer, A. W. Feinberg, ‘In situ volumetric imaging and analysis of FRESH 3D bioprinted constructs using optical coherence tomography’, *Biofabrication*, vol. 15, 2023, doi: 10.1088/1758-5090/ac975e.
[65] J. Newton, ‘3D Printing with Gels - continuous feed extruder experiment’, Final Year Report, Univ. of Cape Town, Cape Town, South Africa, 2020.
[66] PattysLab, ‘Peristaltic Pump Open Source Any Shape Any Size by PattysLab - Thingiverse’, Thingiverse. Accessed: Jan. 26, 2024. [Online]. Available: https://www.thingiverse.com/thing:5409562.
[67] Y. A. Cengel and A. J. Ghajar, *Heat and Mass Transfer: Fundamentals & Applications, Fifth Edition in SI Units*, 5th ed. New York: McGraw-Hill Education, 2015.

[68] G. Chambon, A. Ghemmour, and M. Naaim, 'Experimental investigation of viscoplastic free-surface flows in a steady uniform regime', *J Fluid Mech*, vol. 754, pp. 332–364, Sep. 2014, doi: 10.1017/jfm.2014.378.
[69] A. B. Metzner and J. C. Reed, 'Flow of Non-Newtonian Fluids-Correlation of the Laminar, Transition, and Turbulent-flow Regions', *A.I.Ch.E Journal*, pp. 434–440, Dec. 1955.
[70] J. J. J. Uicker, G. R. Pennock, and J. E. Shigley, *Theory of Machines and Mechanisms*, 4th International. New York: Oxford University Press, 2011.
[71] 'Overview of materials for Polypropylene, Molded', MatWeb. Accessed: May 10, 2024. [Online]. Available: https://matweb.com/search/DataSheet.aspx?MatGUID=08fb0f47ef7e454fbf7092517b2264b2&ckck=1.
[72] 'Yield Strength of Plastics – Basic Principles - Matmatch', Matmatch. Accessed: May 10, 2024. [Online]. Available: https://matmatch.com/learn/property/yield-strength-of-plastics.
[73] 'Coefficient of Friction Equation and Table Chart'. Accessed: Mar. 25, 2024. [Online]. Available: https://www.engineersedge.com/coeffients_of_friction.htm.
[74] 'EN 1.0503 (C45) Non-Alloy Steel : MakeItFrom.com'. Accessed: Mar. 25, 2024. [Online]. Available: https://www.makeitfrom.com/material-properties/EN-1.0503-C45-Non-Alloy-Steel.

Appendix A: Methodologies

Note that the chemicals used in these methodologies can be dangerous, and one should take appropriate measures to ensure safety when working with these substances.

A.1. Carbopol 980 gel preparation

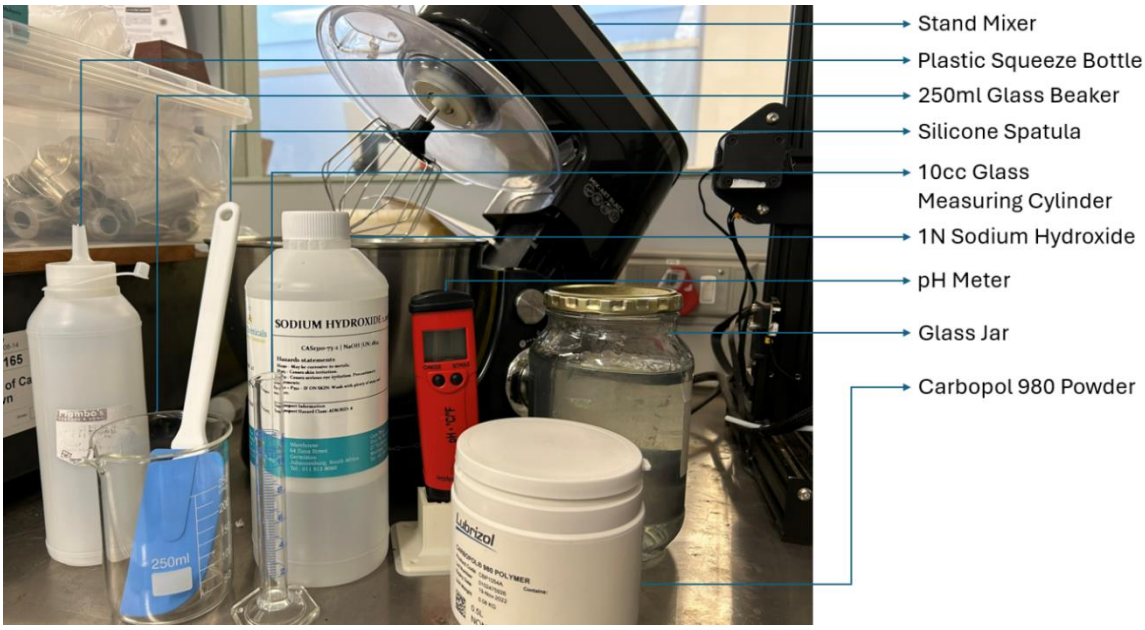

Figure 58: *The apparatus and chemicals required for Carbopol 980 gel preparation.*

Note that sodium hydroxide solution is a strong base and Carbopol in water is acidic, so one should wear gloves and eye protection when working with these substances.

A.1.1. Apparatus

- Stand mixer
- 10 cc glass measuring cylinder
- 250 ml glass beaker
- Silicone spatula
- Digital scale
- pH meter
- Plastic squeeze bottle
- Glass jar

- Paper towel
- Vacuum chamber

A.1.2. Chemicals

- Distilled water
- 1 N sodium hydroxide solution (NaOH)
- Carbopol 980 powder
- Dish soap

A.1.3. Procedure

1. Ensure that the glass beaker, measuring beaker, spatula, pH meter, plastic squeeze bottle, glass jar and portions of the stand mixer that will likely contact the gel mixture have all been cleaned and rinsed with distilled water.
2. Measure all the required distilled water for the gel mixture using the glass beaker and decant into the bowl of the stand mixture. Note the amount of distilled water in the bowl.
3. Use the digital scale to measure the required amount of Carbopol powder for the gel mixture and add it to the water in the bowl of the stand mixture. Note the amount of powder in the bowl.
4. Decant a small amount of NaOH into the squeeze bottle.
5. Decant some distilled water into the glass beaker and leave the pH meter on in the beaker with the cap off.
6. Secure the lid and let the stand mixer mix the Carbopol mixture for 15 minutes using the whisk attachment on low.
7. Once the stand mixer has finished mixing the mixture, stop the stand mixer and lift the lid. Scape down the sides with the spatula.
8. Remove the pH meter from the distilled water and insert it into the gel mixture with the pH meter on.
9. Once the pH meter has been in the mixture for 5 minutes, note the pH. Remove and allow to sit in the beaker. If the gel is stuck to the pH meter, wipe off the gel using a paper towel.
10. Measure out an appropriate amount of NaOH from the squeeze bottle using the measuring cylinder and add it to the gel mixture. The amount depends on the pH and the concentration of Carbopol. Note how much NaOH has been added.
11. Repeat steps 6 through 9, mixing for 10 minutes instead of 15, stopping once adding 1cc of NaOH will likely push the pH past seven.
12. Spoon the mixture into a glass jar using the spatula, filling it to at most half full.
13. Place the jar into the vacuum chamber and run the vacuum until all the gel stops bubbling rapidly. Observe the gel while the vacuum is running and ensure the gel does not bubble over the rim of the jar.
14. Remove the jar. Seal and label it.
15. Clean all apparatus using soap and store chemicals.

A.2. Ink preparation

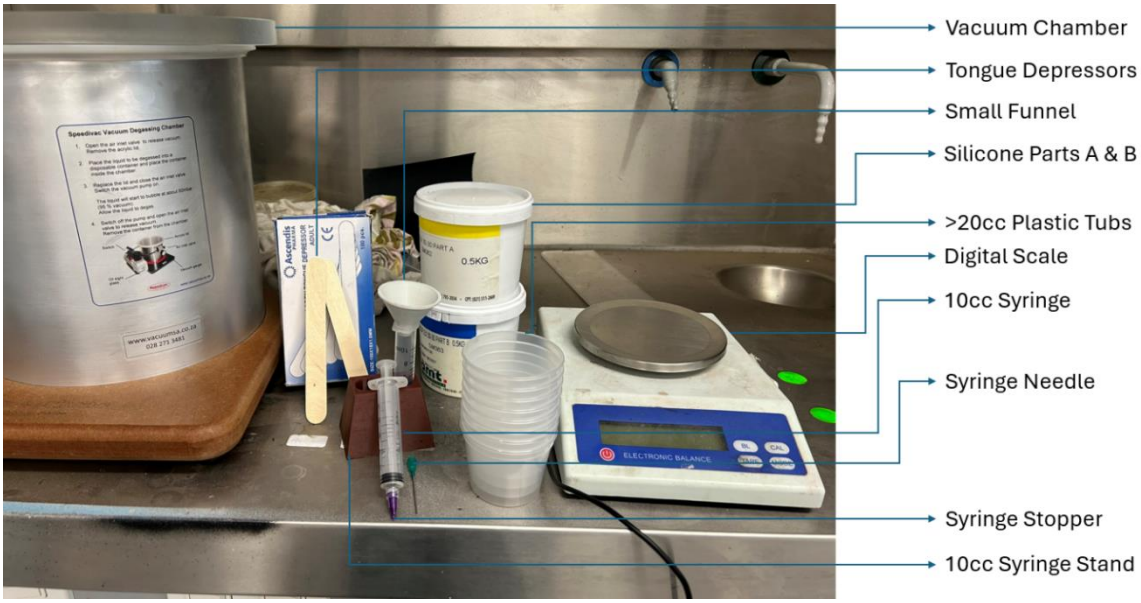

Figure 59: *The apparatus and chemicals required for Ink preparation.*

A.2.1. Apparatus

- >20 cc plastic tubs
- Tongue depressors
- Digital scale
- Vacuum chamber
- Small funnel
- 10 cc syringe
- Syringe stopper
- Syringe needle
- 10 cc syringe stand

A.2.2. Chemicals

- Silicone ink parts A and B
- Dish soap

A.2.3. Procedure

1. Ensure the small plastic tubs and funnel are clean.
2. Place a clean plastic tub on the digital scale and turn on the scale to zero the weight displayed.
3. Use a clean tongue depressor to spoon part A of the silicone ink chemical mixture into one of the tubs until the desired weight is displayed on the digital scale.
4. Replace the tub with part A on the scale with another clean tub. Use a clean tongue depressor to spoon part B of silicone ink until the desired weight for part B is displayed on the scale.
5. Use another clean tongue depressor to spoon part A into B and mix the two with that tongue depressor for 30 seconds. Wet the tip of the tongue depressor with a pigment or dye if desired. To mix parts A and B more completely, pour the mixture back into the tub containing what is left of part A and mix again. Repeat if needed.
6. Place the tub containing the mixture into the vacuum chamber and run until most of the bubbles disappear. If the ink expands too much under vacuum, consider splitting the mixture equally between the two tubs and placing both in the vacuum chamber.
7. Remove the stopper on the syringe and screw the stopper into the tip of the syringe, and place the tip down into the stand. Place the funnel tip down into the now open syringe body and pour the degassed mixture of parts A and B.
8. Carefully replace the plunger while removing the stopper. Ensure that the plunger is first replaced before turning the syringe upwards, allowing any bubbles to float towards the stopper before removing the stopper. Use the plunger to push out any bubbles and minimize pushing out ink.
9. Screw the needle into place for use.
10. Discard or clean any apparatus with dish soap that has come into direct contact with mixed parts A and B.

A.3. Gel rheology testing

A.3.1. Apparatus

- RheolabQC rheometer
- Concentric cylinder geometry
- Computer with appropriate rheology software
- 20 cc syringe
- Paper towel

A.3.2. Chemicals

- Dish soap
- Gel mixture

A.3.3. Procedure

1. Clean the syringe and portions of the rheometer that will contact the gel.
2. Turn on the computer
3. Turn on the Peltier temperature control system and the rheometer.
4. Measure 20 cc of gel using the syringe and decant into the rheometer testing barrel. Clean the syringe with soap.
5. Insert cylindrical geometry into the testing barrel.
6. Screw the cap off the bottom of the rheometer.
7. Insert the testing barrel and cylindrical geometry into the rheometer through the hole on the bottom of the rheometer. Once fully inserted, pull the collar down onto the top shaft of the cylindrical geometry until it clicks and screw the bottom cap of the rheometer back on.
8. Start rheology testing software on the computer and fill in the relevant fields.
9. Run the rheology tests. Clean the barrel and geometry with soap between tests if required. Remove the testing barrel and cylindrical geometry in reverse order from insertion before cleaning, and use steps 4 through 7 to add new samples.
10. Save results.
11. Clean the testing barrel, cylindrical geometry and syringe with soap.
12. Put the testing barrel and cylindrical geometry back into their containers.
13. Close the rheology testing program.
14. Turn off the Peltier and rheometer.
15. Turn off the computer.

A.4. Ink extrudability testing

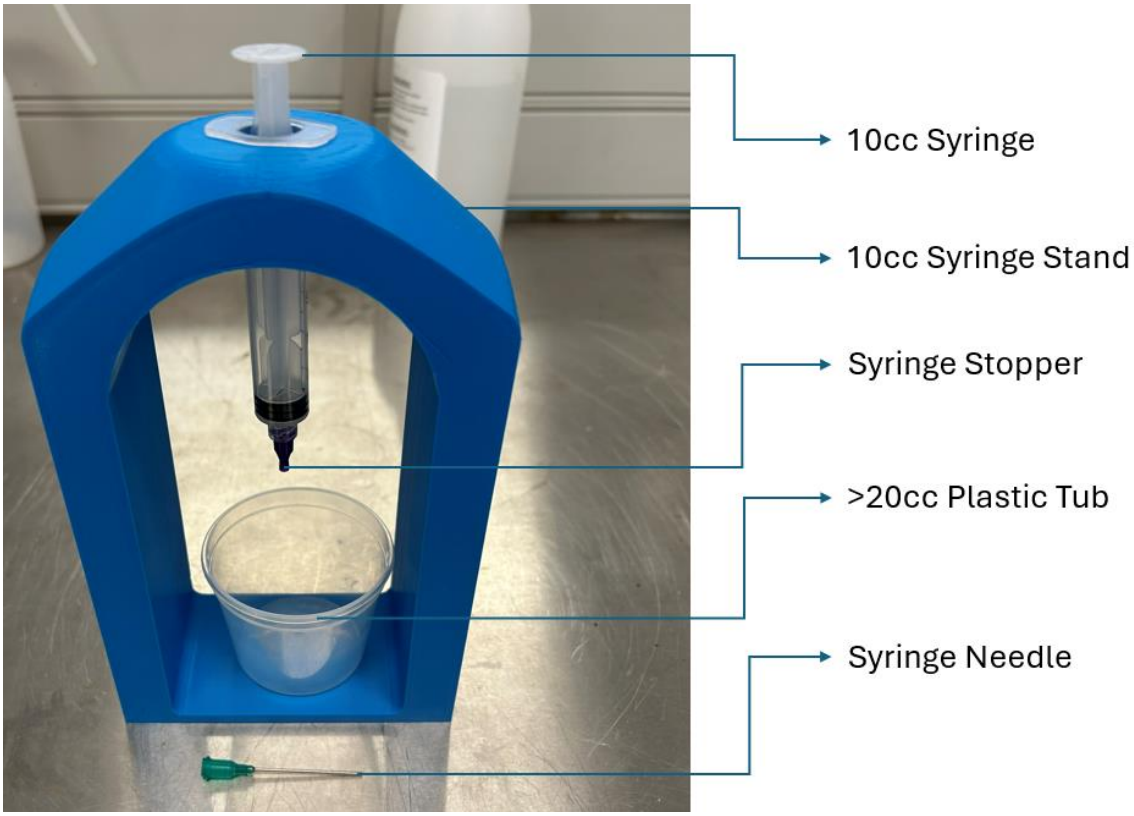

Figure 60: *The apparatus required for ink extrudability testing.*

A.4.1. Apparatus

- 20 cc syringe
- Syringe needle
- Syringe stopper
- Instron Universal Loading Frame
- 1000 N loadcell
- Computer with appropriate software
- Syringe stand (Solidworks part file can be downloaded in https://drive.google.com/drive/folders/1mXSRrU1Rug7xi4EunPfRDUiUuODyCZJ4?usp=drive_link)
- Plastic tub
- Paper towel

A.4.2. Chemicals

- Ink
- Dish soap

A.4.3. Procedure

1. Attach the loadcell sensor to the loading apparatus.
2. Turn on the loading apparatus.
3. Turn on the computer and open the load testing software.
4. Fill in the relevant fields in the software.
5. Prepare the ink for testing and decant it into the syringe with the syringe plunger removed and a stopper on the end of the syringe.
6. Remove the stopper and quickly replace it with a needle tip.
7. Place the plunger back in the syringe.
8. Turn the syringe so the needle faces up and allow bubbles to collect below the needle. Once the bubbles have collected, depress the plunger to push out the bubbles.
9. Once the bubbles have been removed, place the syringe in the syringe stand.
10. Raise the load cell so that the syringe stand with the syringe in it may fit under the load cell. Place the syringe stand so the syringe's plunger is centred below the loadcell sensor. Place the plastic tub below the needle. Refer to Figure 62.
11. Lower the loadcell sensor until it is in contact with the syringe plunger.
12. Start the test.
13. Save the results.
14. Repeat steps 5 through 13 to do repeat tests.
15. Close the software and turn off the computer and loading apparatus
16. Remove the syringe and stand and unload the load cell sensor.
17. Place the loadcell sensor back into its container.
18. Clean any spilt ink with paper towels and soap.

A.5. Gel extrudability testing

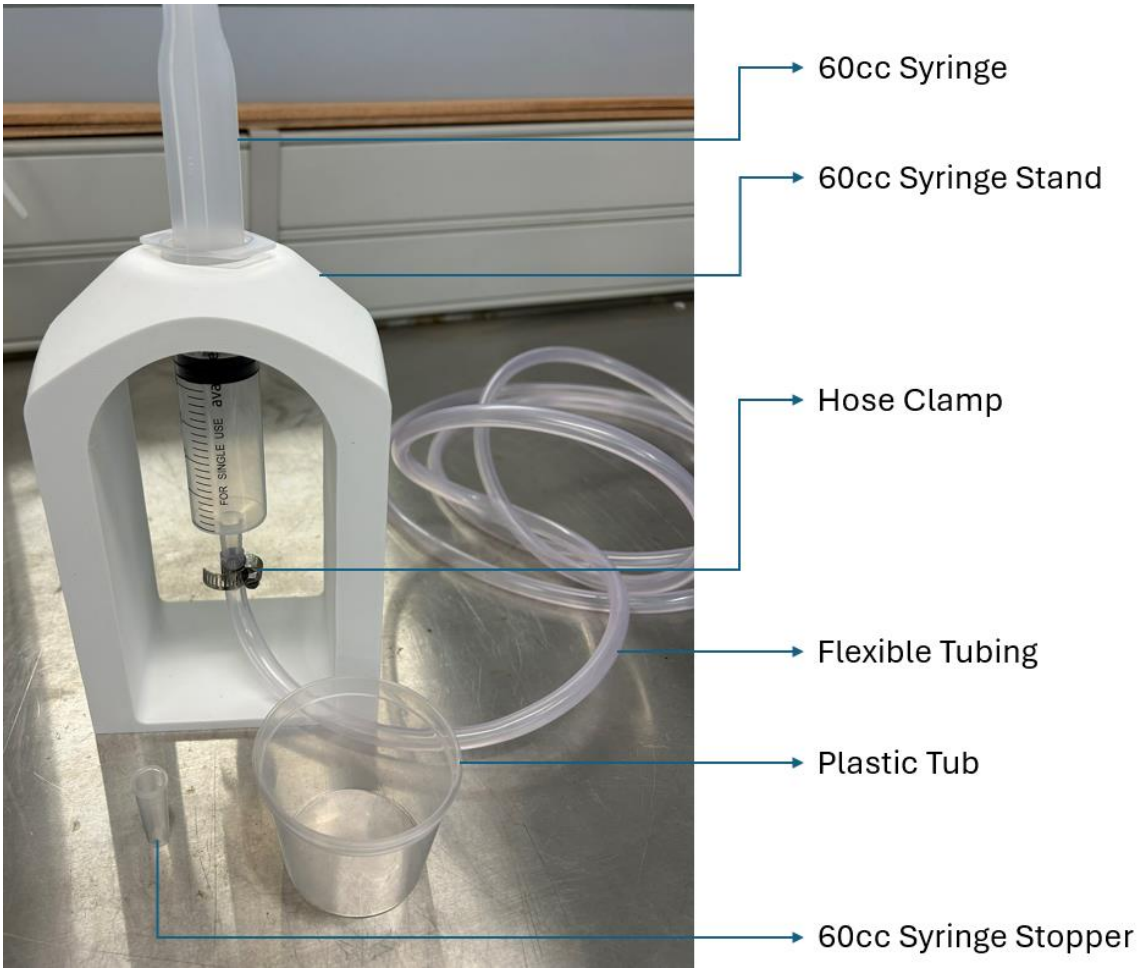

Figure 61: *The apparatus required for gel extrudability testing.*

A.5.1. Apparatus

- 60 cc syringe
- Syringe stopper
- Loadcell
- Computer with appropriate software
- Syringe stand (Solidworks part file can be downloaded in https://drive.google.com/drive/folders/1mXSRrU1Rug7xi4EunPfRDUiUuODyCZJ4?usp=drive_link)
- Plastic tub
- Paper towel
- 8 mm x 10 mm x 1m flexible tubing
- Hose clamp

A.5.2. Chemicals

- Carbopol Gel
- Dish soap

A.5.3. Procedure

Figure 62: *The stand and syringe set up in the loading apparatus.*

1. Attach the loadcell sensor to the loading apparatus.
2. Turn on the loading apparatus.
3. Turn on the computer and open the load testing software.
4. Fill in the relevant fields in the software.
5. Decant the prepared Carbopol gel into the syringe with the syringe stopper attached and the plunger removed.
6. Place the plunger back in the syringe after removing the stopper.
7. Turn the syringe tip upwards and allow bubbles to gather below the tip. Depress the syringe to remove all the bubbles.
8. Reattach the stopper once the bubbles have been removed and place the syringe in the stand.
9. Raise the load cell so that the syringe stand with the syringe in it may fit under the load cell. Place the syringe stand so the syringe's plunger is centred below the loadcell sensor. Place the plastic tub below the needle. Refer to Figure 62.

10. Lower the load cell sensor until it is in contact with the syringe plunger, and remove the stopper.
11. Start the test.
12. Save the results.
13. Repeat steps 5 through 12 to do repeat tests.
14. Once enough repeat tests have been done, repeat steps 5 through 10, but after 10, fit the flexible tubing into place over the syringe tip using an appropriate hose clamp and fill the tubing with gel. Carry on with steps 11 through 13.
15. Now cut the 0.25m off the tubing and do as step 14 stipulates. Once results have been gathered, cut the tubing again so that in the end, one has results for no tubing, 1m, 0.75m, 0.5m and 0.25m of tubing.
16. Close the software and turn off the computer and loading apparatus.
17. Remove the syringe and stand, and unload the load cell sensor.
18. Place the loadcell sensor back into its container.
19. Clean the tubing, syringe and spilt gel with paper towels and soap.

A.6. Peristaltic pump flow testing

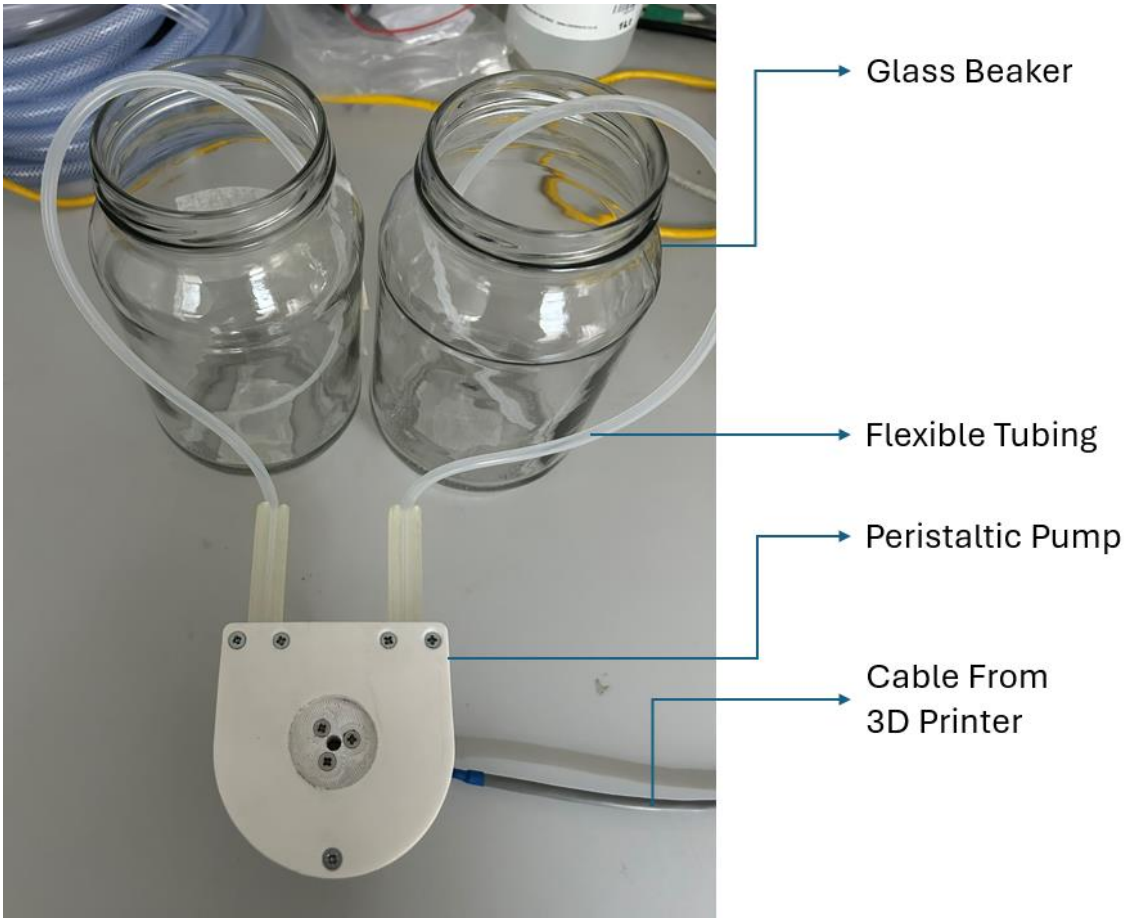

Figure 63: *The apparatus required for peristaltic pump flow testing.*

A.6.1. Apparatus

- Peristaltic pump (Solidworks parts and assembly files can be downloaded in https://drive.google.com/drive/folders/1mXSRrU1Rug7xi4EunPfRDUiUuODyCZJ4?usp=drive_link)
- Two 1000 ml glass beakers
- Small plastic tub
- Digital scale
- Paper towels

A.6.2. Chemicals

- Test liquid

- Water
- Dish soap

A.6.3. Procedure

1. Measure the weight of the empty small plastic tub using the digital scale and note that weight.
2. Put the test liquid in the beaker and put one end of the peristaltic pump's pipe in the beaker so that the end of the pipe is at the bottom of the beaker.
3. Put the other end of the peristaltic pump into the other beaker.
4. Send commands to the peristaltic pump to extrude enough test material to fill the pipe from the filled beaker to the empty beaker, ensuring that the peristaltic pump never sucks air during the execution of the commands.
5. Remove the outlet beaker and refill the inlet beaker as needed. Put the empty tub at the outlet. Clean the outlet beaker with soapy water and dry it with paper towels.
6. Send a command to the peristaltic pump to extrude a specific volume of test liquid at a specified speed. Ensure the inlet never sucks air. Note that speed and volume.
7. Measure the weight of the tub that now has a volume of test fluid in it.
8. Clean the tub using soapy water and dry off with paper towels.
9. Repeat steps 6-8 for repeat tests or testing the same test fluid at different speeds and volumes.
10. If testing different test fluids, empty the test fluid beaker, rinse it with soapy water, dry it with paper towels, and fill it with water. Place the inlet side of the pipe in the filled beaker and the outlet in the empty beaker. Run the peristaltic pump until all test fluid in the pipe has been replaced with water. Repeat steps 4-9 as needed.
11. When finished with testing, run water through the pipe as in step 10. Once filled with water, remove the inlet beaker and run the pipe, sucking air until the water has been mostly replaced with air. Squeeze the pipe to remove the last large drops of water.
12. Clean all surfaces that have contacted test fluid with soapy water and dry with paper towels.

A.7. Syringe pump flow testing

A.7.1. Apparatus

- Syringe pump
- Reservoir for holding test liquid
- 2x Plastic tubs or beakers
- Digital scale
- Paper towels

A.7.2. Chemicals

- Test liquid
- Water
- Dish soap

A.7.3. Procedure

1. Measure the weight of the tub or beaker using the digital scale and note that weight.
2. Put the test liquid in the reservoir and put the input pipe of the syringe pump in the reservoir such that the end of the pipe is at the bottom of the reservoir.
3. Put the pipe outlet out of the syringe pump into one of the tubs or beakers.
4. Send the GEL_PRIME macro detailed in Appendix C.2 to the syringe pump to extrude enough test material to completely fill the pump and pipes from the reservoir to the outlet beaker, ensuring that the syringe pump never sucks air during the execution of the commands.
5. Remove the outlet beaker and refill the reservoir as needed. Put the other empty tub or beaker at the outlet. Clean the removed outlet beaker with soapy water and dry it with paper towels.
6. Use the Fluidd interface to extrude a specific volume of test liquid at a specified speed. Ensure the inlet never sucks air.
7. Measure the weight of the tub or beaker that now has a volume of test fluid in it and note that weight.
8. Clean the tub or beaker using soapy water and, dry off with the paper towels and replace the tub or beaker at the outlet of the syringe pump.
9. Repeat steps 6-8 for repeat tests or testing the same test fluid at different speeds.
10. If testing different test fluids, empty the reservoir, rinse it with soapy water, dry it with paper towels, and fill it with water. Place the inlet side of the pipe in the filled reservoir and the outlet in the empty beaker or tub. Run the syringe pump until all test fluid in the pipe has been replaced with water. Repeat steps 2-9 as needed.
11. When finished with testing, run water through the pipes as in step 10. Once filled with water, remove the inlet beaker and run the pipe, sucking air until the water has been mostly replaced with air. Squeeze the pipe to remove the last large drops of water.
12. Clean all surfaces that have contacted test fluid with soapy water and dry with paper towels.

Appendix B: Slicer part preparation

Presented below is a short explanation on how to set up a part using Cura installed on an appropriate computer.

1. Open Cura and set the material to the ink material profile.
2. Set up the profile for the print job. Pay special attention to the line width and the print speed. Set the z-seam alignment to behind the part.
3. Place the ink part in the centre of the build place. Add a prime tower offset in front of the part. Add a dwell tower behind the part and set the flow of the dwell tower to 0.1% using per-model settings.
4. Slice the part and save the G-code output after checking the preview.
5. Clear the build plate and set the material to the gel material profile. Do not forget to double-check the line width.
6. Place the geometry of the inside of the container you will be printing support gel within in the centre of the build plate.
7. Slice the gel part, check the G-code output and save it.
8. Run the Python scripts found in Appendix C.3.
9. Open the G-code output of the scripts in Cura and inspect them to ensure that the ink part, including any towers, skirts, brims or draft shields, is totally encased in the gel support material. No part of the ink part should be taller than the gel part, plus the minimum depth required to avoid recirculation wake and hydrostatic crevasse formation minus the length of the needle used.

Appendix C: 3D printer configuration

The following sections show how to adjust Ultimaker Cura (5.5) and Klipper/Fluidd (0.12) to work together and 3D print embedded parts using the DIGEX print head as shown in this project.

The files presented here can also be found in the following Google Drive folder:

https://drive.google.com/drive/folders/1mXSRrU1Rug7xi4EunPfRDUiUuODyCZJ4?usp=drive_link

C.1. Cura configuration

The following subsections detail the start and end G-code, the values of the settings, and the values used in this project. The start and end G-code settings fields can be found by looking at the top-left menu and clicking Settings > Printer > Manage Printers > Machine Settings. The extruder settings can be found under Print Settings on the right-hand side of the screen.

To create a material file and give it the values shown in the material settings section, one will need to navigate to the folder containing the materials in C:\Users\User\AppData\Roaming\cura\5.5\materials and copy the code presented in the Material Settings section into a text file and give it the suffix of .fdm_material.xml for each material.

C.1.1. Cura start G-code

```
START_PRINT BED_TEMP={material_bed_temperature_layer_0}
EXTRUDER_TEMP={material_print_temperature_layer_0, 0}
```

C.1.2. Cura end G-code

```
G91 ;Relative positioning
G1 E-1 F30 ;Retract a bit
G1 E-1 Z10 F2400 ;Retract and raise Z
G1 X5 Y5 F3000 ;Wipe out
G1 Z40 ;Raise Z more
G90 ;Absolute positioning

G1 X{machine_width} Y{machine_depth} ;Present print
M106 S0 ;Turn-off fan
M104 S0 ;Turn-off hotend
```

```
M140 S0 ;Turn-off bed

M84 X Y E ;Disable all steppers but Z
```

C.1.3. Cura settings

C.1.3.1. Extruder 1

```
[values]
bottom_layers = 0
cool_fan_enabled = False
cool_min_layer_time = 10
cool_min_speed = 1
infill_overlap = 30.0
infill_pattern = lines
infill_sparse_density = 0
line_width = 1.6
material_alternate_walls = True
material_initial_print_temperature = 20
material_print_temperature = 20
prime_tower_min_volume = 100
retract_at_layer_change = True
retraction_amount = 0.01
retraction_enable = True
retraction_speed = 0.33
skirt_brim_minimal_length = 50
skirt_brim_speed = 5
skirt_gap = 1.6
skirt_height = 1
speed_layer_0 = 5
speed_print = 5
speed_topbottom = 5
speed_travel = 30
speed_wall = 5
speed_wall_x = 5
support_infill_rate = 15
top_bottom_pattern = concentric
top_bottom_thickness = 1.8
top_layers = 0
top_thickness = 1.6
wall_line_count = 3
z_seam_corner = z_seam_corner_outer
z_seam_type = back
```

C.1.3.2. Extruder 2

```
[values]
bottom_layers = 0
cool_fan_enabled = False
cool_min_layer_time = 10
cool_min_speed = 1
infill_pattern = concentric
infill_sparse_density = 100
infill_sparse_thickness = =resolveOrValue('layer_height')
line_width = 60
material_alternate_walls = True
material_flow = 15.972
material_initial_print_temperature = 20
material_print_temperature = 20
retraction_enable = False
speed_layer_0 = 50
speed_print = 50
speed_topbottom = 10
speed_wall = 50
top_bottom_pattern = concentric
top_bottom_thickness = 0
top_layers = 0
wall_line_count = 999
wall_thickness = =wall_line_width_0 if magic_spiralize else 0.8
z_seam_type = random
```

C.1.3.3. General

```
[values]
adhesion_type = skirt
draft_shield_dist = 5
layer_height = 0.8
magic_spiralize = True
material_bed_temp_wait = False
material_bed_temperature = 20
material_print_temp_wait = False
prime_tower_enable = False
prime_tower_position_x = 100
prime_tower_position_y = 100
prime_tower_size = 30
relative_extrusion = True
support_enable = False
```

C.1.4. Material settings

C.1.4.1. Embedded ink

```
<?xml version='1.0' encoding='utf-8'?>
<fdmmaterial xmlns="http://www.ultimaker.com/material"
xmlns:cura="http://www.ultimaker.com/cura" version="1.3">
  <metadata>
    <name>
      <brand>Custom</brand>
      <material>Embedded Ink</material>
      <color>Generic</color>
      <label>Custom Material</label>
    </name>
    <version>1</version>
    <color_code>#ffc924</color_code>
    <GUID>b7c49195-827a-4bc9-9980-da6e72971b80</GUID>
    <adhesion_info />
    <description />
  </metadata>
  <properties>
    <diameter>15</diameter>
    <density>1.24</density>
  </properties>
  <settings>
    <setting key="standby temperature">0</setting>
    <setting key="print cooling">0</setting>
    <setting key="retraction amount">0</setting>
    <setting key="print temperature">0</setting>
    <setting key="heated bed temperature">0.0</setting>
    <setting key="retraction speed">0</setting>
  </settings>
</fdmmaterial>
```

C.1.4.2. Support gel

```
<?xml version='1.0' encoding='utf-8'?>
<fdmmaterial xmlns="http://www.ultimaker.com/material"
xmlns:cura="http://www.ultimaker.com/cura" version="1.3">
  <metadata>
    <name>
      <brand>Custom</brand>
      <material>Support Gel</material>
      <color>Generic</color>
      <label>Custom Material</label>
```

```
    </name>
    <version>1</version>
    <color_code>#ffc924</color_code>
    <GUID>b7c49195-827a-4bc9-9980-da6e72971b80</GUID>
    <adhesion_info />
    <description />
  </metadata>
  <properties>
    <diameter>29.2</diameter>
    <density>1.24</density>
  </properties>
  <settings>
    <setting key="standby temperature">0</setting>
    <setting key="print cooling">0</setting>
    <setting key="retraction amount">0</setting>
    <setting key="print temperature">0</setting>
    <setting key="heated bed temperature">0.0</setting>
    <setting key="retraction speed">0</setting>
  </settings>
</fdmmaterial>
```

C.2. Klipper configuration

```
[include fluidd.cfg]

[stepper_x]
step_pin: PE9
dir_pin: PF1
enable_pin: !PF2
microsteps: 16
rotation_distance: 40
endstop_pin: ^!PB10
position_endstop: 160
position_max: 160
homing_speed: 30

[stepper_y]
step_pin: PE11
dir_pin: PE8
enable_pin: !PD7
microsteps: 16
rotation_distance: 40
endstop_pin: ^!PE12
position_endstop: 160
position_max: 160
homing_speed: 30
```

```
[stepper_z]
step_pin: PE13
dir_pin: PC2
enable_pin: !PC0
microsteps: 16
rotation_distance: 4
endstop_pin: ^!PG8
position_endstop: 0.0
position_max: 250

[extruder]
step_pin: PD13
dir_pin: PG9
enable_pin: !PF0
microsteps: 16
rotation_distance: 0.7
gear_ratio: 3.6:1
nozzle_diameter: 1.6
filament_diameter: 14.8
heater_pin: PB1 # Heat0
sensor_pin:  PF4 # T1 Header
sensor_type: EPCOS 100K B57560G104F
max_power: 1.0
control: pid
pid_Kp: 22.2
pid_Ki: 1.08
pid_Kd: 114
min_temp: 0
max_temp: 250
max_extrude_only_distance: 100.0
min_extrude_temp: 0
max_extrude_cross_section: 9999

[extruder_stepper gel_extruder]
extruder: extruder
step_pin: PD15
dir_pin: !PE7
enable_pin: !PA3
microsteps: 16
rotation_distance: 1.25

[manual_stepper nozzle_stepper]
step_pin: m1:PE9
dir_pin: !m1:PF1
enable_pin: !m1:PF2
microsteps: 16
rotation_distance: 48.695
```

```
[heater_bed]
heater_pin: PD12
sensor_pin: PF3 # T0
sensor_type: EPCOS 100K B57560G104F
control: watermark
min_temp: 0
max_temp: 130
control: pid
pid_Kp: 54.027
pid_Ki: 0.770
pid_Kd: 948.182

[fan]
pin: PE5

[heater_fan fan1]
pin: PC8

[controller_fan fan2]
pin: PE6
heater: extruder,heater_bed
stepper: stepper_x,stepper_y,stepper_z,extruder

[controller_fan m1_fan2]
pin: m1:PE6
heater: extruder,heater_bed
stepper: stepper_x,stepper_y,stepper_z,extruder

[mcu]
serial: /dev/serial/by-path/platform-fd500000.pcie-pci-0000:01:00.0-usb-
0:1.1:1.0

[mcu m1]
serial: /dev/serial/by-path/platform-fd500000.pcie-pci-0000:01:00.0-usb-
0:1.2:1.0

[printer]
kinematics: cartesian
max_velocity: 300
max_accel: 500
max_z_velocity: 5
max_z_accel: 100

########################################
# TMC2209 configuration
########################################

[tmc2209 stepper_x]
uart_pin: PC13
```

```
run_current: 0.800
stealthchop_threshold: 999999

[tmc2209 stepper_y]
uart_pin: PE3
run_current: 0.800
stealthchop_threshold: 999999

[tmc2209 stepper_z]
uart_pin: PE1
run_current: 0.8
stealthchop_threshold: 999999

[tmc2209 extruder]
uart_pin: PD6
run_current: 0.8
stealthchop_threshold: 999999

[tmc2208 extruder_stepper gel_extruder]
uart_pin: PD1
run_current: 0.800
stealthchop_threshold: 999999

[tmc2208 manual_stepper nozzle_stepper]
uart_pin: m1:PC13
run_current: 0.8
stealthchop_threshold: 999999

########################################
# EXP1 / EXP2 (display) pins
########################################

[board_pins]
aliases:
    # EXP1 header
    EXP1_1=PG4, EXP1_3=PD11, EXP1_5=PG2, EXP1_7=PG6, EXP1_9=<GND>,
    EXP1_2=PA8, EXP1_4=PD10, EXP1_6=PG3, EXP1_8=PG7, EXP1_10=<5V>,
    # EXP2 header
    EXP2_1=PB14, EXP2_3=PG10, EXP2_5=PF11, EXP2_7=PF12,  EXP2_9=<GND>,
    EXP2_2=PB13, EXP2_4=PB12, EXP2_6=PB15, EXP2_8=<RST>, EXP2_10=PF13

[display]
lcd_type: emulated_st7920
spi_software_miso_pin: EXP2_1
spi_software_mosi_pin: EXP1_3
spi_software_sclk_pin: EXP1_5
spi_speed: 1000000
en_pin: EXP1_4
encoder_pins: ^EXP2_3, ^EXP2_5
```

```
click_pin: ^!EXP1_2

########################################
# MACROS
########################################

[virtual_sdcard]
path: /home/pi/printer_data/gcodes
on_error_gcode: CANCEL_PRINT

[display_status]

[pause_resume]

[exclude_object]

[gcode_macro CANCEL_PRINT]
description: Cancel the actual running print
rename_existing: CANCEL_PRINT_BASE
gcode:
  TURN_OFF_HEATERS
  CANCEL_PRINT_BASE

[gcode_macro CENTER]
gcode:
  G90
  G1 Z75 F1500
  G1 X90 Y90 F1500

[force_move]
enable_force_move: true

[gcode_macro M201]
gcode:
     G4

[gcode_macro M203]
gcode:
     G4

[gcode_macro M108]
gcode:
     G4

[gcode_macro M205]
gcode:
     G4

[gcode_macro M109]
```

```
rename_existing: M99109
gcode:
  {% set s = params.S|default(20)|float %}
  {% set min_ext = s-10 %}
  {% set max_ext = s+10 %}

  TEMPERATURE_WAIT SENSOR=extruder minimum={min_ext} maximum={max_ext}

[gcode_macro START_PRINT]
gcode:
  {% set BED_TEMP = params.BED_TEMP|default(20)|float %}
  {% set EXTRUDER_TEMP = params.EXTRUDER_TEMP|default(20)|float %}
  {% set min_ext = EXTRUDER_TEMP-10 %}
  {% set max_ext = EXTRUDER_TEMP+10 %}
  {% set min_bed = BED_TEMP-10 %}
  {% set max_bed = BED_TEMP+10 %}

  M104 S20
  M140 S{BED_TEMP}

  #Start heating extruder to temp when bed completes:
  M104 S{EXTRUDER_TEMP} T0
  # Use absolute coordinates
  G90
  # Home the printer
  G28
  CENTER

  # Wait for nozzle to reach temperature
  TEMPERATURE_WAIT SENSOR=extruder minimum={min_ext} maximum={max_ext}

  G92 E0 ;Reset Extruder
  G1 Z50 F3000 ;Move Z Axis up
  G1 X110 Y110 Z0.28 F5000.0 ;Move to start position
  G92 E0 ;Reset Extruder
  G1 Z2.0 F1000 ;Move Z Axis up

[gcode_macro T0]
gcode:
     SET_GCODE_OFFSET Z=0 MOVE=1 SPEED=5
  SYNC_EXTRUDER_MOTION EXTRUDER=gel_extruder MOTION_QUEUE=
  SYNC_EXTRUDER_MOTION EXTRUDER=extruder MOTION_QUEUE=extruder

[gcode_macro T1]
gcode:
     SET_GCODE_OFFSET Z=0.8 MOVE=1 SPEED=5
  SYNC_EXTRUDER_MOTION EXTRUDER=extruder MOTION_QUEUE=
  SYNC_EXTRUDER_MOTION EXTRUDER=gel_extruder MOTION_QUEUE=extruder
```

```
[gcode_macro NOZZLE_DOWN]
gcode:
     MANUAL_STEPPER STEPPER=nozzle_stepper MOVE=0.8 SPEED=10

[gcode_macro NOZZLE_UP]
gcode:
  MANUAL_STEPPER STEPPER=nozzle_stepper MOVE=0 SPEED=10

[gcode_macro NOZZLE_HOLD]
gcode:
  MANUAL_STEPPER STEPPER=nozzle_stepper ENABLE=1 SET_POSITION=0

[gcode_macro NOZZLE_RELEASE]
gcode:
  MANUAL_STEPPER STEPPER=nozzle_stepper ENABLE=0

[gcode_macro GEL_FILL]
gcode:
  {% set extruder_offset = printer.gcode_move.position[2] -
printer.gcode_move.gcode_position[2] %}
  {% if extruder_offset > 0 %}
  G1 E0 F180
  G4 P10000
  {% endif %}

[gcode_macro NOZZLE_PRIME]
gcode:
     {% set nozzle_prime_distance = 1.7 | float %}
  G90
  M82
  G92 E0
  G1 E{1.7268*nozzle_prime_distance+5.2029} F180
  G1 E0 F180
  G4 P10000
  M83

[gcode_macro GEL_PRIME]
gcode:
     T1
     G90
  M82
  G92 E90
     {% set n = 6 %}
     {% for pumps in range(n) %}
     G1 E0 F180
  G4 P10000
     G1 E90 F180
     {% endfor %}
     G1 E0 F180
```

```
 [gcode_macro GEL_LAYER]
 gcode:
      {% set layer_height = 0.8 | float %}
      {% set layer_diameter_sq = 121.642*121.642 | float %}
      {% set syringe_diameter_sq = 28.6*28.6 | float %}
      {% set flow_multiplier = 1 | float %}
      {% set layer_fill =
flow_multiplier*layer_height*layer_diameter_sq/syringe_diameter_sq | float %}
   G90
   M82
   G92 E0
   G1 E{1.384*layer_fill+7.548} F180
   G4 P10000
   G1 E0 F180
   G4 P10000
   M83

 [gcode_macro NOZZLE_PRIME_GEL_LAYER]
 gcode:
      {% set nozzle_prime_distance = 1.7 | float %}
      {% set layer_height = 0.8 | float %}
   {% set layer_diameter_sq = 121.642*121.642 | float %}
      {% set syringe_diameter_sq = 28.6*28.6 | float %}
      {% set flow_multiplier = 1 | float %}
      {% set layer_fill =
flow_multiplier*layer_height*layer_diameter_sq/syringe_diameter_sq | float %}
      {% set nozzle_prime_layer_fill = nozzle_prime_distance + layer_fill |
float %}
   G90
   M82
   G92 E0
   G1 E{1.384*nozzle_prime_layer_fill+7.548} F180
   G4 P10000
   G1 E0 F180
   G4 P10000
   M83
```

C.3. Python G-code post-processing scripts

```
 # The following scripts take an ink and gel file output by a slicer into the
Python Scripts file and
 # meshes them together and performs some fixes to prepare the output file
for embedded 3D
 # printing. Outputs from the files can be checked along the way to
investigate behaviour.

 def offset_ink_gcode(input_file, output_file, offset_value):
     # Raises the part printed with the ink to ensure it is well embedded in
the gel
     with open(input_file, 'r') as f:
         lines = f.readlines()

     modified_lines = []

     for line in lines:
         if line.startswith('G1') or line.startswith('G0'):
             # Extract current Z-coordinate value
             z_index = line.find('Z')

             if z_index != -1:
                 try:
                     # Extract the Z value before any space or comment
                     z_value = float(line[z_index+1:].split()[0])
                     z_value += offset_value # Offset the Z-coordinate
                     line = line[:z_index+1] + str(z_value) +
line[line.find(' ', z_index):]
                     # Update the line with the new Z-coordinate

                 except ValueError: # Handle the case where conversion to
float fails
                     pass

         modified_lines.append(line)

     with open(output_file, 'w') as f:
         f.writelines(modified_lines)

 ink_gcode_file = 'C:\\Users\\User\\Documents\\Project\\Python
Scripts\\Ink_test.gcode'
 offset_gcode_file = 'C:\\Users\\User\\Documents\\Project\\Python
Scripts\\Ink_test_offset.gcode'
 z_offset_value = 10  # Adjust this value based on your requirement

 offset_ink_gcode(ink_gcode_file, offset_gcode_file, z_offset_value)
```

```
 def reset_extruder_gcode(input_file, output_file):
     # Sums all the extrusion values in a layer and retracts them to reset
the gel syringe pump
     with open(input_file, 'r') as f:
         lines = f.readlines()

     modified_lines = []
     cumulative_extrusion = 0.0

     for i, line in enumerate(lines):
         if line.startswith('G92 E0'):
             # Discard lines that would reset the extrusion amount to zero
             continue
         # Extract the E value from the line if it contains an extrusion
command
         e_index = line.find('E')

         if e_index != -1:
             try:
                 # Extract the E value and add to cumulative extrusion
                 extrusion_value = float(line[e_index + 1:].split()[0])
                 cumulative_extrusion += extrusion_value

             except ValueError: # Handle the case where conversion to float
fails
                 pass

         modified_lines.append(line)

         if line.startswith(';MESH:NONMESH'):
             # Retract the accumulated extrusion before the start of the next
layer
             retract_distance = round(-cumulative_extrusion, 5)
             modified_lines.append(f'G1 E{retract_distance} F180 ;Retract\nG4
P10000\n')
             cumulative_extrusion = 0.0  # Reset the cumulative extrusion for
the next layer

     with open(output_file, 'w') as f:
         f.writelines(modified_lines)

 gel_gcode_file = 'C:\\Users\\User\\Documents\\Project\\Python
Scripts\\Gel_test.gcode'
 fixed_gcode_file = 'C:\\Users\\User\\Documents\\Project\\Python
Scripts\\Gel_test_fixed.gcode'

 reset_extruder_gcode(gel_gcode_file, fixed_gcode_file)

 def read_gcode(file_path):
```

```
    #Reads all the lines from a gcode file and returns them in blocks
defined by their 'Z height'
    z_blocks = []
    current_block = {'z': None, 'lines': []}
    capture_lines = False

    with open(file_path, 'r') as file:
        # Defining a start and end point to read between
        for line in file:
            if 'M107' in line:
                capture_lines = True
                continue
            elif 'G91' in line:
                capture_lines = False
                continue
            elif 'M82' in line:  # Skip lines containing 'M82'
                continue

            if capture_lines:
                # Capture lines between valid values of Z
                z = None

                for token in line.split():
                    if token.startswith('Z') and len(token) > 1:
                        # Assigning a value for Z from number immediately
after
                        try:
                            z = float(token[1:])
                        except ValueError: # Handle the case where the value
after Z is not a valid float
                            continue

                if z is not None:
                    if current_block['z'] is not None:
                        #Appending valid lines to blocks
                        z_blocks.append(current_block.copy())
                        current_block['lines'] = []
                    current_block['z'] = z
                current_block['lines'].append(line.strip())

    if current_block['z'] is not None:
        z_blocks.append(current_block)

    return z_blocks

 def merge_gcode(file1_path, file2_path, output_path):
    # Merges two files together by concatenating blocks in order of their 'Z
height'
    file1_blocks = read_gcode(file1_path)
```

```
    file2_blocks = read_gcode(file2_path)
    file1_layer = 0
    file2_layer = 0
    prev_source_file = None

    # Combine the Z values from both files
    all_z_values = set(block['z'] for block in
file1_blocks).union(block['z'] for block in file2_blocks)

    # Sort Z values in ascending order
    sorted_z_values = sorted(all_z_values)

    # Merge blocks based on Z values
    merged_blocks = []
    for z_value in sorted_z_values:
        blocks_with_z_value_file1 = [block for block in file1_blocks if
block['z'] == z_value]
        blocks_with_z_value_file2 = [block for block in file2_blocks if
block['z'] == z_value]

        for block in blocks_with_z_value_file1: # Merge blocks with a
toolchange script between
            merged_blocks.append(['M117 Ink Layer {}'.format(file1_layer)])
            # Check if the previous block was not from file1
            if prev_source_file is None or prev_source_file != 'file1':
                merged_blocks.append(['NOZZLE_UP'] + ['T0'])
                prev_source_file = 'file1'

            merged_blocks.append(block['lines'])
            file1_layer += 1

        for block in blocks_with_z_value_file2:
            merged_blocks.append(['M117 Gel Layer {}'.format(file2_layer)])
            # Check if the previous block was not from file2
            if prev_source_file is None or prev_source_file != 'file2':
                merged_blocks.append(['T1'])
                merged_blocks.append(['NOZZLE_DOWN'] +
['NOZZLE_PRIME_GEL_LAYER'])
                prev_source_file = 'file2'

            elif prev_source_file == 'file2':
                merged_blocks.append(['GEL_LAYER'])

            merged_blocks.append(block['lines'])
            file2_layer += 1

    # Write merged blocks to the output file
    with open(output_path, 'w') as output_file:
        for lines in merged_blocks:
```

```
            for line in lines:
                output_file.write(line + '\n')

 Ink_file = 'C:\\Users\\User\\Documents\\Project\\Python
Scripts\\Ink_test_offset.gcode'
 Gel_file = 'C:\\Users\\User\\Documents\\Project\\Python
Scripts\\Gel_test_fixed.gcode'
 Merged_file = 'C:\\Users\\User\\Documents\\Project\\Python
Scripts\\Ink_gel_merged.gcode'

 merge_gcode(Ink_file, Gel_file, Merged_file)

 def append_start_end(file1_path, file2_path, output_path):
     # Appends the lines taken out in read_gcode
     start_lines = [] # Read the lines of the first file up to 'M107'
     with open(file1_path, 'r') as file1:
         for line in file1:
             if 'T1' in line:
                 continue
             start_lines.append(line.strip())
             if 'M107' in line:
                 break

     end_lines = [] # Read the lines of the first file from 'G91' to the end
     capture_lines = False
     with open(file1_path, 'r') as file1:
         for line in file1:
             if 'G91' in line:
                 capture_lines = True
             if capture_lines:
                 end_lines.append(line.strip())

     second_file_lines = [] # Read the lines of the second file
     with open(file2_path, 'r') as file2:
         second_file_lines = [line.strip() for line in file2]
     # Concatenate the lines and write to the output file
     all_lines = start_lines + second_file_lines + ['M82 ;absolute extrusion
mode'] + end_lines
     with open(output_path, 'w') as output_file:
         for line in all_lines:
             output_file.write(line + '\n')

 file1_path = 'C:\\Users\\User\\Documents\\Project\\Python
Scripts\\Gel_test_fixed.gcode'
 file2_path = 'C:\\Users\\User\\Documents\\Project\\Python
Scripts\\Ink_gel_merged.gcode'
 output_path = 'C:\\Users\\User\\Documents\\Project\\Python
Scripts\\Dual_extrusion.gcode'
```

```
append_start_end(file1_path, file2_path, output_path)
```

C.4. Micro-controller pin-out

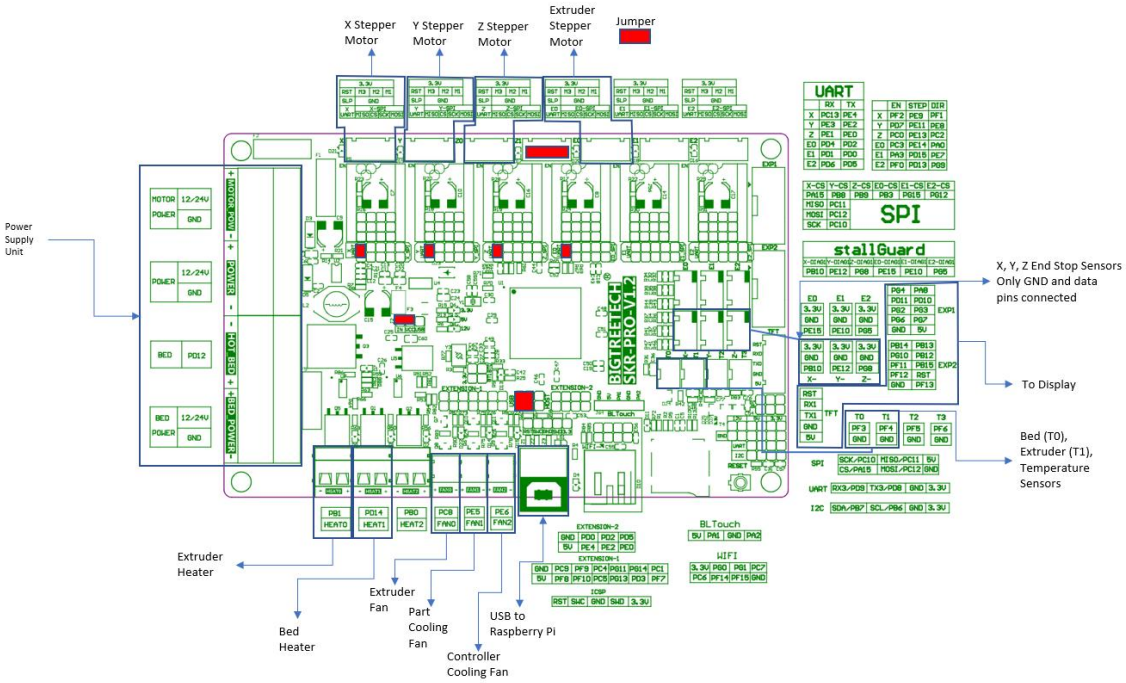

Figure 64: *Micro-controller pin-out*

Both the microcontroller boards used for this project had faulty stepper motor driver circuits. Both controllers were connected to the Raspberry Pi to work around this. On the second microcontroller, the jumpers are in the same positions, the power supply unit is only connected to power and motor power, another cooling fan is connected to PE6, and a motor is connected to one of the motor drivers.

Appendix D: Calculations

D.1. Ink syringe plunger buckling limit

Calculating the buckling limit of the polypropylene plunger will help design the syringe pump to avoid damaging the 10 cc syringe plunger in the ink syringe pump.

The syringe plunger buckling limit may not be calculated well using the Euler column formula for buckling. It is only about five times longer than it is wide during use. It is then prudent to check if Johnson's parabolic equation for buckling serves better. The following relation for the slenderness ratio can be used to check if Johnson or Euler is better in this scenario [70]:

$$(S_r)_D = \pi \sqrt{\frac{2CE}{\sigma^y}} \tag{D-1}$$

In the slenderness ratio $(S_r)_D$, E is the Young's modulus of the column, σ^y is the yield strength of the column, and C is the end condition constant. Euler applies to values greater than the critical slenderness ratio, and Johnson applies to values below.

The syringe plunger is most likely made from polypropylene (PP). PP can have a Young's modulus of 1 GPa and a yield strength of 20 MPa [71][72]. This case will use a C value of 0.25 since the bottom is fixed while the top is free [70]. Substituting these values into Equation D-1 gives:

$$(S_r)_D = \pi \sqrt{\frac{2(0.25)(1\ GPa)}{(20\ MPa)}}$$

$$(S_r)_D = 15.708$$

To calculate the slenderness ratio, S_r, to determine which equation is better, one must know L and k for this scenario. L is the length of the column, which for the plunger is 50 mm. k is the radius of gyration of the column. k can be calculated using Equation D-2 [70]:

$$k = \sqrt{\frac{I}{A}} \tag{D-2}$$

In Equation D-2, I is the area moment of inertia, and A is the cross-sectional area of the column. The cross-sectional area and the area moment of inertia vary over the length of the plunger. For the sake of simplicity, the area will be assumed to be constant since buckling will likely occur mid-way along the length of the plunger, and the variations are only at the ends of the plunger.

Buckling will likely occur between the ribs of the plunger, so the area moment of inertia will be calculated as an "X" shape instead of a "+" shape. To this end, the inertia will be calculated as a square with four triangles removed, as shown in Figure 65.

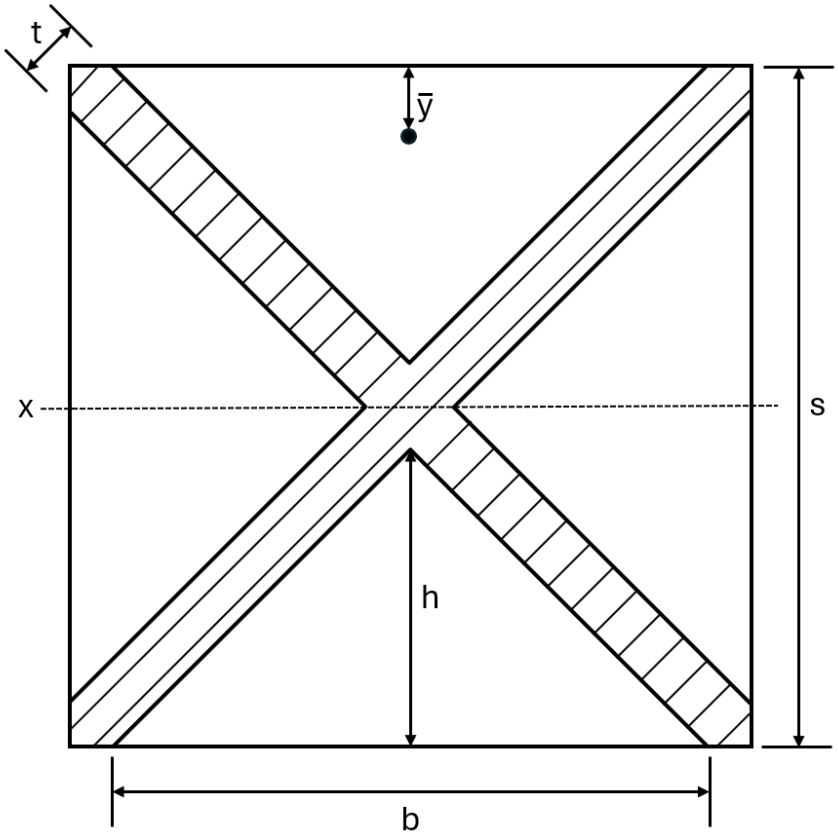

Figure 65: *Cross-section of the syringe plunger.*

$$I = I_{xx\,Square} - 2I_{yy\,Triange} - 2\left(I_{xx\,Triange} + A_{Triangle}\left(\frac{s}{2} - \bar{y}_{Triagle}\right)\right) \quad \text{(D-3)}$$

$$I = \frac{s^4}{12} - 2\left(\frac{hb^3}{48}\right) - 2\left(\frac{bh^3}{36} + \frac{bh}{2}\left(\frac{s}{2} - \frac{h}{3}\right)\right) \quad \text{(D-4)}$$

For the plunger, the distance s is 9.7 mm, and the thickness, t is 0.9 mm. Knowing the thickness and the side lengths, one can use Equation D-5 and Equation D-6 to calculate b and h or the base and the height of the triangles, respectively:

$$b = s - 2t\sin(45°) \quad \text{(D-5)}$$

$$b = 9.7 - 2(0.9)\sin(45°)$$

$$b = 8.427\ mm$$

$$h = \frac{s}{2} - t\sin(45°) \quad \text{(D-6)}$$

$$h = \frac{9.7}{2} - 0.9\sin(45°)$$

$$h = 4.214\ mm$$

Knowing b and h, one may begin substituting values into Equation D-4:

$$I = \frac{9.7^4}{12} - 2\left(\frac{(4.214)(8.427)^3}{48}\right) - 2\left(\frac{(8.427)(4.214)^3}{36} + \frac{(8.427)(4.214)}{2}\left(\frac{9.7}{2} - \frac{4.214}{3}\right)\right)$$

$$I = 475.285\ mm^4$$

The cross-sectional area can be calculated using Equation D-7 and Equation D-8:

$$A = A_{Square} - 4A_{Triangle} \tag{D-7}$$

$$A = s^2 - 4\left(\frac{bh}{2}\right) \tag{D-8}$$

$$A = 9.7^2 - 4\left(\frac{(8.427)(4.214)}{2}\right)$$

$$A = 23.067\ mm^2$$

Knowing the cross-sectional area and the area moment of inertia of the plunger, one may continue and calculate the radius of gyration of the plunger using Equation D-2:

$$k = \sqrt{\frac{475.285}{23.067}}$$

$$k = 20.604$$

One may now calculate the slenderness ratio, S_r of the plunger, using Equation D-8:

$$S_r = \frac{L}{k} \tag{D-8}$$

$$S_r = \frac{50}{20.604}$$

$$S_r = 2.437$$

$$(S_r)_D > S_r$$

Having shown that the slenderness ratio is above the critical point $(S_r)_D$, one may rest assured Jackson's relation for buckling is appropriate [70], using Equation D-9:

$$F = A\left(\sigma^y - \frac{1}{E}\left(\frac{\sigma^y}{2\pi}\right)^2\left(\frac{L}{k}\right)^2\right) \tag{D-9}$$

$$F = (23.067 \times 10^{-6})\left(20 \times 10^6 - \frac{1}{1 \times 10^9}\left(\frac{20 \times 10^6}{2\pi}\right)^2\left(\frac{0.05}{20.604}\right)^2\right)$$

$$F = 461.34\ N$$

Knowing the buckling limit of the plunger, one may take appropriate measures to avoid damaging the ink deposition syringe pump by not forcing fluid out of the pump that requires more than 460 N of force.

D.2. Ink syringe pump threaded rod force output

It would be wise to assess whether an M4 threaded rod driven by a NEMA17 motor can produce enough force to depress the syringe and determine whether the single start M4 threaded rod is appropriate for the ink syringe pump. One may use Equation D-10 and Equation D-11 to determine this [39]:

$$T = \frac{F d_m B}{2} \tag{D-10}$$

$$B = \frac{l + \pi f d_m \sec(\alpha)}{\pi d_m - f l \sec(\alpha)} \tag{D-11}$$

In Equation D-10 and Equation D-11, T is torque, F is force, d_m is the mean diameter of the threaded rod, l is the lead of the thread, f is the coefficient of friction, and α is half the thread angle. Making force the subject of the equation:

$$F = \frac{2T}{d_m B} \tag{D-12}$$

The mean diameter can be calculated with Equation D-13:

$$d_m = d - \frac{p}{2} \tag{D-13}$$

Where d is the diameter of the thread, and p is the pitch of the thread. In single-start M4 threaded rods, the diameter is 4 mm, and the pitch is 0.7 mm. Substituting this all into Equation D-13:

$$d_m = 4 - \frac{0.7}{2}$$

$$d_m = 3.65\ mm$$

NEMA17 motors can output a torque of 0.45 Nm, the lead of the M4 threaded rod is 0.7 mm, the coefficient of friction of steel on steel is 0.16 [73], and the thread angle is 30°. Substituting this all into Equation D-11 and Equation D-10:

$$B = \frac{0.7 + \pi(0.16)(3.65)\sec(30)}{\pi(3.65) - (0.16)(0.7)\sec(30)}$$

$$B = 0.2486$$

$$F = \frac{2(0.45)}{\left(\frac{3.65}{1000}\right)(0.2486)}$$

$$F = 991.86\ N$$

992 N is more than double the required force of 400 N to depress the 20 cc syringe. At least by this metric, a M4 threaded rod is appropriate for this application.

D.3. Linear rod deflection

When the 20 cc syringe in the syringe pump is extruding material, a reaction force is applied, which results in a moment of acting on the linear rods that the syringe depressor mechanism slides along. One should choose linear rods that do not deflect large amounts under this moment to ensure that the material is accurately and consistently extruded as expected.

One may simplify and model the problem as a single beam with a circular cross-section with half the applied moment applied to it with clamped ends, as Figure 66 shows:

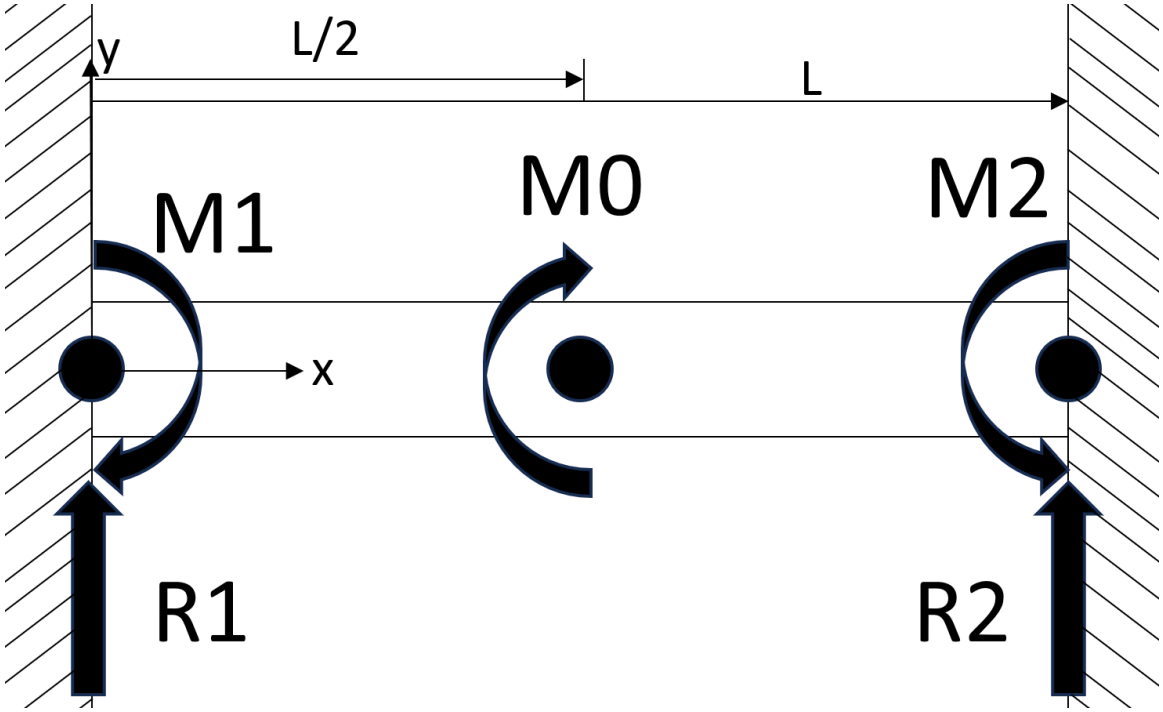

Figure 66: *Moments and forces on the linear rods.*

M_0 is the applied bending moment, M_1 and M_2 are reaction moments, R_1 and R_2 are reaction forces, and l is the length of the beam.

One may calculate the moment M_0 as half (as there are two linear rods) the force being applied to the syringe plunger times the distance the axis of the plunger is away from the plane running through the axes of the linear rods. This moment can be shown by Equation D-14:

$$M_0 = \frac{F_R d}{2} \tag{D-14}$$

Where F_R is the reaction force, and d is the distance of the moment arm. In this case, 400 N should be a worst-case scenario for the force being applied to the plunger and the distance for the moment arm is 30 mm. This yields:

$$M_0 = \frac{400 * 0.003}{2}$$

$$M_0 = 6\ Nm$$

As a worst-case scenario, the reaction moment M_0 may be applied in the middle of the beam where it can cause the most bending. Reaction moments and forces are present at both clamped ends, as shown. The following constraints may be put on the system:

$$\theta_1 = \theta_2 = 0$$

$$\delta_1 = \delta_0 = \delta_2 = 0$$

The angular displacement of the clamped ends will naturally be zero as they cannot rotate. The deflection at the clamped ends can likewise be said to be zero. The centre where the moment is being applied can also be said to be zero since no force is applied on the beam by the load. Then, doing a moment balance around the midpoint of the beam:

$$0 = M_0 + M_1 - M_2 + R_1 \cdot \frac{l}{2} - R_2 \cdot \frac{l}{2}$$

Doing a force balance on the beam yields:

$$0 = R_1 + R_2$$

$$R_1 = -R_2$$

Using this to simplify the moment balance yields:

$$M_2 = M_0 + M_1 + R_1 l$$

One can then use Equation D-15 and Equation D-16 for deflection due to bending [39]:

$$\theta = \int \frac{M}{EI} dx \tag{D-15}$$

$$\boldsymbol{y = \int \theta\, dx} \tag{D-16}$$

Where M is the bending moment being subjected to the beam, E is the Young's Modulus of the material in the beam, I is the moment of inertia, y is the deflection of the beam, x is the length along the beam and θ is the angular deflection of the beam.

Knowing this and noting that in this case, EI is constant for the entire length of the beam since the cross-section remains constant, one may make the following equations, with a and b being used to denote the first and second half of the linear rod respectively:

$$\theta_a = {M_1 x + \frac{1}{2} R_1 x^2}\Big/_{EI}$$

$$\theta_b = {M_0 x + M_1 x + \frac{1}{2} R_1 x^2 - \left(M_0 + M_1 + \frac{1}{2} R_1 l\right) l}\Big/_{EI}$$

$$y_a = {\frac{1}{2} M_1 x^2 + \frac{1}{6} R_1 x^3}\Big/_{EI}$$

$$y_b = {\frac{1}{2} M_0 x^2 + \frac{1}{2} M_1 x^2 + \frac{1}{6} R_1 x^3 - \left(M_0 + M_1 + \frac{1}{2} R_1 l\right) l x + \frac{1}{2}\left(M_0 + M_1 + \frac{2}{3} R_1 l\right) l^2}\Big/_{EI}$$

$$M_1 = -\frac{1}{2}(M_0 + R_1 l)$$

$$R_1 = -\frac{3M_0}{2l}$$

With the reaction forces and loads being known, the only unknowns left are Young's Modulus and the moment of inertia. The linear rods are made from C45 steel, with a Young's Modulus of 190 GPa [74]. To calculate the moment of inertia, the Equation D-17 can be used (Budynas & Nisbett, 2015):

$$I = \frac{\pi D^4}{64} \tag{D-17}$$

Equation D-17 only requires the diameter, D, of the linear rod, which stays a constant 6 mm throughout:

$$I = \frac{\pi(6)^4}{64}$$

$$I = 63.617\ mm^4$$

MATLAB was used to generate Figure 67. The code may be found in the following Google Drive:

https://drive.google.com/drive/folders/1mXSRrU1Rug7xi4EunPfRDUiUuODyCZJ4?usp=drive_link

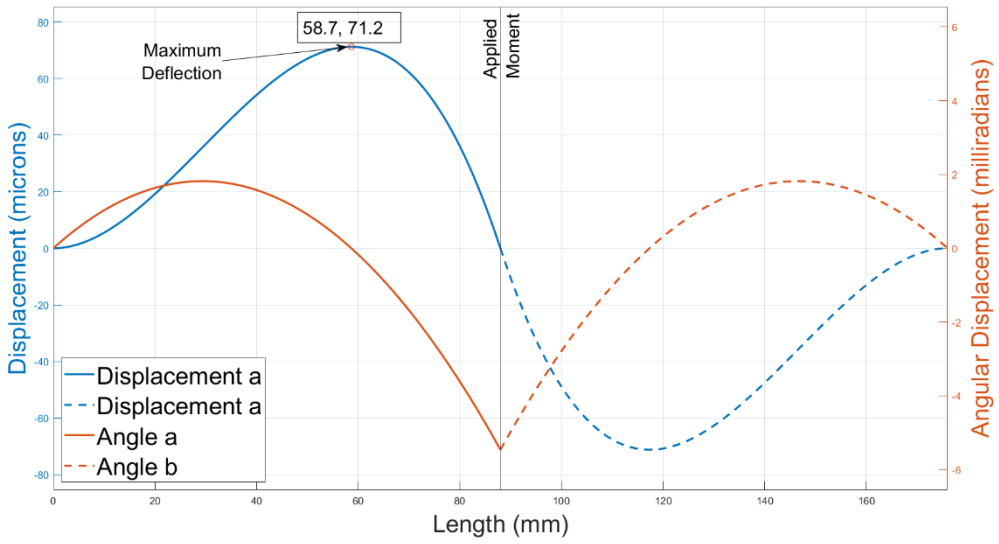

Figure 67: *Calculated displacement and angular displacement of the linear rods.*

Figure 67 shows the maximum displacement is 71.2 microns. Considering the small displacement due to the moment, in addition to the metal backplate to which the linear rods are mounted and the lower housing in which the syringe is being held, should adequately ensure that the syringe pump will extrude material accurately and consistently.

D.4. Peristaltic pump volumetric flowrate

An open-source parametric peristaltic pump developed by PattysLab [66] was used as a starting point for developing a peristaltic pump specific to this application. Three 625RS radial ball bearings were used as rollers to occlude a flexible, 5 mm outer diameter hose with 1 mm walls. The centre of the rollers is 18.2 mm from the centre of the motor axis. Knowing all this, one may begin to calculate the volume of fluid extruded per revolution of the peristaltic pump.

The first step to calculate the volume per revolution of a peristaltic pump is to approximate the pump as a torus using Equation D-18:

$$V = 2\pi^2 r^2 R \tag{D-18}$$

In Equation D-18, V is the volume, r is the internal radius of the tube, and R is the radius from the centre of the motor axis to the centre of the tube. The peristaltic pump in question has an internal tube radius of 1.5 mm and an arm radius of 25.5 mm. This yields the below results:

$$V = 2\pi^2(1.5)^2(25.5)$$

$$V = 1132.25\ mm^3$$

One should note that the rollers depress the tube, which needs to be considered. This can be done by subtracting the volume segment of the circular profile of the rollers from the volume of the torus calculated above. The segment, however, also covers a volume that is not depressing the tube, so one must subtract that volume using another segment. The two areas are shown in Figure 68:

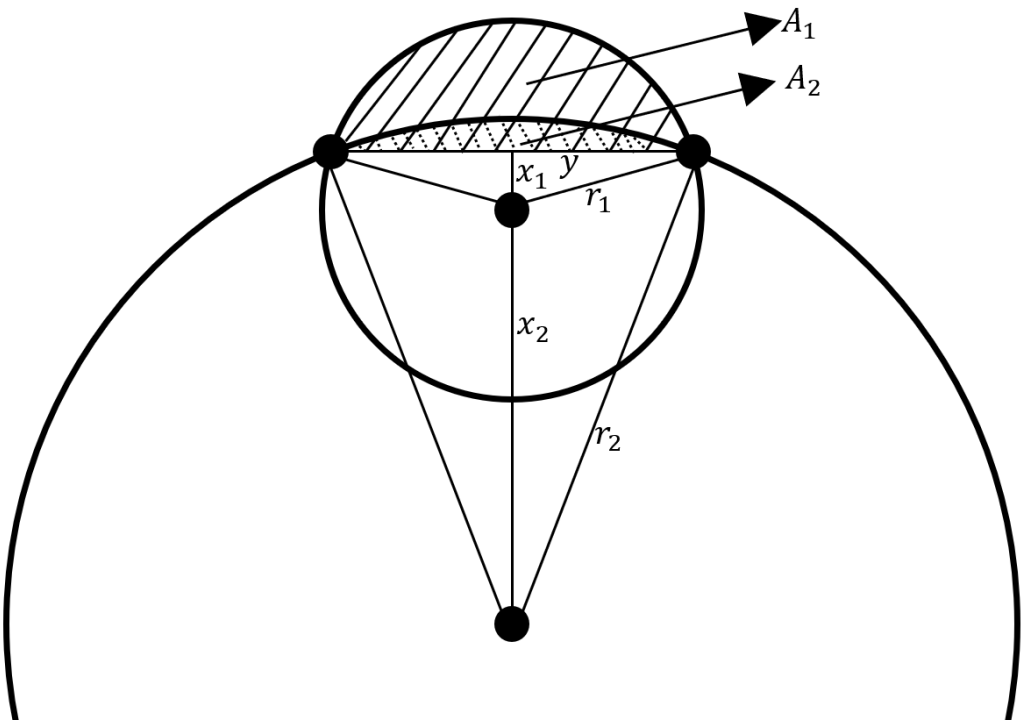

Figure 68: *Aid in the calculation of the occluded area of the peristaltic pump.*

The equation for the area of a segment is given below in Equation D-19:

$$A = r^2\left(\frac{\pi\theta}{360} - \frac{\sin\theta}{2}\right) \tag{D-19}$$

Where A is the area of the segment, r is the radius of the circle, and θ is the angle opposite of the segment of the circle. In this case, the line cutting the segment from the rest of the circle is shared between the two circles. This allows the depressed area of the peristaltic pump to be shown by Equation D-20:

$$A_d = A_1 - A_2 \tag{D-20}$$

Where A_d is the depressed area, A_2 is the segment of the circle drawn by the roller with the thickness of the tubing since the thickness of the tubing also depresses the tube and A_1 is the segment of the circle drawn by the centre of the tubing minus the internal radius of the tubing. With this knowledge, the radii required can be calculated for the segment area calculations, but the angle is still unknown. Some trigonometry can be done to find these angles using Figure 69.

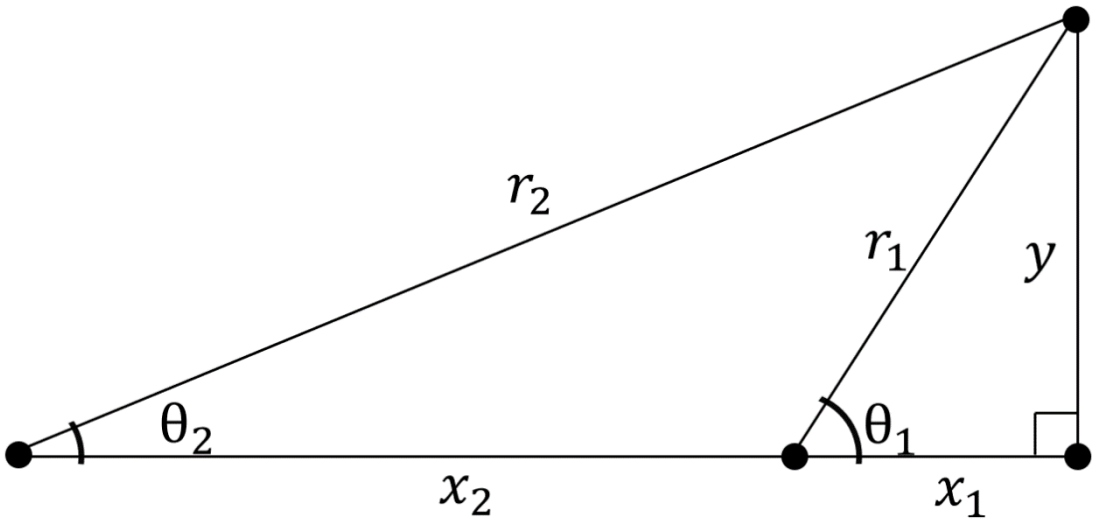

Figure 69: *Aid in the finding of the unknown angles required to find the occluded area of the peristaltic pump.*

Looking at Figure 69, r_1, r_2 and x_2 are known while x_1, θ_1, θ_2 and y are unknown. However, y is shared, so using Pythagoras:

$$y = \sqrt{{r_2}^2 - (x_1 + x_2)^2} \tag{D-21}$$

And

$$y = \sqrt{{r_1}^2 - {x_1}^2} \tag{D-22}$$

Making x_1 the subject after making Equation D-21 and Equation D-22 equal:

$$x_1 = \frac{{r_2}^2 - {r_1}^2 - {x_2}^2}{2x_2} \tag{D-23}$$

With $r_1 = 9\ mm$, $r_2 = 25.5\ mm$ and $x_2 = 18.2\ mm$, this yields:

$$x_1 = \frac{25.5^2 - 9^2 - 18.2^2}{2 \times 18.2}$$

$$x_1 = 6.539\ \text{mm}$$

Substituting x_1 along with the values for r_1, r_2 and x_2 into either Equation D-21 or Equation D-22 yields:

$$y = 6.184\ mm$$

Using the above information and Equation D-24:

$$\theta = \sin^{-1}\frac{y}{r} \tag{D-24}$$

Which yields:

$$\theta_1 = 43.4°$$

And

$$\theta_2 = 14°$$

However, the angles opposite the segment are double θ_1 and θ_2, yielding a θ_{s1} and θ_{s2} of 86.8° and 28.1°. With all this said, the areas depressed area can be calculated using Equation D-25.

$$A_d = {r_1}^2\left(\frac{\pi\theta_{s1}}{360} - \frac{\sin\theta_{s1}}{2}\right) - {r_2}^2\left(\frac{\pi\theta_{s2}}{360} - \frac{\sin\theta_{s2}}{2}\right) \tag{D-25}$$

$$A_d = 9^2\left(\frac{\pi \times 86.8}{360} - \frac{\sin 86.8}{2}\right) - 25.5^2\left(\frac{\pi \times 28.1}{360} - \frac{\sin 28.1}{2}\right)$$

$$A_d = 14.603\ mm^2$$

Multiplying this area with the height of the channel, in this case, $5\ mm$, yields an approximate volume depressed by a single roller of $73.013\ mm^3$. With this known, the volume of all the rollers, 3, in the pump tested, may be subtracted from the volume calculated for a torus above. Note this value can be expressed as a volumetric flow rate since this is the theoretical fluid output per revolution.

$$\dot{V} = V - 3A_d \tag{D-26}$$

$$\dot{V} = 1132.54 - 3 \times 73.013$$

$$\dot{V} = 913.45\, mm^3/rev = 0.913\, ml/rev$$

This volumetric flow rate can be used to determine the efficiency of the pump's output. This will determine how well the peristaltic pump performs compared to the piston pump by seeing how well the peristaltic pump performs when attempting to print at a rate of 913.45 mm^3/s.

D.5. Gel yield stress prediction equations

In the case where none of the gels that had undergone rheology testing had the appropriate yield stress or viscosity properties, an effort was made to formulate an equation to predict the properties of a gel with a different concentration.

The rheology tests tested concentrations of 3, 5 and 7 g/1000ml. For these concentrations, the yield stress behaviour is known. In water, the concentration of Carbopol gel should be zero. Water has a yield stress of zero. Water can then give a fourth point to create an equation describing the relation between concentration and yield stress in Carbopol 940 gel. This can take the form of Equation D-27:

$$y = ax^3 + bx^2 + cx + d \tag{D-27}$$

Where y is the yield stress, x is the concentration of the Carbopol gel and a, b, c and d are constants. Knowing that water has zero concentration of Carbopol and zero yield stress and that each concentration, the following is true:

$$For\ Concentration\ of\ 0\ \frac{g}{1000ml};\quad 0 = a(0)^3 + b(0)^2 + c(0) + d$$

$$For\ Concentration\ of\ 3\ \frac{g}{1000ml};\quad \tau_y[3] = a(3)^3 + b(3)^2 + c(3) + d$$

$$For\ Concentration\ of\ 5\ \frac{g}{1000ml};\quad \tau_y[5] = a(5)^3 + b(5)^2 + c(5) + d$$

$$For\ Concentration\ of\ 7\ \frac{g}{1000ml};\quad \tau_y[7] = a(7)^3 + b(7)^2 + c(7) + d$$

This data can be contained within a table as shown below in Table 9:

Table 9: *Carbopol concentration variables*

Concentration	a	b	c	d	y
0 g/1000ml	0	0	0	1	0
3 g/1000ml	27	9	3	1	$\tau_y[3]$
5 g/1000ml	125	25	5	1	$\tau_y[5]$
7 g/1000ml	343	49	7	1	$\tau_y[7]$

Returning then to Equation D-27, this gives us that d must be zero as well. Knowing the row for 0 g/1000ml and the d column are only filled with zeroes, one can disregard this row and column, as shown in Table 10.

Table 10: *Simplified Carbopol concentration variables*

a	b	c	y
27	9	3	$\tau_y[3]$
125	25	5	$\tau_y[5]$
343	49	7	$\tau_y[7]$

Several transforms were performed, resulting in the values in Table 11.

Table 11: *Calculated variable equations*

a	b	c	y
15	1	0	$(\tau_y[7] - 2\tau_y[5] + \tau_y[3])/8$
-71	-7	1	$2\tau_y[3] - \tau_y[5]$
1	0	0	$(\frac{17}{8}(\tau_y[7] - 2\tau_y[5] + \tau_y[3]) - \frac{1}{4}\tau_y[7] + \frac{9}{4}\tau_y[3] - \tau_y[5])/105$

$$a = \frac{1}{24}\tau_y[3] - \frac{1}{20}\tau_y[5] + \frac{1}{56}\tau_y[7]$$

$$b = \frac{1}{8}\tau_y[3] - \frac{1}{4}\tau_y[5] + \frac{1}{8}\tau_y[7] - 15a$$

$$c = 2\tau_y[3] - \tau_y[5] + 71a + 7b$$

$$d = 0$$

R was used to create a plot showing the predicted yield stress of Carbopol 940 gel using the equations formulated in this appendix sub-section. That code may be found in the following Google Drive:

https://drive.google.com/drive/folders/1mXSRrU1Rug7xi4EunPfRDUiUuODyCZJ4?usp=drive_link

D.6. The average radius of a truncated cone

Two methods are investigated here to calculate the average radius of a truncated cone. The first was used to calculate the radius at which the volume above and below that point would be equal. The second method investigated was to make the volume of truncated being printed equal to the volume of a cylinder with the same height as the cone.

Equation D-28 describes the volume of a truncated cone:

$$V = \frac{1}{3}\pi h(r^2 + rR + R^2) \tag{D-28}$$

Where V is the volume of the truncated cone, h is the height of the truncated cone, r is the bottom radius of the truncated cone, and R is the top radius of the truncated cone.

Using the truncated cone equivalence method with t and b denoting the top truncated cone and bottom truncated cone:

$$V_t = V_b \tag{D-29}$$

$$\frac{1}{3}\pi h_t\left({r_t}^2 + r_t R_t + {R_t}^2\right) = \frac{1}{3}\pi h_b\left({r_b}^2 + r_b R_b + {R_b}^2\right) \tag{D-30}$$

One may divide out the constants present on both sides of the equation and replace r_t and R_b with r_x since they are all equal and r_x will clearly denote that this is the unknown in this equation. R_t will also be replaced with r_t to make the equation more manageable to read in its final form. Another property to take note of is that r increases linearly with h. Linear increases can be described with the equation for a straight line:

$$y = mx + c \tag{D-31}$$

Where m is a constant gradient, and c is a constant. One may substitute r for y and h for x in this case. Applying these substitutions yields:

$$r = mh + c \tag{D-32}$$

Or alternatively:

$$h = \frac{r}{m} - \frac{c}{m} \tag{D-33}$$

The height then from the bottom of the truncated cone to the point where the volume is equal above and below can be shown as:

$$h_b = \left(\frac{r_x}{m} - \frac{c}{m}\right) - \left(\frac{r_b}{m} - \frac{c}{m}\right)$$

$$h_b = \left(\frac{r_x}{m} - \frac{r_b}{m}\right) \tag{D-34}$$

Similarly, the height from that same point up to the top of the truncated cone can be simplified to:

$$h_t = \left(\frac{r_t}{m} - \frac{r_x}{m}\right) \tag{D-35}$$

Substituting Equation D-34 and Equation D-35 into the Equation D-30 yields:

$$\left(\frac{r_t}{m} - \frac{r_x}{m}\right)\left({r_x}^2 + r_x r_t + {r_t}^2\right) = \left(\frac{r_x}{m} - \frac{r_b}{m}\right)\left({r_b}^2 + r_b r_x + {r_x}^2\right)$$

Simplifying this all yields:

$$r_x = \sqrt[3]{\frac{{r_t}^3 + {r_b}^3}{2}} \tag{D-36}$$

This radius will be called the volumetric average radius.

Another method for calculating the average radius would be to make the volume of the truncated cone equal to that of a cylinder of an equal height, which looks like the following:

$$\frac{1}{3}\pi h({r_b}^2 + r_b r_t + {r_t}^2) = \pi h {r_x}^2$$

The above equation simplifies down to:

$$r_x = \sqrt{\frac{{r_b}^2 + r_b r_t + {r_t}^2}{3}} \tag{D-37}$$

This radius will be called the equivalent cylindrical radius.

D.7. Nozzle fill function volume

The dual extruder has a design utilising a drop-down nozzle. To ensure this nozzle is full when printing gel, the nozzle should be filled with gel before gel deposition can occur. One should then calculate the volume between the end of the nozzle and the outlet of the tubes running down into the nozzle.

The volume of the upper and middle portions of the nozzle is simple to compute since they are annuli with constant radii over their height, which can be shown as:

$$V_u = \pi h_u({r_{uo}}^2 - {r_{ui}}^2) \tag{D-38}$$

$$V_m = \pi h_m({r_{mo}}^2 - {r_{mi}}^2) \tag{D-39}$$

Where V_u and V_m are the volumes of the upper and middle portions of the nozzle, h_u and h_m are the heights of the upper and middle portions of the nozzle, r_{uo} and r_{mo} are the outer radii of the upper and middle portions of the nozzle and r_{ui} and r_{mi} are the inner radii of the upper and middle portions of the nozzle. A cross-section of the nozzle is shown in Figure 70.

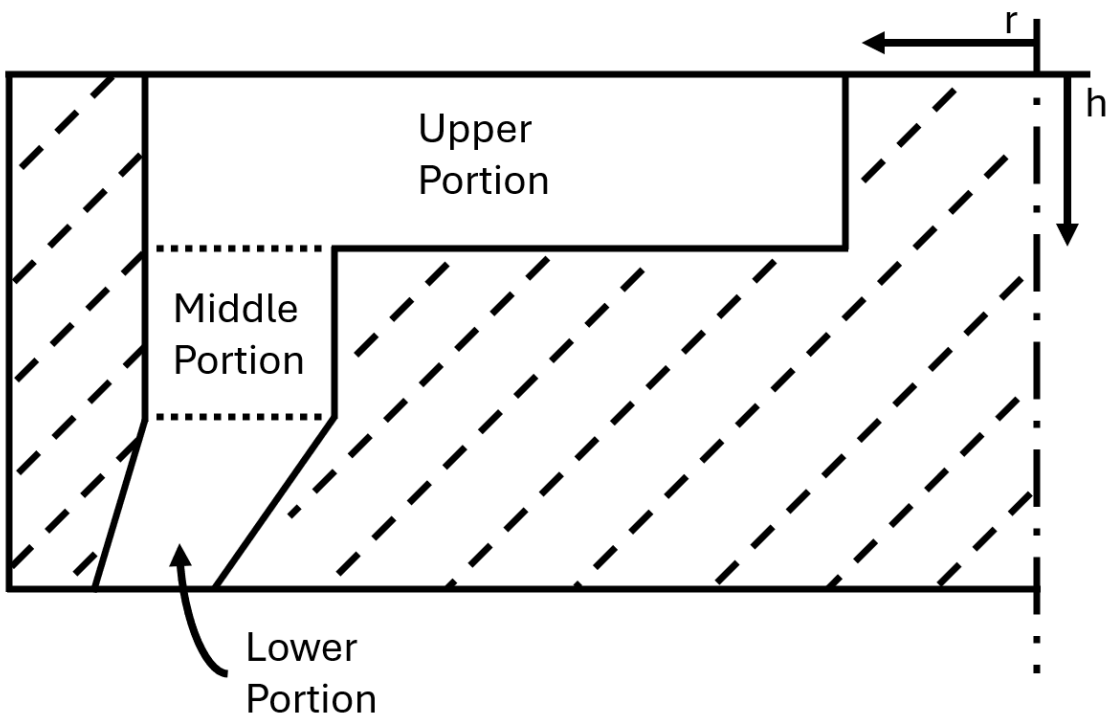

Figure 70: *Cross-sectional view of the annular nozzle.*

Calculating the volume of the lower portion of the nozzle will be somewhat more complicated since the outer and inner radii of the annulus change with its height. To calculate the volume of an annulus with varying inner and outer radii, one may use Equation D-40:

$$V = \pi \int_{h_1}^{h_2} ({r_o}^2 - {r_i}^2)\, dh \tag{D-40}$$

The radii of the annulus, in this case, have a constant slope and so can be represented with the following equations:

$$r_o = m_o h + c_o$$

$$m_o = \frac{r_{oend} - r_{ostart}}{h_{tot}}$$

$$c_o = r_{ostart}$$

$$r_i = m_i h + c_i$$

$$m_i = \frac{r_{iend} - r_{istart}}{h_{tot}}$$

$$c_o = r_{istart}$$

Where r_o and r_i are the outer and inner radii, respectively, m_o and m_i are the constant gradients of the outer and inner radii, c_o and c_i are constants, r_{oend} and r_{iend} are the outer and inner radii at the ends of the annuli, r_{ostart} and r_{istart} are the outer and inner radii at the start of the annuli and h_{tot} is the distance between the start and the end of the annulus.

Since the integral above squares both the equations for r_o and r_i, that may also be done:

$$r_o{}^2 = m_o{}^2h^2 + 2m_ohc_o + c_o{}^2$$

$$r_i{}^2 = m_i{}^2h^2 + 2m_ihc_i + c_i{}^2$$

Substituting that back into Equation D-40:

$$V_l = \pi \int_0^{h_l} (m_o{}^2h^2 + 2m_ohc_o + c_o{}^2 - m_i{}^2h^2 - 2m_ihc_i - c_i{}^2)\, dh$$

$$V_l = \pi \int_0^{h_l} \left((m_o{}^2 - m_i{}^2)h^2 + (2m_oc_o - 2m_ic_i)h + (c_o{}^2 - c_i{}^2)\right) dh$$

$$V_l = \pi \left(\left(\frac{1}{3}(m_o{}^2 - m_i{}^2)h_l{}^3 + \frac{1}{2}(2m_oc_o - 2m_ic_i)h_l{}^2 + (c_o{}^2 - c_i{}^2)h_l\right) - 0\right)$$

$$V_l = \pi h_l \left(\frac{1}{3}(m_o{}^2 - m_i{}^2)h_l{}^2 + \frac{1}{2}(2m_oc_o - 2m_ic_i)h_l + (c_o{}^2 - c_i{}^2)\right)$$

Combining the volumes for the upper and lower nozzle yields:

$$V = \pi \left(h_u(r_{uo}{}^2 - r_{ui}{}^2) + h_m(r_{mo}{}^2 - r_{mi}{}^2) + h_l \left(\frac{1}{3}(m_o{}^2 - m_i{}^2)h_l{}^2 + (m_oc_o - m_ic_i)h_l + (c_o{}^2 - c_i{}^2)\right)\right)$$

One may split this to make it easier to read and calculate:

$$V = \pi\big(A1 + A2 + h_l(B + C + D)\big) \tag{D-41}$$

$$A1 = h_u(r_{uo}{}^2 - r_{ui}{}^2) \tag{D-42}$$

$$A2 = h_m(r_{mo}{}^2 - r_{mi}{}^2) \tag{D-43}$$

$$B = \frac{1}{3}((r_{oend} - r_{ostart})^2 - (r_{iend} - r_{istart})^2) \tag{D-44}$$

$$C = (r_{oend} - r_{ostart})r_{ostart} - (r_{iend} - r_{istart})r_{istart} \tag{D-45}$$

$$D = r_{ostart}{}^2 - r_{istart}{}^2 \tag{D-46}$$

One may then take the volume calculated in Equation D-41 and divide it by the area of the syringe in the syringe pump extruding gel to find the distance that should be requested to be extruded:

$$D_{extrude} = \frac{V}{\pi {R_s}^2} \tag{D-47}$$

Where $D_{extrude}$ is the distance to be extruded and R_s is the inner radius of the syringe extruding the gel.

D.8. Ink maximum extrusion rate

The maximum extrusion rate of the ink syringe pump can be determined by looking at the maximum nozzle translation speed, as stated in Section 3.3.3, to calculate the deposition speed and relate that to the volumetric flow rate out of the syringe pump. This is shown as:

$$\boldsymbol{Q = v_n d_n h} \qquad \boldsymbol{Q = v_p \pi r_s^2}$$

$$v_n d_n h = v_p \pi r_s^2$$

$$v_p = \frac{v_n d_n h}{\pi r_s^2} \tag{D-48}$$

Where Q is the volumetric flow rate, v_n and v_p is the velocity of the nozzle and the plunger respectively, d_n is the diameter of the nozzle, h is the printed layer height, and r_s is the radius of the syringe. In this maximum case, the nozzle velocity will be assumed to be 100 mm/s, d_n is 0.57 mm (assuming a 21 GA general application needle), h is 1 mm, and r_s is measured to be 7.285 mm in a 10 cc syringe. Substituting these values into Equation D-48 yields:

$$v_p = \frac{(100)(0.57)(1)}{\pi(7.825)^2}$$

$$v_p = 0.296\ mm/s$$

This shows that the ink syringe pump plunger's maximum expected extrusion rate is 0.3 mm/s.

D.9. Peristaltic pump torque equation derivation

A force balance can be done between the pressure difference over the length of the tube through which fluid flow occurs and the losses due to the shear stresses acting on the fluid in contact with the walls of the tube to determine the torque requirement on the motor driving a peristaltic pump.

$$F_a = F_s \tag{D-49}$$

$$F_a = P_a A_t \qquad \text{(4-50)} \qquad F_s = \tau_w A_s \tag{D-51}$$

$$\mathrm{F_a = \Delta P \cdot \frac{\pi D_t^{\,2}}{4}} \qquad \text{(4-52)} \qquad \mathrm{F_s = \tau_w \cdot \pi D_t L_t} \tag{D-53}$$

$$\Delta P \cdot \frac{\pi D_t^{\,2}}{4} = \tau_w \cdot \pi D_t L_t \tag{D-54}$$

$$\Delta P = \frac{4L_t}{D_t} \cdot \tau_w \tag{D-55}$$

In the first two lines of this derivation, F_a is the force being applied to push fluid through the tube, P_a is the pressure of the fluid in the tube, A_t is the cross-sectional area of the tube, F_s is the shear force on the tube walls and A_s is the internal surface area of the tube. In the last lines of the derivation, ΔP is the pressure drop across the length of the pipe, D_t is the internal diameter of the pipe and L_t is the length of the pipe.

Since F_a is the force applied to push fluid through the tube, and we now have an expression for ΔP and τ_w, the torque required to push the fluid can be expressed like so:

$$T = F_a R \tag{D-56}$$

$$T = \frac{4L_t}{D_t}\left(\frac{\pi {D_t}^2}{4}\right) R \cdot \tau_w \tag{D-57}$$

$$T = \pi D_t L_t R\left(\tau_0 + K\left(\left(\frac{3n+1}{4n}\right)\left(\frac{8V}{D_t}\right)\right)^n\right) \tag{4-13}$$

D.10. Gel syringe pump threaded rod force output

The syringe pump design uses a NEMA17 stepper motor rotating an M4 threaded rod, which then drives the plunger on the 60 cc syringe back and forth. One may approximate the output force of this arrangement with Equation D-58 [39]:

$$F = \frac{2T_R}{d_m}\left(\frac{\pi d_m - f l \sec(\alpha)}{l + \pi f d_m \sec(\alpha)}\right) \tag{D-58}$$

Where T_R is the required torque, F is the sum of the forces acting in the axial direction of the screw, d_m is the mean diameter of the screw, l is the lead of the screw, f is the coefficient of friction, and α is half the thread angle.

We know the maximum output torque of a NEMA17 motor is 0.4 Nm. The lead of an M4 screw is 0.7 mm, the coefficient of friction of lubricated steel rubbing against steel is 0.16 [73], and half the thread angle is 30° for ISO Metric threads. To calculate the mean diameter, one may use Equation D-13 [39]:

$$d_m = d - \frac{p}{2} \tag{D-13}$$

Where d is the diameter of the thread, and p is the pitch of the thread. The M4 lead screw is a single start thread with a pitch of 0.7 mm, allowing us to calculate the mean diameter:

$$d_m = 4 - \frac{0.7}{2}$$

$$d_m = 3.65\ mm$$

Using the rated torque of the NEMA17 motor, the maximum thrust force can be calculated:

$$F = \frac{2 \cdot 0.4}{\frac{3.65}{1000}}\left(\frac{\pi \cdot \frac{3.65}{1000} - 0.16 \cdot \frac{0.7}{1000}\sec(30)}{\frac{0.7}{1000} + \pi \cdot 0.16 \cdot \frac{3.65}{1000}\sec(30)}\right)$$

$$F = 882\ N$$

D.11. Annular nozzle flow modifier

Since the original nozzle had an internal radius of 12 mm, that was the target used to determine the size of the new annular nozzle. A desirable overflow was selected as 0.5 mm to ensure the gel was pushed to the edge of the nozzle. Using this overflow value, along with the diameter of the nozzle being 60 mm, gave an external radius of 29.5 mm for the annular nozzle. Only the internal radius of the annular nozzle is unknown. To determine the internal radius, one may equate the area of a circle with the radius of the old nozzle with the area of the new annular nozzle:

$$A_{old} = A_{new} \tag{D-59}$$

$$\pi r^2 = \pi\left({R_o}^2 - {R_i}^2\right) \tag{D-60}$$

In Equation D-59 and Equation D-60, A_{old} and A_{new} are the old and new areas, respectively, r is the radius of the old nozzle, and R_o and R_i are the outer and inner radii of the new nozzle, respectively. Additionally, one should consider the overflow of 0.5 mm, which can be given the variable r_{over}.

The inner and outer radii, r_i and r_o, respectively, of the new nozzle can then be displayed in the following way when considering the overflow radius:

$$R_o = r_o + r_{over} \tag{D-61}$$

$$R_i = r_i - r_{over} \tag{D-62}$$

Substituting Equation D-61 and D-62 into Equation D-60 gives:

$$\pi r^2 = \pi((r_o + r_{over})^2 - (r_i - r_{over})^2) \tag{D-63}$$

$$r_i = \sqrt{(r_o + r_{over})^2 - r^2} + r_{over} \tag{D-64}$$

$$r_i = \sqrt{(29.5 + 0.5)^2 - 12^2} + 0.5$$

$$r_i = 28\ mm$$

Therefore, the new annular nozzle would need an internal radius of 28 mm and an external radius of 29.5 mm with an allowance of a 0.5 mm overflow. In the slicer software, this would be represented by the flow multiplier being reduced to the ratio of the cross-sectional areas of the outlets of the annular nozzle and the radius given to the slicer for the nozzle diameter increasing to the outer diameter of the gel nozzle. Only one new variable is introduced to find the ratio of the cross-sectional areas. The new variable being R, which is the bottom radius of the gel nozzle with a value of 30 mm.

$$F = \frac{A_{new}}{A_{bottom}} \tag{D-65}$$

$$F = \frac{\pi\left({R_o}^2 - {R_i}^2\right)}{\pi R^2} \tag{D-66}$$

$$F = \frac{\pi(30^2 - 27.5^2)}{\pi(30)^2}$$

$$F = 15.972\%$$

One may use 15.972% to modify the flow from a conventional nozzle with a radius of 30 mm to an annular nozzle with an internal radius of 28 mm and an external radius of 29.5 mm while allowing overflow to the edge of the 30 mm radius.

Appendix E: MATLAB code and outputs

This appendix shows the MATLAB code and its outputs.

Maximum Allowable Needle Length shows the ink deposition needle's maximum allowable length for each given gauge.

Soft Tubing Expansion shows the amount of expansion the soft tubing in the peristaltic pump would experience during use.

Linear Rod Deflection and Angular Deflection show the deflection the linear rods in the DIGEX print head would experience while pressing down the syringe plunger in the ink syringe pump at the maximum allowable force.

Nozzle Fill Volume is the small amount of gel the gel nozzle needs to be filled in addition to the normal extrusion amounts during typical printing to combat under-extrusion.

This code may also be found in the following Google Drive:

https://drive.google.com/drive/folders/1mXSRrU1Rug7xi4EunPfRDUiUuODyCZJ4?usp=drive_link

E.1. Maximum allowable needle length

```
% Initialising variables
F = 400;
Rs = (1*14.8e-3)/2;
v = 0.33e-3;
mu = 3.5;
% https://www.hamiltoncompany.com/laboratory-products/
% needles-knowledge/needle-gauge-chart
Dn = [0.051; 0.108; 0.133; 0.159; 0.184; 0.21; 0.26; 0.311; 0.337; 0.413;
0.514; ...
      0.603; 0.686; 0.838; 1.067; 1.194; 1.372; 1.6; 1.804; 2.159; 2.388;
2.693];
Ga = ["34"; "33-32"; "31"; "30"; "29-28"; "27"; "26-25"; "24"; "23"; "22";
"21"; ...
      "20"; "19"; "18"; "17"; "16"; "15"; "14"; "13"; "12"; "11"; "10"];

Rn = (Dn/2)*1e-3;
A = pi*(Rs^2);
dp = F/A;
Q = v*A;
L = (Rn.^4).*dp*pi/(8*mu*Q);
% Creating a bar graph to help visualise allowable needle lengths
bar(Dn, L*1000),
set(gca, 'YScale', 'log'),
```

```
title("Maximum allowable needle length for each gauge")
xlabel("Internal Diameter of Needle Gauges [mm]")
ylabel("Maximum Allowable Needle Length [mm]")
```

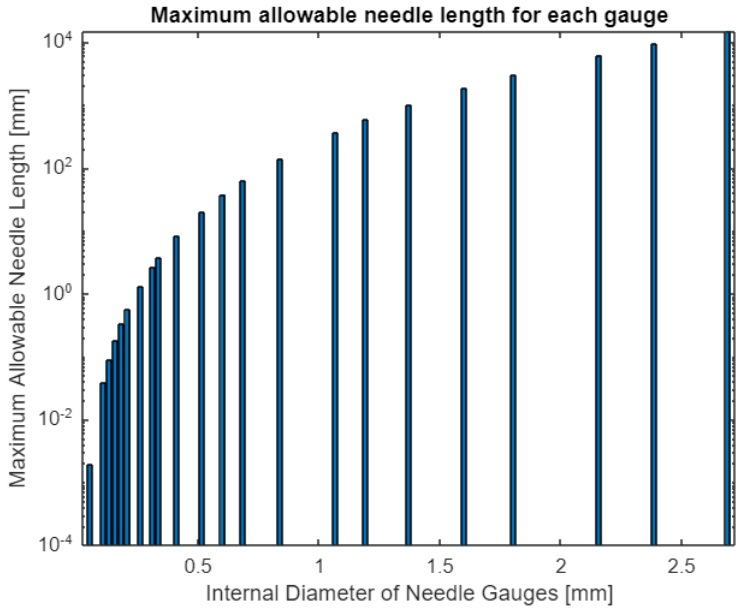


```
% Creating a table to store the maximum allowable needle lengths
varSize = [22 3];
varTypes = ["string", "double", "double"];
varNames = ["Needle Gauge", "Internal Diameter [mm]", "Max Length [mm]"];
needleLengths = table('Size', varSize, 'VariableNames', varNames, ...
                      'VariableTypes', varTypes);
needleLengths.("Needle Gauge") = Ga;
needleLengths.("Internal Diameter [mm]") = Dn;
needleLengths.("Max Length [mm]") = L*1000;
needleLengths
```

needleLengths = 22×3 table

	Needle Gauge	Internal Diameter [mm]	Max Length [mm]
1	"34"	0.0510	0.0019
2	"33-32"	0.1080	0.0391
3	"31"	0.1330	0.0899
4	"30"	0.1590	0.1836
5	"29-28"	0.1840	0.3292
6	"27"	0.2100	0.5586
7	"26-25"	0.2600	1.3125

	Needle Gauge	Internal Diameter [mm]	Max Length [mm]
8	"24"	0.3110	2.6868
9	"23"	0.3370	3.7043
10	"22"	0.4130	8.3559
11	"21"	0.5140	20.0467
12	"20"	0.6030	37.9717
13	"19"	0.6860	63.6045
14	"18"	0.8380	141.6339
15	"17"	1.0670	372.2622
16	"16"	1.1940	583.7254
17	"15"	1.3720	1.0177e+03
18	"14"	1.6000	1.8822e+03
19	"13"	1.8040	3.0418e+03
20	"12"	2.1590	6.2402e+03
21	"11"	2.3880	9.3396e+03
22	"10"	2.6930	1.5106e+04

```
% Saving the table
path = "C:\Users\Adrian\Documents\UCT Dissertation\";
filename = "Max_allowable_ink_needle.xlsx";
writetable(needleLengths,path+filename);
```

E.2.Soft tubing expansion

```
% Initializing variables
p_i = 6e5;
p_o = 0;
r_i = 1.5/1000;
r_o = 2.5/1000;
E = 0.05e9;
% Calculating parts A, B, C and D for
```

```
% thick-walled pressure vessel equation
A = p_i*(r_i^2);
B = p_o*(r_o^2);
C_i = (r_i^2)*(r_o^2)*(p_o - p_i)/(r_i.^2);
C_o = (r_i^2)*(r_o^2)*(p_o - p_i)/(r_o.^2);
D = (r_o^2) - (r_i^2);
% Calculating tangential stresses
s_t_i = (A - B - C_i)/D
```

```
s_t_i = 1.2750e+06
```

```
s_t_o = (A - B - C_o)/D
```

```
s_t_o = 6.7500e+05
```

```
% Calculating ring stresses
s_r_i = (A - B + C_i)/D
```

```
s_r_i = -6.0000e+05
```

```
s_r_o = (A - B + C_o)/D
```

```
s_r_o = 5.5511e-11
```

```
% Calculating expansion of tubing and
% change in cross-sectional area
format long
r_s = r_i*((abs(s_r_i)/E) + 1)
```

```
r_s =

   0.001518000000000
```

```
format
percent_change = 100*((r_s^2) - (r_i^2))/(r_i^2)
```

```
percent_change = 2.4144
```

E.3.Linear rod deflection and angular deflection

```
% start fresh plot each time code is run
close all;
% Initialise variables
Mo = 400*0.030/2;
L = 0.176;
a = L/2;
E = 190*10^9;
I = (pi*0.006^4)/64;
EI = E*I;
% Equations defining forces and moments
```

```
R1 = -(3/2)*(Mo/L);
M1 = -0.5*(Mo + R1*L);
R2 = -R1;
M2 = M1 + Mo + R1*L;
% Making values along x-axis before and after where Mo is applied
x1 = linspace(0, L/2);
x2 = linspace(L/2, L);
% Equations defining angles and deflections
theta1 = (M1*x1 + 0.5*R1*(x1.^2))/EI;
theta2 = (0.5*R1*(x2.^2) + (M1 + Mo)*x2 - (M1 + Mo + 0.5*R1*L)*L)/EI;
y1 = (0.5*M1*(x1.^2) + (R1*(x1.^3))/6)/EI;
y2 = (R1*(x2.^3)/6 + 0.5*(M1 + Mo)*(x2.^2) - (M1 + Mo + 0.5*R1*L)*L*x2 +...
      0.5*(Mo + M1 + (2/3)*(R1*L))*(L^2))/EI;
% Deleting some left-over annotations from previous iterations of plots
delete(findall(gcf, 'Type', 'annotation'));
delete(findall(gca, 'Type', 'text', 'Tag', 'XLineText'));
hold on
% Creating Displacement portion of the plot
yyaxis left
plot(x1.*1000, y1.*10^6, x2.*1000, y2.*10^6, 'LineWidth', 2);
ylabel("Displacement (microns)", FontSize=24);
% Putting limits on the Displacement axis
maxyy = 1.2*max([abs(y1.*10^6), abs(y2.*10^6)], [], "all");
ylim([-maxyy maxyy]);
% Creating Angular Displacement portion of the plot
yyaxis right
plot(x1.*1000, theta1.*10^3, x2.*1000, theta2.*10^3, 'LineWidth', 2);
ylabel("Angular Displacement (milliradians)", FontSize=24)
% Putting limits on the Angular Displacement axis
maxyt = 1.2*max([abs(theta1.*10^3), abs(theta2.*10^3)], [], "all");
ylim([-maxyt maxyt]);
% Defining the legend
legend("Displacement a", "Displacement a", "Angle a", "Angle b",...
        Location="southwest", Fontsize=24);
title("Displacement and angular displacement of beam", Fontsize=28);
xlabel("Length (mm)", Fontsize=24);
xlim([0 L*1000]);

yyaxis left
% Creating annotations for midline and point of maximum deflection
legend("AutoUpdate","off");
midline = xline(L*1000/2, "-");
text('Position', [L*1000/2, 60, 0], 'String', ["Applied", "Moment"],...
      'Tag', 'XLineText', 'Rotation', 90, 'FontSize', 18);
midline.Tag = 'XLine';
[maxy, xmaxy] = max(y1);
xmax = x1(xmaxy)*1000;
ymax = maxy*10^6;
annotation("textarrow", [(xmax-10)./(L*1000) (xmax+9)./(L*1000)],...
```

```
            [ymax./maxyy (ymax+2)./maxyy], "String",...
            ["Maximum", "Deflection"], FontSize=18);
plot(xmax, ymax, "o", "Color", "r");
annotation("textbox", [(xmax+1.5)./(L*1000) (ymax+4)./maxyy .048 .035],...
           "String", "58.7, 71.2", 'FitBoxToText', 'on', FontSize=18);
yline(maxyy);

grid on

hold off
```

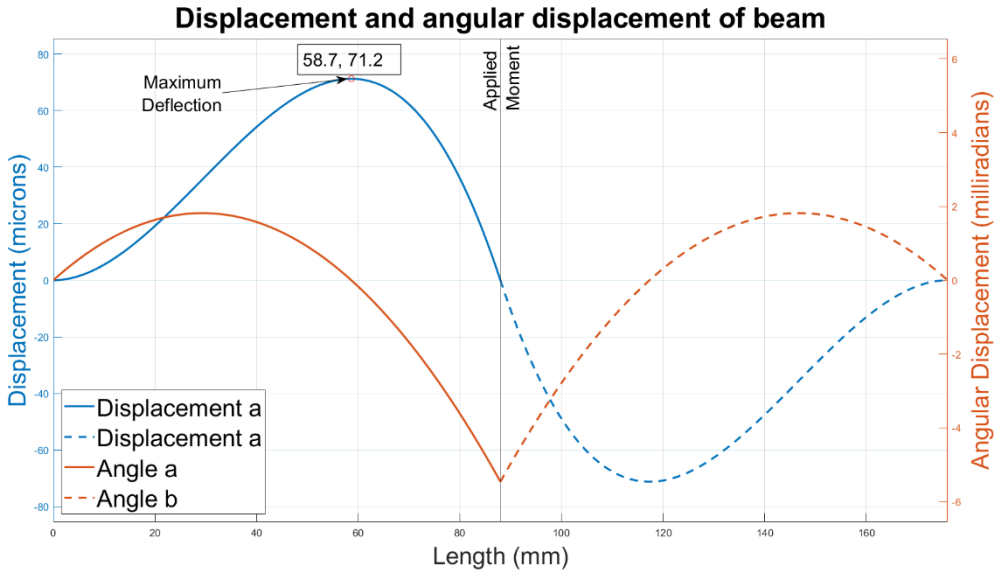


```
% Display maximum and minimum deflections
max(y1)
```

```
ans = 7.1186e-05
```

```
min(y2)
```

```
ans = -7.1186e-05
```

E.4.Nozzle fill volume

```
% Initialise variables
hu = 1;
hl = 4;
ruo = 27.25;
rui = 19.8;
roend = 29.5;
rostart = 27.25;
riend = 28;
ristart = 24.25;
```

```
hm = 5;
rmi = ristart;
rmo = rostart;
rs = 28.6/2;
% Calculate volume of gel nozzle when lowered
A1 = hu*(ruo^2 - rui^2);
A2 = hm*(rmo^2 - rmi^2);
B = ((roend - rostart)^2 - (riend - ristart)^2)/3;
C = rostart*(roend - rostart) - ristart*(riend - ristart);
D = rostart^2 - ristart^2;
V = pi*(A1 + A2 + hl*(B + C + D))
```

```
V = 5.0596e+03
```

```
% Calculate extrude distance of the gel syringe pump
Dextrude = V/(pi*rs^2)
```

```
Dextrude = 7.8758
```

Appendix F: Gel rheological properties and extrusion analysis

A large amount of processing was done on the rheological and extrusion properties of the Carbopol gels tested. It would be impractical to include it all in this document. A summary is written below to help explain what was done and the reasoning behind some of the calculations and the processing. The code can be found in the following Google Drive:

https://drive.google.com/drive/folders/1mXSRrU1Rug7xi4EunPfRDUiUuODyCZJ4?usp=drive_link

F.1. Initial gel rheological data processing

This section will deal with the first 250 lines of code written in "Gel Testing 18C", "Gel Testing 22C" and "Gel Testing 30C". As these names might suggest, they deal with the rheological data of the Carbopol gels collected at 18, 22 and 30°C.

After the data was imported in such a way as to make it useful for analysis, 3x3 grids of shear stress vs shear rate and viscosity vs torque were plotted in Figure 71. This was done as a quick way to investigate the data for any apparent interesting phenomena or check for errors in collecting or importing that data.

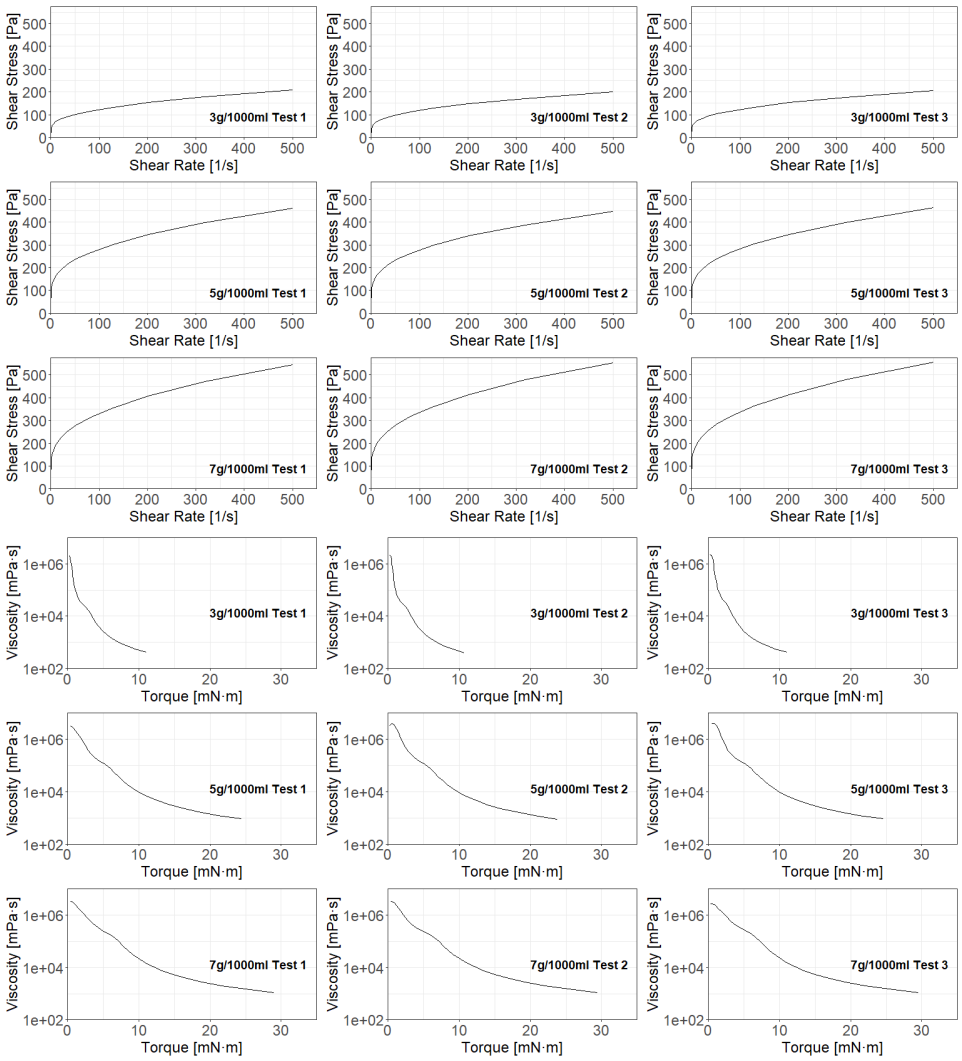

Figure 71: *3x3 grids of shear stress vs shear rate and viscosity vs torque rheology data.*

Three graphs were then plotted to show each test's shear stress against its shear rate, grouped by the concentration of the Carbopol Gel (3, 5 and 7 g/1000ml). This was again done to see if there was much variation between the tests with the same concentrations at the same temperatures. Since these graphs are all plotted together in Figure 72, they will not be shown here.

Next, all the shear stress and shear rate graphs were plotted on the same axes and compared. It was noted that each concentration was separated from the other concentrations on the plot and that the tests done at the same temperatures and concentrations gave similar results.

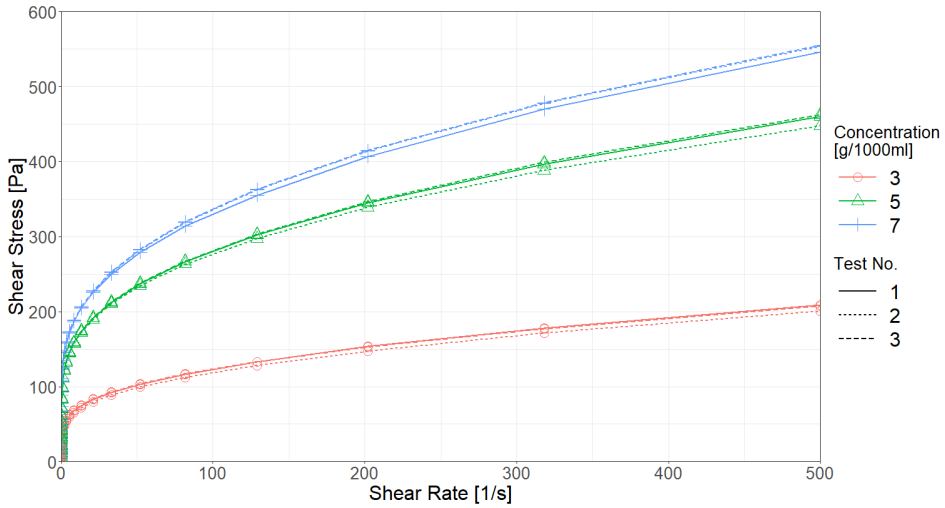

Figure 72: *All rheology test data at a given temperature.*

Finally, three more graphs were plotted to investigate how closely the averaged output Herschel-Bulkley constants matched the shear stress vs shear rate data. Each test output these constants, and a simple average was made between the three tests per plot. This showed that for the data collected, one might use the theoretical Herschel-Bulkley equation to predict the behaviour, noting that the theoretical result underestimates the shear stress above shear rates of 300/s. One plot shall be shown in Figure 73:

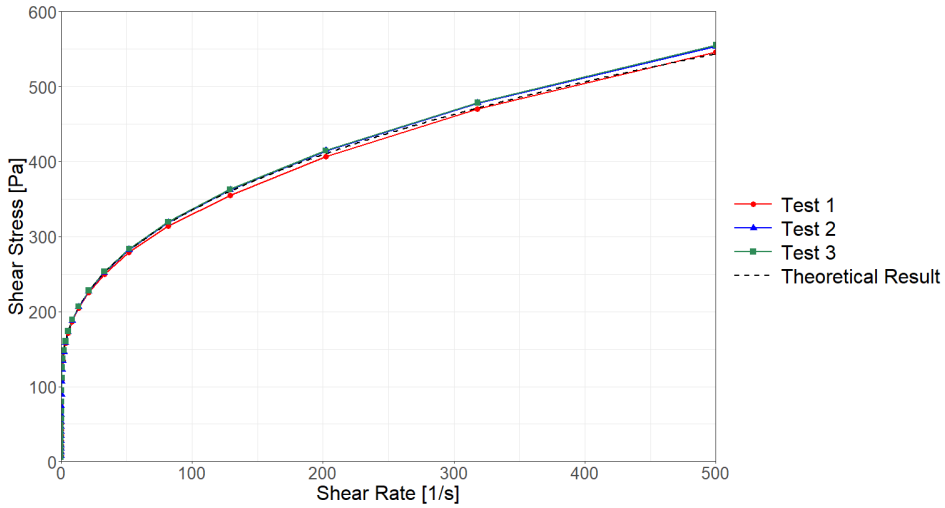

Figure 73: *Rheology test data compared against theoretical results.*

F.2. Comparison of the averaged data plots

Seeing that the data was consistent at different temperatures and concentrations, an effort was made to compare all these data points and see if controlling the temperature of the gel was necessary for this project.

To this end, the data was imported into and processed in the "Gel Testing Averages" file. All the data recorded at the same temperature and concentration were averaged and plotted on the same graph, Figure 74. Investigating this plot showed that each concentration remained distinct in the graph and separated from the other concentrations. Investigation of the plot also revealed that over the range of 18 to 30°C, no temperature yielded a consistently more or less viscous gel across all the gel concentrations. From this, it was concluded that temperature control was not needed over normal room temperatures for embedded 3D printing using Carbopol gel.

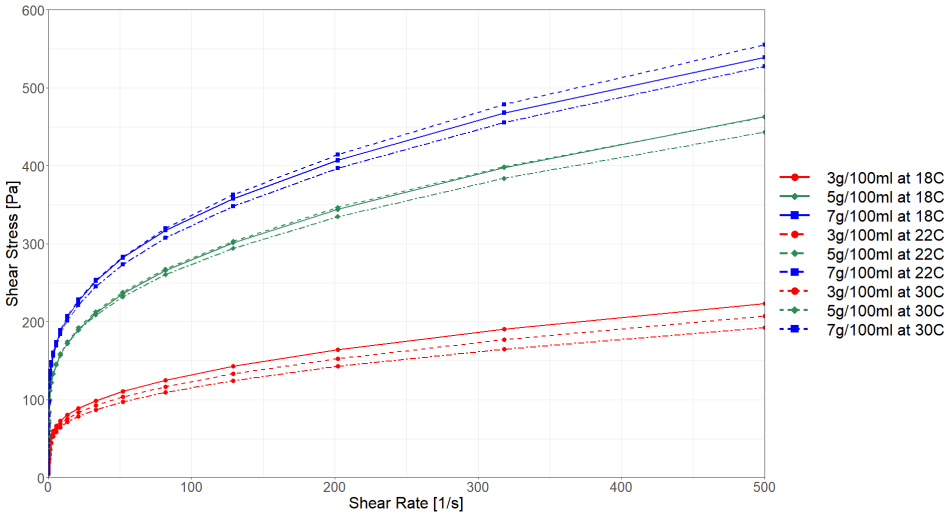

Figure 74: *Comparison of all the averaged rheological data*

F.3. Pump selection and printing criteria investigation

After it had been determined that temperature control was not necessary to control the support gel's rheological properties, further investigations with the data could go forward in any of the "Gel Testing" files. Lines of code after line 300 in "Gel Testing 22C" were used for this analysis.

The first plot showed the theoretical pump head required against the flow rate of the peristaltic pump designed for this project, shown in Figure 75. This used the averaged Herschel-Bulkley constants from earlier in the code. The required pump head plot was used to ensure that the output of the pump head calculations was still sensible and as an intermediate step to determining if a NEMA17 stepper motor would be appropriate for this use case.

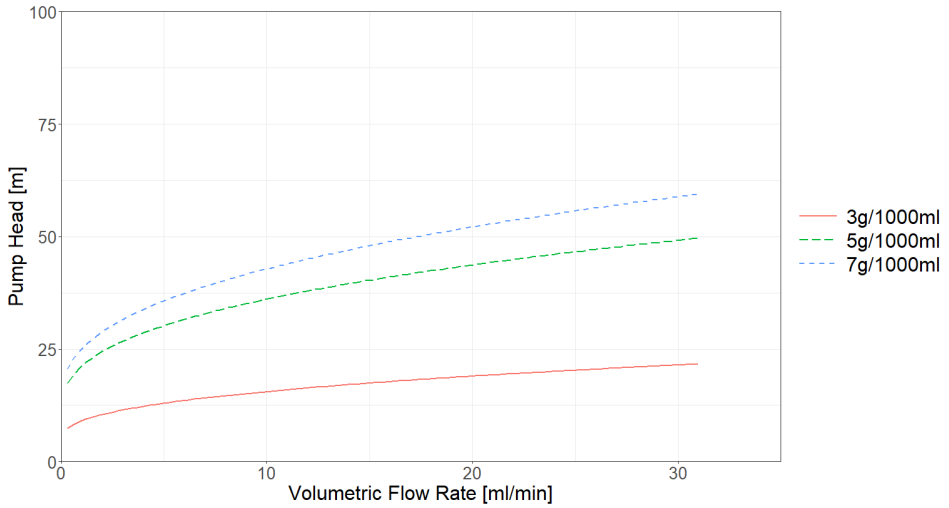

Figure 75: *The required pump head at a given flow rate for the peristaltic pump*

Having seen what appeared to be reasonable results for the pump head, Master's equation for determining the required torque was used to plot the required torque for the gel concentrations at different revolutions per minute and volumetric flow rates [41], shown in Figure 76. The author developed a relation to check the required torque and plot it to double-check the results in Section 6.2, shown in Figure 77. Both plots showed that the required was well below that of the maximum torque of a NEMA17 motor. With this known, it was decided to build the peristaltic pump and begin testing.

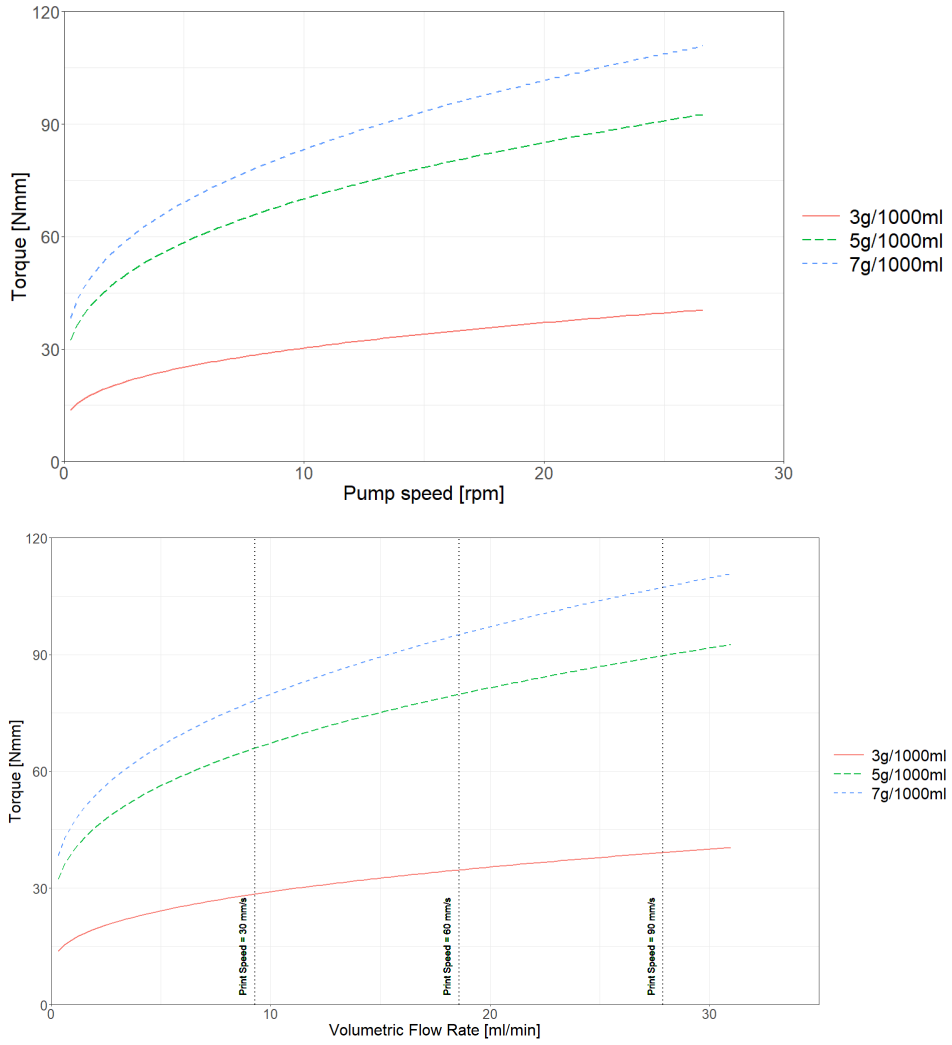

Figure 76: *The required torque for the peristaltic pump using Masters' relation*

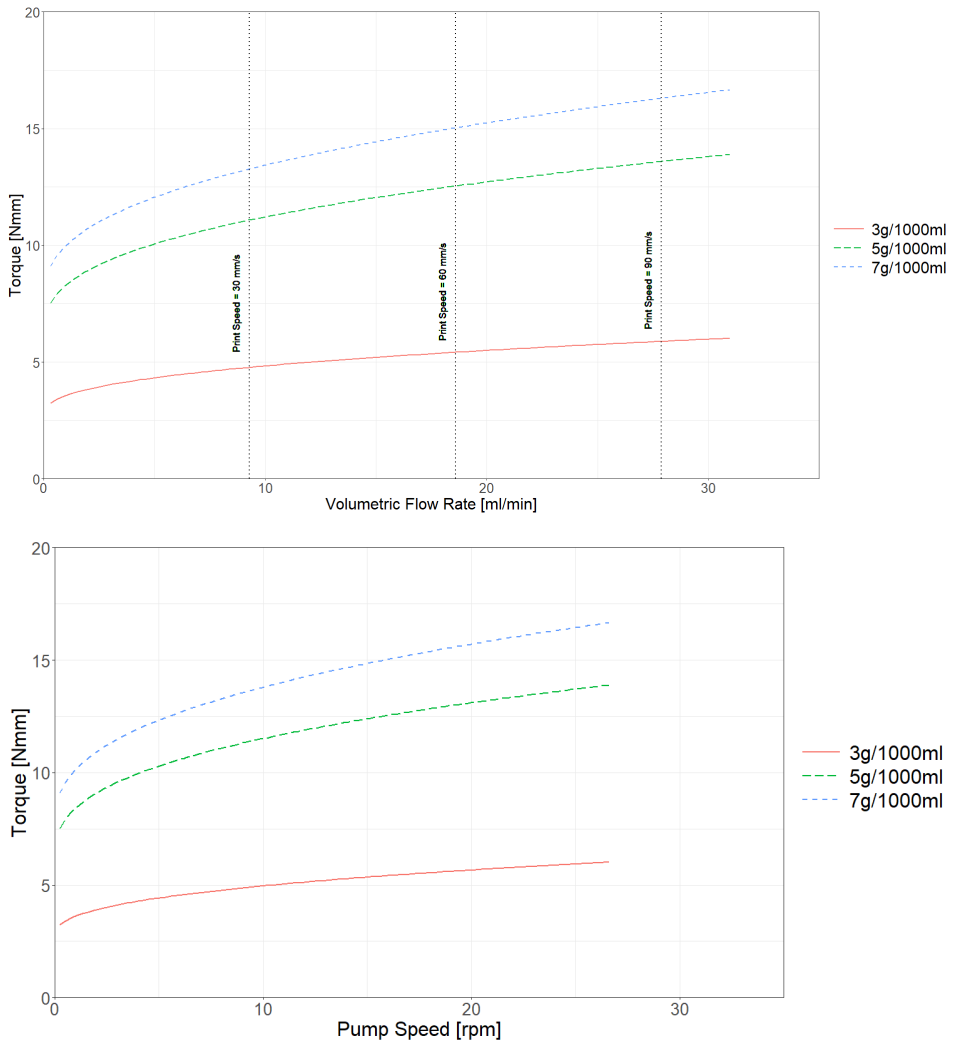

Figure 77: *The required torque for the peristaltic pump using the author's relation*

After this, it was briefly investigated at what needle translation speeds would yielding occur in the Carbopol gels since an attraction of using this gel as a support gel is that it may act as a gel when experiencing low shear rates but may act as a liquid. To this end, a plot was made to show at what translation speeds yielding may be caused in the Carbopol gels at different concentrations, shown in Figure 78. Additionally, a relation was made to estimate the shear stress vs shear rate behaviour Appendix D.5, which was also used to estimate at what point yielding may be seen in this other concentration of Carbopol gel, in this case, 2 g/1000ml.

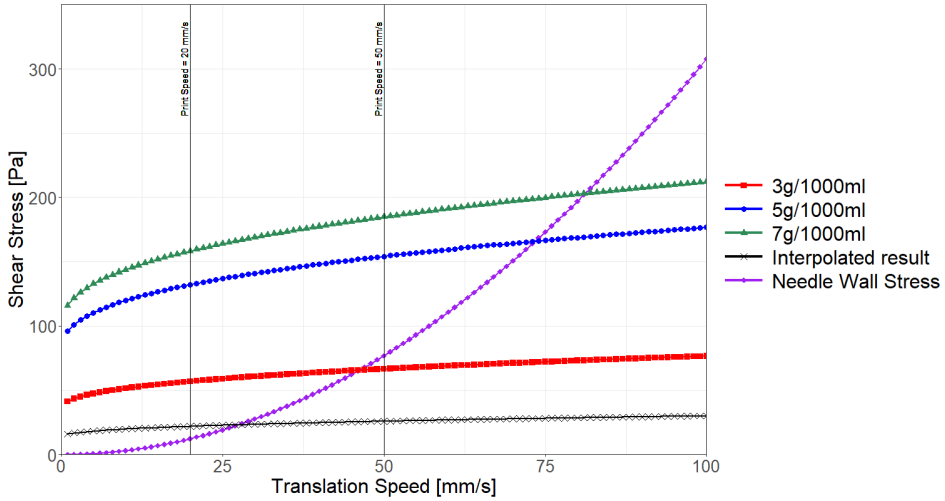

Figure 78: *The required shear stress to cause yielding in the Carbopol gel*

Finally, a plot was made to show the minimum length of the ink syringe needle that should be submerged during printing at different translation speeds to avoid recirculation wake-based instabilities, shown in Figure 79.

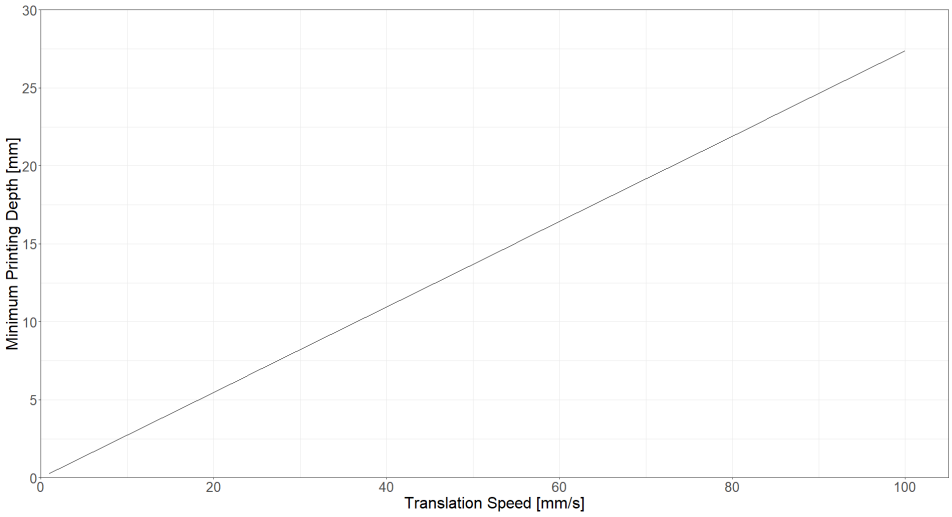

Figure 79: *The minimum printing depth to avoid recirculation wake instabilities at different translation speeds.*

F.4. Gel syringe pump extrudability data analysis

In the "Gel extrusion comparison" file, data from the gel extrudability tests were imported and compared. Tests were done with gel extruded by a syringe, and the force-displacement data was measured, shown in Figure 80. These tests measured the force required to extrude gel out of just the syringe and with 0.25, 0.5, 0.75 and 1 m of tubing attached to the tip of the syringe. Analysing the plots shows a low amount of force required to extrude the gel. This led to the conclusion that a NEMA17 stepper motor was more than capable of extruding the gel as needed.

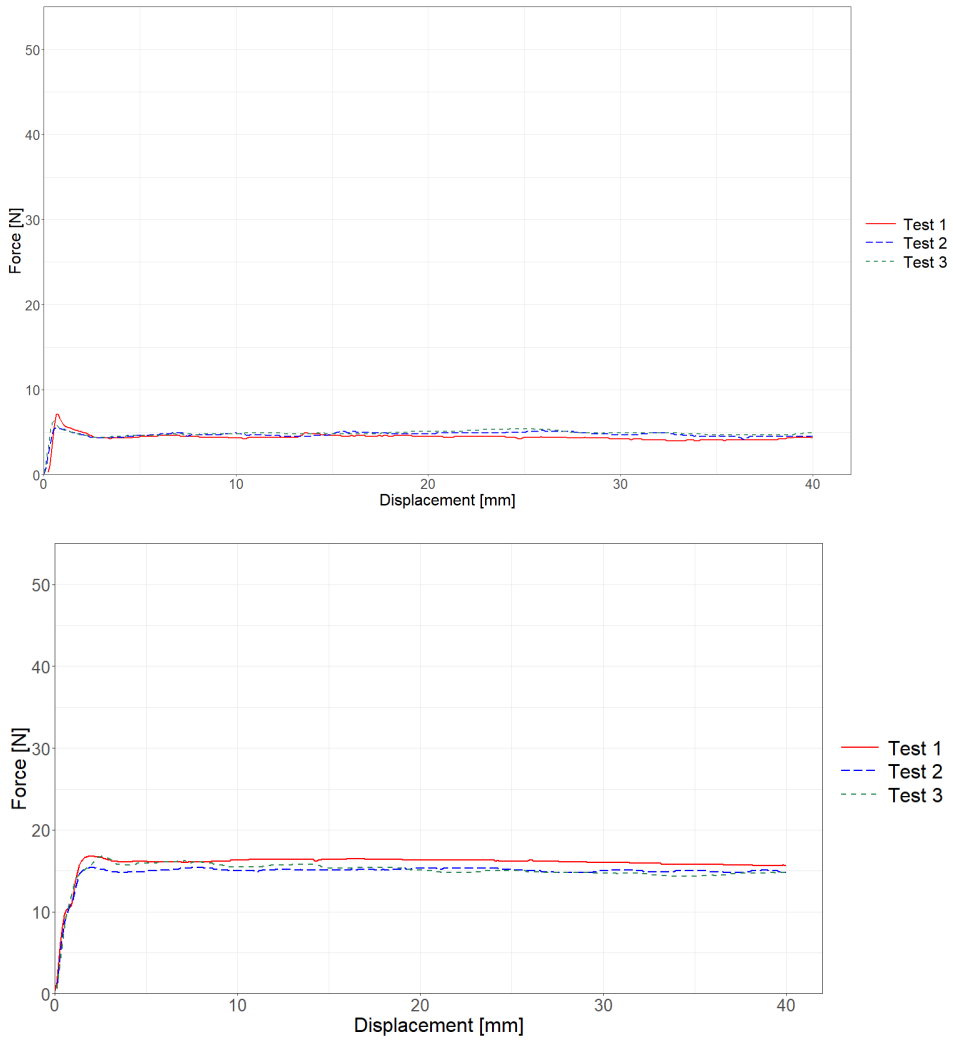

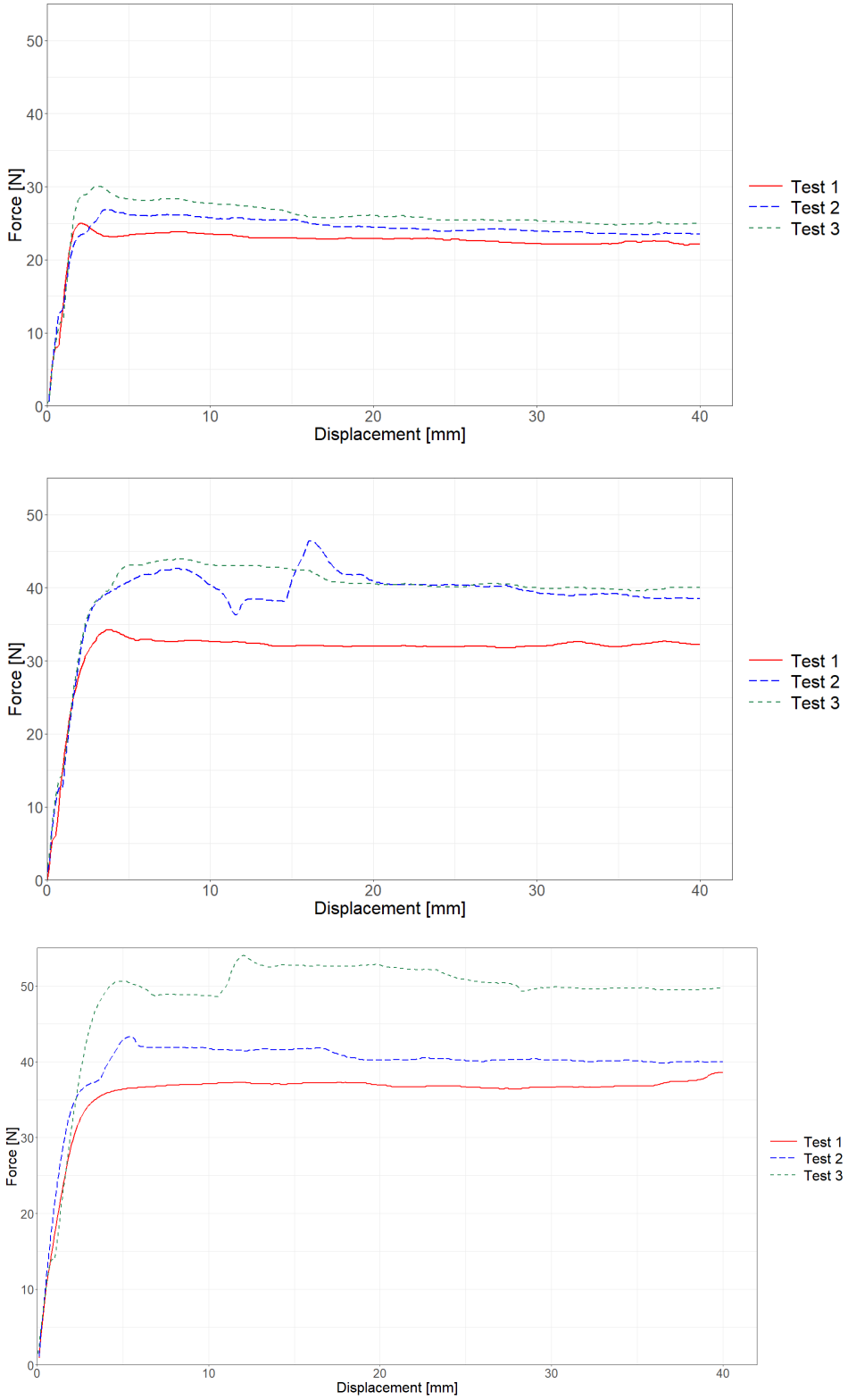

Figure 80: *Force-displacement data when extruding support gel out of a 60 cc syringe through varying tube lengths.*

Appendix G: Pump data

This project collected data from the peristaltic pump and the gel syringe pump. That data is shown in this appendix. This data may also be found in the following Google Drive:

https://drive.google.com/drive/folders/1mXSRrU1Rug7xi4EunPfRDUiUuODyCZJ4?usp=drive_link

G.1. Peristaltic pump tests

Table 12: *Peristaltic pump data printer settings*

Printer settings:	
microsteps	16
rotation_distance	40

Test command:

```
 force_move stepper=stepper_x distance=(Distance [mm]) velocity=(Velocity [mm/s])
```

Table 13: *Peristaltic pump data variables*

Gel Density [kg/m^3]:	1026
Volumetric flowrate [ml/rev]:	0.944
Mass flowrate [g/rev]	0.9685

Table 14: *Peristaltic pump data*

Tub weight [g]:	5.7
Test 1:	
Result #	Weight (including tub) [g]
1	9.35
2	9.41
3	9.51
4	9.42
5	9.46
6	9.55
7	9.57
8	9.58
Avg:	9.4813
Avg-Tub:	3.7813

Test 2:	
Result #	Weight (including tub) [g]
1	16.44
2	12.9
3	13.37
4	17.02
5	20.58
6	15.72
7	17.66
8	19.51
9	20.39
Avg:	17.066
Avg-Tub:	11.366
Test 3:	
Result #	Weight (including tub) [g]
1	38
2	38.57
3	39.55
Avg:	38.707
Avg-Tub:	33.007
Test 4:	
Result #	Weight (including tub) [g]
1	39.99
2	39.51
3	39.48
Avg:	39.66
Avg-Tub:	33.96
Test 5:	
Result #	Weight (including tub) [g]
1	34.64
2	36.35
3	33.37
Avg:	34.787
Avg-Tub:	29.087

Table 15: *Peristaltic pump variability testing*

Test #	Concentration [g/l]	Distance [mm]	Velocity [mm/s]	Measured Average [g]	Theoretical amount [g]	Percentage [%]
1	3	5000	100	3.7813	121.07	3.1232
2	3	15000	100	11.366	363.2	3.1292
3	1.2	2000	100	33.007	48.427	68.157
4	1.2	2000	50	33.96	48.427	70.126
5	1.2	2000	110	29.087	48.427	60.063

G.2. Syringe pump tests

Table 16: *Syringe pump test results*

Test 1			
Number	Concentration [g/l]	Speed [mm/min]	Weight [g]
1	0	180	146.1
2	0	180	149.43
3	0	180	147.49
4	0	180	145.02
5	0	180	140.14
		Average Weight [g]	145.64

Notes: First test with water

Test 2			
Number	Concentration [g/l]	Speed [mm/min]	Weight [g]
1	0	90	87.64
2	0	90	98.12
3	0	90	96.85
		Average Weight [g]	94.203

Notes: Testing effect of pumping water at slower speed

Test 3			
Number	Concentration [g/l]	Speed [mm/min]	Weight [g]
1	0	24	19.14
2	0	24	7.47
3	0	24	8.36
		Average Weight [g]	11.657

Notes: Testing effect of pumping water much slower

Test 4			
Number	Concentration [g/l]	Speed [mm/min]	Weight [g]
1	1.6	180	163.67
2	1.6	180	152.42
3	1.6	180	146.7
4	1.6	180	146.22
5	1.6	180	141.85
6	1.6	180	138.2
7	1.6	180	139.12
		Average Weight [g]	146.88

Notes: Testing pumping 1.6 g/l Carbopol gel Replaced M4 screw with M8 screw after wear observed

Test 5			
Number	Concentration [g/l]	Speed [mm/min]	Weight [g]
1	3	180	138.6
2	3	180	114.53
3	3	180	91.47
		Average Weight [g]	114.87

Notes: Testing pumping 3 g/l gel

Test 6			
Number	Concentration [g/l]	Speed [mm/min]	Weight [g]
1	3	90	156.45
2	3	90	162.26
3	3	90	160.18
		Average Weight [g]	159.63

Notes: Testing pumping 3 g/l at slower speed
Installed new reservoir
Tightened fittings
Replaced inlet hose with
10 mm ID reinforced hose

Test 7			
Number	Concentration [g/l]	Speed [mm/min]	Weight [g]
1	3	90	162.49
2	3	90	164.06
3	3	90	161.92
4	3	90	162.09
		Average Weight [g]	162.64

Notes: Testing adding a dwell command of 10 seconds after every suction stroke

G.3. Low flow rate gel syringe pump tests

After some testing, it was found that the syringe pump would under-extrude when pumping at lower flow rates. This would result in low-quality gel layers. An effort was made to measure the syringe pump's performance at these low flow rates.

G.3.1. Tests measuring the output of the pump after the non-return valve

Table 17: *Syringe pump results after non-return valve*

Test 1			
No.	Velocity [mm/s]	Distance [mm]	Weight [g]
1	3	5	0.36
2	3	5	0.35
3	3	5	0.37
4	3	5	0.38
5	3	5	0.29
		Avg	0.35

Notes: Extrude command sent, wait for 10 seconds and then send an equal retract command

Test 2			
No.	Velocity [mm/s]	Distance [mm]	Weight [g]
1	3	10	2.92
2	3	10	2.44
3	3	10	2.88
4	3	10	2.39
5	3	10	2.31

Notes: Extrude command sent, wait for 10 seconds and then send an equal retract command

6	3	10	2.71
		Avg	2.6083

Test 3

No.	Velocity [mm/s]	Distance [mm]	Weight [g]
1	3	15	5.13
2	3	15	5.47
3	3	15	4.79
4	3	15	4.78
5	3	15	5.24
6	3	15	5.34
		Avg	5.125

Notes: Extrude command sent, wait for 10 seconds and then send an equal retract command

Test 4

No.	Velocity [mm/s]	Distance [mm]	Weight [g]
1	5	5	0.15
2	5	5	0.36
3	5	5	0.32
4	5	5	0.45
5	5	5	0.27
6	5	5	0.22
		Avg	0.295

Notes: Similar to previous tests but increased extrusion speed

Test 5

No.	Velocity [mm/s]	Distance [mm]	Weight [g]
1	3	5+5	2.15
2	3	5+5	2.45
3	3	5+5	2.02
4	3	5+5	2.07
5	3	5+5	2.13
6	3	5+5	2.15
		Avg	2.1617

Notes: Extrude command sent, wait for 10 seconds, a second extrude command with another wait and then send an equal retract command

Test 6

No.	Velocity [mm/s]	Distance [mm]	Weight [g]
1	3	20	8.57
2	3	20	7.31
3	3	20	7.3
4	3	20	7.95
5	3	20	7.43
6	3	20	7.42
		Avg	7.6633

Notes: Similar to the first 3 tests

Test 7

No.	Velocity [mm/s]	Distance [mm]	Weight [g]
1	3	25	10.97
2	3	25	10.31
3	3	25	10.57
4	3	25	10.58
5	3	25	10.02

Notes: Similar to the first 3 tests

6	3	25	10.46
		Avg	10.485

Test 8			
No.	Velocity [mm/s]	Distance [mm]	Weight [g]
1	3	30	12.67
2	3	30	13.92
3	3	30	13.12
4	3	30	12.85
5	3	30	12.88
6	3	30	13.12
		Avg	13.093

Notes: Similar to the first 3 tests

G.3.2. Tests measuring the output of the pump after the full gel deposition assembly

Table 18: *Syringe pump test results after the full gel deposition assembly*

Test 1			
No.	Velocity [mm/s]	Distance [mm]	Weight [g]
1	3	5	0.14
2	3	5	0.18
3	3	5	0.12
4	3	5	0
5	3	5	0
		Avg	0.088

Notes: Extrude command sent, wait for 10 seconds and then send an equal retract command

Test 2			
No.	Velocity [mm/s]	Distance [mm]	Weight [g]
1	3	10	1.24
2	3	10	1.3
3	3	10	1.58
4	3	10	1.7
5	3	10	2
6	3	10	2.02
		Avg	1.64

Notes: Extrude command sent, wait for 10 seconds and then send an equal retract command

Test 3			
No.	Velocity [mm/s]	Distance [mm]	Weight [g]
1	3	15	3.57
2	3	15	3.78
3	3	15	3.77
4	3	15	4.06
5	3	15	3.47

Notes: Extrude command sent, wait for 10 seconds and then send an equal retract command

6	3	15	3.71
		Avg	3.727

Test 4

No.	Velocity [mm/s]	Distance [mm]	Weight [g]
1	3	15	5.6
2	3	15	6.24
3	3	15	5.54
4	3	15	5.68
5	3	15	5.64
6	3	15	5.17
		Avg	5.645

Notes: Extrude command sent, wait for 10 seconds and then send an equal retract command

Test 5

No.	Velocity [mm/s]	Distance [mm]	Weight [g]
1	3	25	7.76
2	3	25	7.67
3	3	25	7.29
4	3	25	7.37
5	3	25	7.58
6	3	25	7.73
		Avg	7.567

Notes: Extrude command sent, wait for 10 seconds and then send an equal retract command

Test 6

No.	Velocity [mm/s]	Distance [mm]	Weight [g]
1	3	15	9.82
2	3	15	9.81
3	3	15	9.19
4	3	15	9.47
5	3	15	9.43
6	3	15	9.37
		Avg	9.515

Notes: Extrude command sent, wait for 10 seconds and then send an equal retract command

Appendix H: Fittings list

Many fittings are required to build all the assemblies in this project. These lists will aid in gathering the required amounts of each.

The master list is a full inventory of all the required fittings. The per-drawing lists are meant to be used with the drawings with the drawing number at the top of each list.

H.1. Master list

Table 19: *Master fittings list*

Fitting	Type	Number	Drawings
M3	Nut	41	Various
M3	Washer	14	DIGEX005, DIGEX011, DIGEX013, DIGEX201
M3x8	Counter Sunk Head	9	DIGEX007, DIGEX011, DIGEX101
M3x8	Socket Head	7	DIGEX005, DIGEX011, DIGEX201
M3x12	Socket Head	2	DIGEX009
M3x16	Counter Sunk Head	18	DIGEX005, DIGEX101, DIGEX305
M3x18	Socket Head	13	DIGEX007, DIGEX009, DIGEX013, DIGEX201
M3x30	Socket Head	2	DIGEX003, DIGEX007
M3x35	Counter Sunk Head	6	DIGEX011, DIGEX101, DIGEX305
M4	Nut	48	Various
M4	2020 Profile T-nut	4	DIGEX201, DIGEX303
M4	Heat Insert	2	DIGEX003
M4	Washer	12	DIGEX005, DIGEX011
M4x10	Counter Sunk Head	6	DIGEX005, DIGEX011, DIGEX303
M4x12	Socket Head	8	DIGEX003, DIGEX005
M4x16	Counter Sunk Head	10	DIGEX005, DIGEX201
M4x25	Socket Head	6	DIGEX003, DIGEX005, DIGEX009
M4x40	Counter Sunk Head	8	DIGEX007
M4x40	Button Head	1	DIGEX303
M4x45	Socket Head	8	DIGEX009
M4x16	Counter Sunk Wood Screw	46	DIGEX305, DIGEX306
M4x30	Counter Sunk Wood Screw	6	DIGEX306
M5	Nut	2	DIGEX009
M5	Washer	4	DIGEX005
M5x25	Socket Head	1	DIGEX009
M8	Brass Nut	2	DIGEX101
4.8x8 mm	Pop Rivet	4	DIGEX005
	Total	290	

H.2. Per-drawing lists

Table 20: *DIGEX003 fittings list*

DIGEX003			
Fitting	Type	Number	Connecting to
M4x12	Socket Head	2	DIGEX005
M4	Nut	2	
M3x30	Socket Head	2	DIGEX007
M3	Nut	2	
M4x25	Socket Head	2	DIGEX005
M4	Nut	2	
M4x12	Socket Head	2	DIGEX003
M4	Heat Insert	2	

Table 21: *DIGEX005 fittings list*

DIGEX005			
Fitting	Type	Number	Connecting to
4.8x8 mm	Pop Rivet	4	DIGEX005
M5	Washer	4	
M3x16	Counter Sunk	2	DIGEX005
M3	Washer	2	
M3	Nut	2	
M3x16	Counter Sunk	1	DIGEX005
M3	Nut	1	
M4x16	Counter Sunk	8	DIGEX005
M4	Washer	8	
M4	Nut	8	
M4x12	Socket Head	4	DIGEX005
M4	Nut	4	

Table 22: *DIGEX007 fittings list*

DIGEX007			
Fitting	Type	Number	Connecting to
M4x40	Counter Sunk	8	DIGEX007
M4	Nut	8	
M3x18	Socket	4	DIGEX007
M3	Nut	4	
M3x8	Counter Sunk	1	DIGEX007
M3	Nut	1	

Table 23: *DIGEX009 fittings list*

DIGEX009			
Fitting	Type	Number	Connecting to
M5x25	Socket Head	1	DIGEX009
M5	Nut	2	
M3x12	Socket Head	2	DIGEX009
M3	Nut	2	
M4x45	Socket Head	8	DIGEX009
M4	Nut	8	
M3x18	Socket Head	4	DIGEX009
M3	Nut	4	
M4x25	Socket Head	4	DIGEX009
M4	Nut	4	
M4	Nut	3	DIGEX013

Table 24: *DIGEX011 fittings list*

DIGEX011			
Fitting	Type	Number	Connecting to
M4x10	Counter Sunk	4	DIGEX005
M4	Washer	4	
M4	Nut	4	
M3x8	Socket Head	3	DIGEX005
M3	Washer	3	
M3	Nut	3	
M3x35	Counter Sunk	3	DIGEX011
M3	Nut	3	
M3x8	Counter Sunk	4	DIGEX011

Table 25: *DIGEX013 fittings list*

DIGEX013			
Fitting	Type	Number	Connecting to
M3x18	Socket Head	4	DIGEX013
M3	Washer	8	
M3	Nut	4	

Table 26: *DIGEX101 fittings list*

DIGEX101			
Fitting	Type	Number	Connecting to
M3x8	Counter Sunk	4	DIGEX101
M3x16	Counter Sunk	2	DIGEX101
M3	Nut	2	
M3x16	Counter Sunk	4	DIGEX101
M3	Nut	4	
M3x16	Counter Sunk	1	DIGEX305
M3	Nut	1	
M8	Brass Nut	2	DIGEX101
M3x16	Counter Sunk	2	DIGEX101
M3	Nut	2	
M3x35	Counter Sunk	1	DIGEX305
M3	Nut	1	
M3x35	Counter Sunk	2	DIGEX101
M3	Nut	2	
M3x16	Counter Sunk	2	DIGEX101
M3	Nut	2	
M3x16	Counter Sunk	2	DIGEX101
M3	Nut	2	

Table 27: *DIGEX201 fittings list*

DIGEX201			
Fitting	Type	Number	Connecting to
M3x8	Socket Head	4	DIGEX201
M4x16	Counter Sunk	2	DIGEX201
M4	T-Nut	2	
M3x18	Socket Head	1	DIGEX201
M3	Washer	1	
M3	Nut	1	

Table 28: *DIGEX303 fittings list*

DIGEX303			
Fitting	Type	Number	Connecting to
M4x10	Counter Sunk	2	DIGEX303
M4	T-Nut	2	DIGEX303
M4x40	Button Head	1	DIGEX303
M4	Nut	1	

Table 29: *DIGEX305 fittings list*

DIGEX305			
Fitting	Type	Number	Connecting to
M4x16	Wood Screw	4	DIGEX306
M4x16	Wood Screw	6	DIGEX306
M3x16	Counter Sunk	2	DIGEX305
M3	Nut	2	
M4x16	Wood Screw	36	DIGEX306
M4x30	Wood Screw	6	DIGEX306

Appendix I: Sub-assembly drawings

The drawings that are shown here as well as the sub-assembly part files may be found in the following Google Drive:

https://drive.google.com/drive/folders/1mXSRrU1Rug7xi4EunPfRDUiUuODyCZJ4?usp=drive_link